IRE
Transactions
on ANTENNAS and PROPAGATION

Volume AP-5 APRIL, 1957 Number 2

Published Quarterly

TABLE OF CONTENTS

PUBLISHED BY THE
ofessional Group on Antennas and Propagation

IRE TRANSACTIONS® PGAP IS A QUARTERLY PUBLICATION DEVOTED TO EXPERIMENTAL AND THEORETICAL PAPERS ON ANTENNAS AND WIRELESS PROPAGATION OF ELECTROMAGNETIC WAVES

MANUSCRIPTS should be submitted to John B. Smyth, Editor, SRA, 3930 4th Avenue, San Diego 3, California. Manuscripts should be original typewritten copy, double spaced, plus one carbon copy. References should appear as footnotes and include author's name, title, journal, volume, initial and final page numbers, and date. Each paper must have an abstract of not more than 200 words. News items concerning PGAP members and group activities should be sent to the News Editor, Mr. Arthur Dorne, Dorne and Margolin, Inc., 30 Sylvester Street, Westbury, L.I., N.Y.

ILLUSTRATIONS should be submitted as follows: All line drawings (graphs, charts, block diagrams, cutaways, etc.) should be inked uniformly and ready for reproduction. If commercially printed grids are used in graph drawings, author should be sure printer's ink is of a color that will reproduce. All half-tone illustrations (photographs, wash, airbrush, or pencil renderings, etc.) should be clean and ready to reproduce. Photographs should be glossy prints. Call-outs or labels should be marked on a registered tissue overlay, not on the illustration itself. No illustration should be larger than 8 x 10 inches.

Copies can be purchased from
THE INSTITUTE OF RADIO ENGINEERS
1 East 79 St., New York 21, N.Y.

PRICE PER COPY: members of the Professional Group on Antennas and Propagation, $1.75; members of the IRE, $2.60; nonmembers, $5.25.

ANNUAL SUBSCRIPTION PRICE: PGAP members, included in PGAP assessment of $4.00; IRE members, $8.50; Colleges and public libraries, $10.00; nonmembers, $17.00.

Entered as second-class matter, at the post office at Menasha, Wisconsin, under the act of August 24, 1912. Acceptance for mailing at a special rate of postage is provided for in the act of February 28, 1925, embodied in Paragraph 4, Section 412, P. L. & R., authorized October 26, 1927.

news and views

Administrative Committee Meeting

The following is abstracted from the minutes of the Administrative Committee meeting held at Jansky and Bailey, Washington, D. C., January 11, 1957. Present were J. I. Bohnert, Vice-Chairman, who presided, P. S. Carter, Arthur Dorne, Coleman Goatley (guest), F. T. Haddock, J. W. Herbstreet, D. D. King, R. L. Mattingly, and D. C. Ports.

1) Mr. Mattingly presented a brief membership and financial report. Membership has grown each year. As of the end of 1956, our membership totaled 2392, of which 365 were student members; whereas, on March 8, 1956, total membership was only 1891. Also, as of the end of 1956, our treasury balance was $3448.00, a deficit having been avoided through the postponement of TRANSACTIONS publications.

2) There was an extended discussion of programs for improving our financial status to ensure that in the future it will not again impede either the publication of our TRANSACTIONS or any other phase of our professional activity. It was concluded that the publication of advertising in the TRANSACTIONS (as just recently permitted by IRE policy) constitutes the most promising avenue for use, and further that our goal should be the sale only of sufficient advertising to meet our actual needs. In view of this, it was decided that we should not engage a commercial sales representative, but instead should handle the sales ourselves. Mr. Ports volunteered to administer this activity. His offer was gratefully accepted by the Committee. He will, with the assistance of other members of the Administrative Committee, organize a program of personal letters and calls to likely prospects. It was the belief of the Committee that the TRANSACTIONS should be a uniquely valuable medium for many advertisers, such as manufacturers of test equipment which meets our particular needs and laboratories seeking personnel in our profession.

3) The next topic was the Affiliate Membership Plan recently approved by IRE headquarters. In this plan the membership of certain selected scientific societies would be extended the privilege of joining the various professional groups on an "affiliate" basis without joining the IRE. Such a member of PGAP would incur less than half the cost of full IRE-PGAP membership and would still receive the TRANSACTIONS. The IRE Executive Committee must approve any such societies selected by the professional groups. After discussion, during which it was brought out that the committee does not yet have a full understanding of the intent of this policy, it was decided to select a few societies, and submit them for approval, together with a request for a clarification of the type of society considered appropriate, and an indication of whether the total number was expected to be limited. The following were then selected: The American Astronomical Society, the American Meteorological Society, the Optical Society of America, and the Royal Astronomical Society. It was noted that the complete list of societies which might possibly be included is a very extensive one, numbering perhaps in the hundreds. In the case of some of these there is a very substantial overlapping of interests with IRE.

4) Mr. Goatley reported on the Symposium on Optics and Microwave Techniques held in November at the George Washington University, pointing out in particular that for its success we are deeply indebted to the University, which cooperated and assisted most completely.

5) Mr. Ports reported that he has been contacted by John P. Hagen in connection with the URSI Spring meeting. The Administrative Committee passed a resolution indicating our approval of the PGAP's joint sponsorship with the URSI of this meeting. The Secretary will advise Dr. Hagen of this action and Dr. J. T. Bolljahn (PGAP Meetings Chairman) will be instructed to

implement this decision. The Secretary will also send a letter to the Executive Committee of the IRE asking for their approval. It is hoped and expected that the abstracts of this Spring meeting will be published in the TRANSACTIONS.

6) Mr. Dorne brought up the matter of how News and Views could best further the development of PGAP and suggested a number of alternative types of material which it might include. After discussion it was agreed that News and Views should concentrate upon reporting specific items of information which best convey a picture of the current activity and concerns of PGAP and its members, with the hope that this will increase the cohesiveness of the organization and stimulate more active and widespread participation in its affairs by the membership. Mr. Dorne also suggested that the society might benefit along these lines if it sponsored social events which would acquaint the members with each other. It was agreed to hold an informal gathering for cocktails sometime during the National Convention.

7) Mr. Ports brought up the special IRE issue dedicated to Radio Astronomy. C. M. Jansky was originally scheduled to handle the task of procuring and editing the material for this issue. Unexpected commitments have made this impossible and Frederick Haddock is now in charge. Dr. Haddock pointed out that there are many ways of handling an issue of this type depending upon the type of reader to which it is most particularly directed. The papers might, for example, emphasize either the techniques of radio astronomy or alternatively astronomy itself. He asked for an expression from the committee of the direction he should take. It was the consensus that the issue should be directed toward nonspecialist electronic people and that it should be balanced to include papers on both the electronic techniques and astronomy, of the type which will give the best over-all picture of the field, despite the fact that this would necessarily exclude much of the type of new detailed material which would be of most interest to individuals working in radio astronomy.

R. L. MATTINGLY
Secretary-Treasurer

OTHER ADMINISTRATIVE NEWS

Delmer Ports reports that initial response to the advertising sales campaign is favorable. To date, as a result of Committee activity, five tentative commitments have been received for the July issue. Note: The deadline for copy for this issue is June 1. All PGAP members are urged to help in this activity. Prospective advertisers should be referred to:

Delmer C. Ports
c/o Jansky & Bailey
1339 Wisconsin Avenue, N.W.
Washington 7, D. C.

The Radio Astronomy Issue of the PROCEEDINGS is now definitely scheduled for December of this year.

S. M. King is the PGAP representative on the National Convention Record Committee.

FUTURE MEETINGS AND SEMINARS

The 1957 WESCON will be held in San Francisco's Cow Palace on August 20, 21, 22, and 23. Four sessions of the technical program are expected to be devoted to antennas and propagation. Your assistance in making these PGAP-sponsored sessions of the highest possible caliber will be greatly appreciated.

Please submit 200-word abstracts of proposed papers before May 1 to: Dr. J. T. Bolljahn, Stanford Research Institute, Engineering Division, Menlo Park, Calif. (Antenna Papers), or Dr. L. A. Manning, Stanford Electronics Laboratory, Stanford University, Stanford, Calif. (Propagation Papers).

A two-week summer statistical seminar will be held at the Endicott House in Dedham, Mass., beginning July 29, 1957. It is understood that the content of this course will make it of interest to propagation people. Further information can be obtained from Dr. M. E. Terry, Bell Telephone Laboratories, Murray Hill, N. J., or the secretary, Dr. Geoffrey Beall, Gillette Safety Razor Company, Boston, Mass.

Ohio State University has again been invited to conduct a classified Radome Symposium for the benefit of the Armed Forces. The meetings are scheduled for June 3 through June 5 in the Ohio Union at Ohio State University.

CHAPTER NEWS

Akron

We are pleased to announce that the formation of the Akron Chapter was approved by IRE, effective February 6, 1957, We have not received word at this time of the officers appointed.

Syracuse

We are also pleased to announce the formation of the Syracuse Chapter, which was approved effective February 6, 1957. We have not been advised to date of the officers appointed.

Washington

A meeting of the Washington Chapter was held February 14, in Tompkins Hall, the new building for the School of Engineering at George Washington University. John E. Jackson, of the Naval Research Laboratory, presented a paper on the latest results of Rocket Studies of Ionospheric Propagation in the 4 to 50-megacycle range.

Personnel Notes

Robert Elliott, formerly head of antenna research at Hughes' Aircraft, has joined with Robert Krausz, formerly head of engineering research at SRI, Southern California Laboratories, to form the RANTEC Corp. in Calabassas, Calif. Other members of the new company are Alvin Clavin, formerly with Canoga Corp., Lou Kurtz, formerly with Hughes, and Bill Harrison, formerly with SRI.

Recently-formed Systems Laboratories Corp., Sherman Oaks, Calif., a group of some 36 scientists and engineers under President John Barnes has announced the election to Vice-President of James Marsh, formerly head of the Autonetics Radar Group. Also at SLC in the antenna and radar field is Don Margerum, formerly with SRI.

George Underberger, formerly with Bendix-Pacific, has joined Kearfott's microwave group in Van Nuys, Calif., which is headed by W. A. Hughes, formerly with Hughes Aircraft.

Bob Blaine has formed Blaine Electronics, 14757 Keswick, Van Nuys, Calif., a company devoted to fabrication of models and electronic equipment for antenna measurements.

L. Cutrona is on a leave of absence from the University of Michigan while heading an antenna group at Ramo-Wooldridge Corp.

contributions

Some Electromagnetic Transmission and Reflection Properties of a Strip Grating*

ROBIN I. PRIMICH†

Summary—**Some theoretical and experimental results for the reflection and transmission of a uniform plane electromagnetic wave, normally incident on an ideal strip grating, are presented. The theory is based on the variational method, and the measurements were made at normal incidence in a parallel plate region operating in the 8- to 10-cms wavelength range. A few results for oblique incidence are also included; the experiments in this case were carried out at 1.24-cm wavelength in a parallel plate spectrometer. Resasonable agreement between theory and experiment was obtained throughout.**

Introduction

A STRIP GRATING of the form shown in Fig. 1 is considered in this paper. The strips are assumed to consist of perfectly conducting, infinitely thin metal and are of uniform width, t, and infinite in extent. Each grating contains an infinite number of equally spaced, identical strips. The problem is of interest for the following reasons.

1) A number of such gratings in sequence will form an artificial medium of refractive index less than unity. However, it has no advantages over the rodded medium[1] and it would be inferior mechanically. Theoretically, this medium illustrates very clearly one of the factors which gives rise to the interface phenomena in artificial dielectrics.[6]

Consider Fig. 2 in which b and t are constant and λ_0. (λ_0 = free space wavelength.)

Suppose that, initially, d is sufficiently large for no appreciable coupling to exist between adjacent gratings.

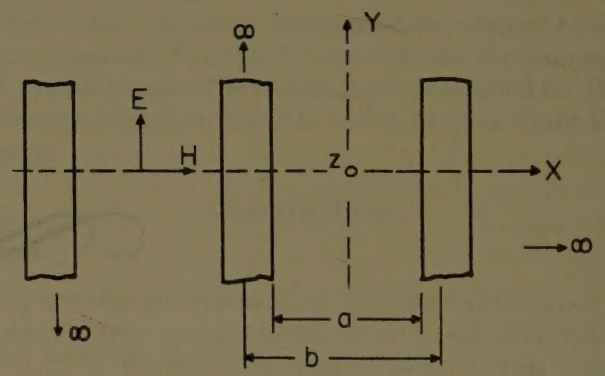

Fig. 1.

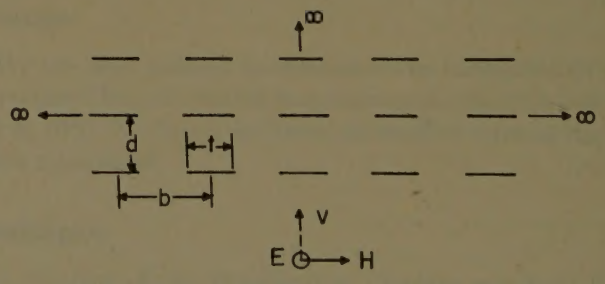

Fig. 2.

Then each grating may be replaced by an equivalent shunt reactance[2] and the behavior of the medium may be determined to a high degree of accuracy by using the

* Manuscript received by the PGAP, September 1, 1956.
† Radio Physics Lab., Defence Res. Board, Ottawa, Canada.
[1] J. Brown, "Artificial dielectrics having refractive indices less than unity," *Proc. IEE*, vol. 100, part 4, pp. 51–62; 1953.

[2] G. G. Macfarlance, "Quasi-stationary field theory and its application to diaphragms and junctions on transmission lines and wave guide," *Proc. IEE*, vol. 93, part 3a, pp. 703–719; 1946.

transmission line analogy.[3] However, for d of the order of $\lambda_0/10$ or less, coupling between gratings can no longer be ignored and the analogy breaks down. The limiting case, $d=0$ (or $d \ll b$) is that of a system of parallel metallic plates of finite thickness, which possess the interface effect to a marked degree; *i.e.*, in particular the reflection coefficient at the interface ($z=0$) of the medium no longer bears a simple relationship to the refractive index of the medium. It is evident that interface effects will be present in all similar medium in which $d \ll \lambda_0 < b$.

2) A single grating can be used for the determination of wavelength and will act also as a polarization filter. A study of the higher-order waves diffracted by the grating serves as an accurate measure of the exciting wavelength. This is a standard optical procedure, but is now of interest in this millimeter wave region.[4] An interesting application is one in which a grating is used to separate out a particular magnetron harmonic.[5]

By restricting the spacing between adjacent strips, the grating is made opaque to waves whose polarization is parallel to the strips. This enables a linearly-polarized wave from an arbitrarily-polarized source to be produced.

3) A strip grating has similar properties to the interface of a semi-infinite system of metallic plates of finite thickness.[6] This is of interest in microwave lens applications so that the possibility of a similar behavior in regard to the surface reflecting properties arises. In fact, an empirical relation involving the grating reactance has been used to determine the effect of plate thickness in a metal plate system.[7] If a rigorous basis for this analogy could be found it would be extremely useful, but a brief consideration of this matter, given at a later stage, indicates that if this analogy does exist, it would be in a form too complicated to be of value for parallel plate lens design.

Basic to the above applications is the requirements that the properties of a single grating be known. Therefore the following sections will review grating theory as applicable to metal strips and it will include the application of the variational method which was used to calculate the reflection coefficient of an ideal strip grating. Experimental results will be included.

Theory of Strip Gratings

Review

In the field of optics, attention has been mostly confined to the angular distribution of waves arising from the grating. These are determined by the periodicity of the grating. The detailed calculation of the scattered fields has been virtually ignored, mainly because of the role of the reactive fields in the vicinity of the grating has not been fully understood (see Wood's anomalies[8]). Palmer has been reexamining these so-called anomalies recently.[9]

In the microwave field, the complex nature of the reflection caused by an arbitrary obstacle is of major interest and it is necessary to solve the complete field problem.

The first attempt to deal with the strip grating was made by Macfarlane.[2] It should be noted at this point that by the use of Babinet's principle[10] the solution of the problem indicated in Fig. 1, for any angle of incidence, is also the solution of the complementary grating in which the metal and aperture regions are interchanged and the polarization is rotated through 90°. Macfarlane, among others, pointed this out and proceeded to solve, using the approximate quasistatic method, the E-plane (or capacitive iris in a waveguide) and H-plane gratings in free space. In a separate paper[11] dealing with a grid of circular wires, he gave the conditions for the existence of higher-order propagating waves.

The "Waveguide Handbook,"[12] using an approximate treatment based on an integral method, gives numerical results for $b<\lambda_0$ (see Fig. 1). In both of the above works the range $b \geq \lambda_0$ is excluded.

Booker[10] has given a more general qualitative discussion.

Miles[13] appears to have been the first to consider all values of b/λ_0, but only for normal incidence. This is an extension of his earlier work.[14] He obtains the reflection and transmission coefficients for the strip grating from a rapidly converging expansion of the integral equation. The resonance in either coefficient at the point $b=\lambda_0$, is specifically mentioned by him for the first time, but surprisingly no recognition is given to the fact that higher-order propagating waves are present and, in particular, that the resonance is due to one of the evanescent waves starting to propagate freely. This does not effect the validity of the results for the main propagating waves, but as he uses the variational method to check the accuracy of the results, it is dubious whether the limiting procedure described has much significance

[3] J. Brown, "The design of metallic delay dielectrics," *Proc. IEE*, vol. 97, part 3a, pp. 45–48; January, 1950.

[4] J. L. Farrands, "The Dielectric Properties of Some Ketones at Cm and Mm Wavelengths," PhD. dissertation, University of London, England; 1953.

[5] J. A. Klein, *et al.*, "Magnetron harmonics at mm wavelengths," *Rev. Sci. Instr.*, vol. 23, pp. 78–82; February, 1952.

[6] R. I. Primich, "A Study of the Properties of Artificial Dielectrics," Ph.D. dissertation, University of London, England; 1954.

[7] D. J. Epstein, "Phase Shift of Microwaves in Passage through Parallel Plate Arrays," M.I.T., Lab. for Insulation Res., Tech. Rep. no. 42; August, 1950.

[8] R. W. Wood, "Physical Optics," The Macmillan Co., New York, N. Y.; 1911.

[9] C. H. Palmer, "Parallel diffraction grating anomalies," *J. Opt. Soc. Amer.*, vol. 42, pp. 269–276; April, 1952.

[10] H. G. Booker, "The elements of wave propagation using the impedance concept." *J. IEE*, vol. 94, part 3, pp. 171–202; 1947.

[11] G. G. Macfarlance, "Surface impedance of an infinite parallel wire grid at oblique angles of incidence," *Proc. IEE*, vol. 93, part 3a, pp. 1523–1527; 1946.

[12] N. Marcuvitz, "Waveguide Handbook," McGraw-Hill Book Co., Inc., New York, N. Y.; 1951.

[13] J. W. Miles, "The diffraction of a plane wave through a grating," *Quart. Appl. Math.*, vol. 7, pp. 45–64; January, 1949.

[14] J. W. Miles, "The analysis of plane discontinuities in cylindrical tubes," *J. Acoust. Soc. Amer.*, vol. 17, pp. 250–285; 1945.

in the presence of higher-order propagation.

A. E. Heins (in a personal communication) has used the Weiner-Hopf technique[15] to obtain a rigorous solution for the special case of the half-open grating and the significance of the higher-order waves is fully realized.

Recent work by Muller[16] seems to have the greatest generality combined with actual numerical computations. In treating an arbitrary strip grating for any angle of incidence, the usual Fourier expansion for the fields is transformed to a pair of Fredholm integral equations of the first order, *i.e.*,

$$A = \int_{-\beta\pi}^{+\beta\pi} P(x-x')\bar{u}(x')dx' \qquad \beta = \frac{a}{b} \qquad \alpha = \frac{b-a}{b}$$

$$B = \int_{-\alpha\pi}^{+\alpha\pi} P(x-x')v(x')dx' \qquad \gamma_m = \text{propagation constant of mth order wave.}$$

$$P(x-x') = \frac{1}{2\pi}\sum_{m=-\infty}^{\infty}\frac{1}{j\gamma_m}\exp\left(jm\overline{x-x'}\right).$$

$\bar{u}(x')$ is related simply to the transverse electric field in the aperture for the E-plane case, $v(x)$ is related to the strip current in the H-plane case, and A and B are simply related to the corresponding field amplitudes. By a simple shift of the coordinate system two further equations are obtained:

$$A = -j/\gamma_0 + \frac{1}{2\pi}\int_{-\alpha\pi}^{+\alpha\pi} x\cdot u'(x)dx \qquad E\text{-plane case.}$$

$$B = -j/\gamma_0 + \frac{1}{2\pi}\int_{-\beta\pi}^{+\beta\pi} x\cdot v'(x)dx \qquad H\text{-plane case.}$$

$u'(x)$ is now associated with the strip current and $v'(x)$ with the aperture electric field. An approximate solution (which was promised for a future publication) is valid for $(b/\lambda_0)\leq 4$; when $[(b-a)/b]<\frac{1}{2}$ the first pair of equations are used, while for $(a/b)<\frac{1}{2}$ the second pair are used. It was demonstrated that the integral equations are encountered in the study of capacitive and inductive irises in rectangular waveguides[16] and that the numerical solutions are equally applicable. Muller has then given a general practical solution although the question of higher-order wave propagation is not specifically discussed.

Twersky[17] has obtained a general rigorous solution for an arbitrary grating, but numerical computation has proved to be too difficult except in some special cases.

The Variational Method

Miles used the variational method to check the accuracy of his results, but apart from the general formulation no details are given. The alternative development to be given here is believed to be more convenient for computation and moreover leads to summations which are identical to those encountered in a previous problem.[6]

An ideal strip grating will be considered. This consists of an infinite number of similar, infinitely thin, perfectly conducting, metallic strips each infinitely long. The strips are equally spaced and have the same width. A uniform plane wave, incident normally to the plane of the grating is assumed. (See Fig. 1.)

Because of the periodicity of the grating plane, it follows that the free space fields may be written[6,18] for $z=0$:

$$E_y = \exp(-j\beta_0 z) + A_0\exp(j\beta_0 z) + \sum_{m=1}^{\infty} A_m\cos\frac{2m\pi x}{b}\exp(j\alpha_m z).$$

$$\frac{\partial E_y}{\partial z} = -j\beta_0\exp(-j\beta_0 z) + j\beta_0 A_0\exp(j\beta_0 z) + j\sum_{m=1}^{\infty}\alpha_m A_m\cos\frac{2m\pi x}{b}\exp(j\alpha_m z).$$

$z=0$:

$$E_y = C_0\exp(-j\beta_0 z) + \sum_{m=1}^{\infty} C_m\cos\frac{2m\pi x}{b}\exp(-j\alpha_m z).$$

$$\frac{\partial E}{\partial z} = -j\beta_0 B_0\exp(-j\beta_0 z) - j\sum_{m=1}^{\infty}\alpha_m C_m\cos\frac{2m\pi x}{b}\exp(-j\alpha_m z).$$

where α_m is the propagation constant of the mth order wave in free space, $\alpha_0=\beta_0$ and A_m and C_m are the amplitudes of the mth order waves on either side of the grating. The time variation $\exp(j\omega t)$ is assumed throughout.

Using the boundary conditions in the grating plane $(z=0)$,

$$\left.\begin{aligned} E_{y_0} &= 1 + A_0 + \sum_{m=1}^{\infty} A_m\cos\frac{2m\pi x}{b} \\ &= C_0 + \sum_{m=1}^{\infty} C_m\cos\frac{2m\pi x}{b} \\ &= 0 \qquad |x| \leq (b-a), \end{aligned}\right\} \quad |x| \leq a.$$

so

$$1 + A_0 = C_0 = \frac{1}{b}\int_{ap} E_{y_0}dx;$$

$$A_m = C_m = \frac{2}{b}\int_{ap} E_{y_0}\cos\frac{2m\pi x}{b}dx.$$

[15] J. F. Carlson and A. E. Heins, "The reflections of an electromagnetic plane wave by an infinite set of plates," *Quart. Appl. Math.*, vol. 4, pp. 313–329; January, 1947.

[16] R. Muller, "Eine strenge behandlung der beugung elecktromagnetischer wellen am streifengitter," *Zeits. Naturforschung*, band 8a, pp. 56–60; January, 1953.

[17] V. Twersky, "Multiple scattering of radiation by an arbitrary configuration of parallel cylinders," *J. Acoust. Soc. Amer.*, vol. 24, pp. 42–46; January, 1952.

[18] F. Berz, "Reflection and refraction of microwaves at a set of parallel metallic plates," *Proc. IEE*, vol. 98, part 3, pp. 47–55; January, 1951.

Equating the magnetic fields in the aperture regions,

$$-j\beta_0(1-A_0)+j\sum_{m=1}^{\infty}\alpha_m A_m\cos\frac{2m\pi x}{b}$$

$$=j\beta_0 C_0-j\sum_{m=1}^{\infty}\alpha_m C_m\cos\frac{2m\pi x}{b}$$

or

$$\beta_0(1-A_0)=\beta_0(1+A_0)$$

$$+\frac{4}{b}\sum_{m=1}^{\infty}\alpha_m\cos\frac{2m\pi x}{b}\int_{ap}E_{y_0}\cos\frac{2m\pi x}{b}\,dx.$$

Multiplying by E_{y_0}, integrating over period "a" and using

$$1+A_0=\frac{1}{b}\int_{ap}E_{y_0}dx.$$

$$\beta_0\cdot\frac{1-A_0}{1+A_0}=\beta_0+4\sum_{m=1}^{\infty}\alpha_m\left\{\frac{\int_{ap}E_{y_0}\cos\frac{2m\pi x}{b}\,dx}{\int_{ap}E_{y_0}\cdot dx}\right\}^2. \quad (1)$$

A similar expression can be obtained in terms of the magnetic field in the grating plane, but for present purposes the above will be sufficient. For computational purposes it is convenient to consider two regions of interest, depending on the value of b/λ_0.

1) $(b/\lambda_0)<1$.

If $\alpha_m/\beta_0=-jQ_m$, Q_m will be real and positive.

Then, if Y_{in} is the input admittance at the grating plane,

$$Y_{in}=1-jB_g=\frac{1-A}{1+A}$$

and

$$B_g=4\sum_{m=1}^{\infty}Q_m\left\{\frac{\int_{ap}E_{y_0}\cdot\cos\frac{2m\pi x}{b}\,dx}{\int_{ap}E_{y_0}dx}\right\}^2. \quad (2)$$

where B_g is the susceptance of the grating.

This expression for B_g can be shown to be stationary and consequently any error in an assumed trial field E_{y_0} will result in only second-order errors in B_g. Furthermore B_g has an absolute minimum (for the correct E_{y_0}) and any error in the assumed E_{y_0} will result in a B_g that is always too large.

From an expression for the aperture magnetic field (which is derived in a manner similar to that above), a value of B_g which is too small can be found and consequently it is possible to limit the error in B_g.

The susceptance of the grating is then known within definite limits.

2) $(b/\lambda_0)>1$.

For any given b/λ_0 a certain number p of the α_m will now be real. Using a trial field of the form (which satisfies the boundary conditions)

$$E_{y_0}=\sum_{n=1}^{\infty}D_n\cos\frac{n\pi x}{a}\qquad |x|\le a$$

in

$$Y_{in}=\frac{1-A_0}{1+A_0}=1+4\sum_{m=1}^{\infty}\frac{\alpha_m}{\beta_0}\left\{\frac{\int_{ap}E_{y_0}\cos\frac{2m\pi x}{b}\,dx}{\int_{ap}E_{y_0}\cdot dx}\right\}^2$$

$$=1+4\sum_{m=1}^{p}\frac{\alpha_m}{\beta_0}\left\{\frac{\int_{ap}E_{y_0}\cos\frac{2m\pi x}{b}\,dx}{\int_{ap}E_{y_0}\cdot dx}\right\}^2$$

$$-j4\sum_{m=p+1}^{\infty}\alpha_m\left\{\frac{\int_{ap}E_{y_0}\cos\frac{2m\pi x}{b}\,dx}{\int_{ap}E_{y_0}\cdot dx}\right\}^2$$

will result in complex D_n's. This means that the grating can no longer be represented by a pure shunt susceptance but has, in addition, a resistive component of impedance. The expression for Y_n is still stationary[6] and the convergence of Y_{in} towards the real value can now be studied best by the methods discussed elsewhere,[6] *i.e.*, convergence towards a single point in the complex plane.

Computations

The assumed trial field used for numerical work is

$$E_{y_0}=\cos\frac{\pi x}{a}+D_3\cos\frac{3\pi x}{a}+D_5\cos\frac{5\pi x}{a}+D_7\cos\frac{7\pi x}{a}$$

$$|x|\le a.$$

Insertion of this in (1) and use of the stationary condition

$$\frac{\partial Y_{in}}{\partial D_n}=0\qquad n=1,3,5,\text{ and }7$$

results in explicit expressions for the grating admittance.

1) $(b/\lambda_0)<1$.

The "Waveguide Handbook" predicts that at the point $b=\lambda_0$, the magnitude of the wave reflected by the grating is zero whereas the variational method showed that the reflection coefficient at this point depended on a ratio a/b. Consequently, the formulas from the former source should not be used in the vicinity $b=\lambda_0$. Experimental results to be given later will give some idea of the range of validity of the "Waveguide Handbook" results.

The variational expressions were used to compute the magnitude of the reflection coefficient for two gratings,

for $(b/\lambda_0) \leq 1$. Experimental work, to be described later, shows that the results are very satisfactory.

2) $(b/\lambda_0) > 1$.

In principle the variational method is still applicable for this region but the computations are laborious. When this study was undertaken originally there was no time available to extend the computations into this range.

Experimental Work

A number of strip gratings were measured in the strip transmission line, which is essentially a parallel plate region of finite width. The instrument and the method of measurement have been fully described elsewhere,[19,20] so that for the present it is sufficient to say that it may be regarded as a large waveguide of about ten wavelengths in width in which the field conditions approximate to those in free space.

The gratings were constructed by cutting out the apertures from a single sheet of 0.001-inch tin foil and supporting this between two blocks of polyfoam held together at their ends by adhesive tape (see Fig. 3).

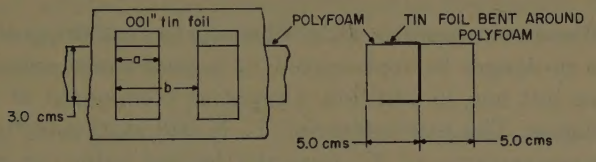

Fig. 3.

By wedging this structure tightly between the plates of the line, the contact with the line conductors was found to be very good, as judged by the consistency and reproducibility of the results.

The measurements were made with a short-circuit termination to the line and then obtaining the usual Weisfloch curve[21] by moving the grating relative to the short circuit and noting the corresponding movement of the minimum in the interference pattern. The complex reflection coefficient follows at once.[20]

Figs. 4 and 5 show the magnitude and phase of the reflection coefficient of some typical gratings. The theoretical curves in these figures were obtained from the "Waveguide Handbook," with allowances for the polyfoam support. The phase is referred to the grating plane. It is worth noting that the two curves which include the points $b=\lambda_0$ reveal the inadequacy of the theory used.

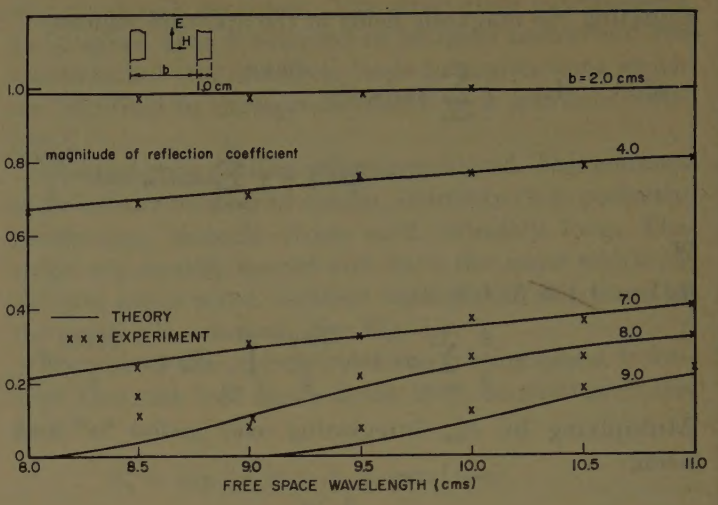

Fig. 4.

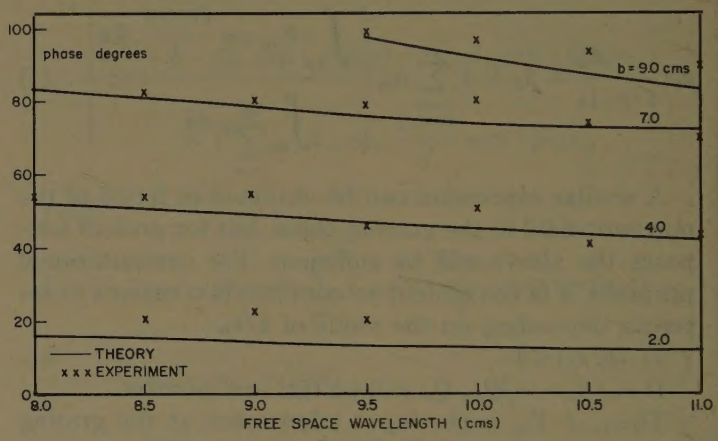

Fig. 5.

Figs. 6 and 7 show the magnitude of the reflection coefficient for two gratings, but the variational method has now been used. The "Waveguide Handbook" results would give zero reflection coefficient at the resonance points $b=\lambda_0$, and it is concluded that the variational method is quite adequate for the region $b=\lambda_0$. No results are shown for $b>\lambda_0$ as the strip transmission line is restricted to normal incidence only, due to the adverse interference of higher-order propagating waves. Fig. 8 shows typical Weissfloch curves[21] in the presence and absence of these higher-order waves. It is evident that the second curve is of little use.

Arbitrary Incidence

At the author's request, some preliminary measurements were made on several gratings by Sollom, who used a parallel plate spectrometer. This is essentially a parallel plate region in which provision is made to rotate the two horns about a fixed center.[22] Figs. 9 and 10 show two typical angular spectra. The theoretical curves were

[19] M. M. Z. El-Kharadly, "Some experiments of artificial dielectrics at centimetre wavelengths," *Proc. IEE*, vol. 102, part B, pp. 17–25; January, 1955.

[20] R. I. Primich, "A general experimental method to determine the properties of artificial media at centimetre wavelengths applied to an array of parallel metallic plates," *Proc. IEE*, vol. 102, part B, pp. 26–36; January, 1955.

[21] A. Weissfloch, "Ein transformationssatz über verlustlose vierpole und seine anwendung auf der experimentelle untersuchung von dezimemter- und zentimeterwellenschaltungen," *Hochfrequenz. U. Elektroak.*, band 60, pp. 67–73; September, 1942.

[22] P. H. Sollom, "An Accurate Parallel-Plate Spectrometer," Ph.D. dissertation, University of London, England; 1954.

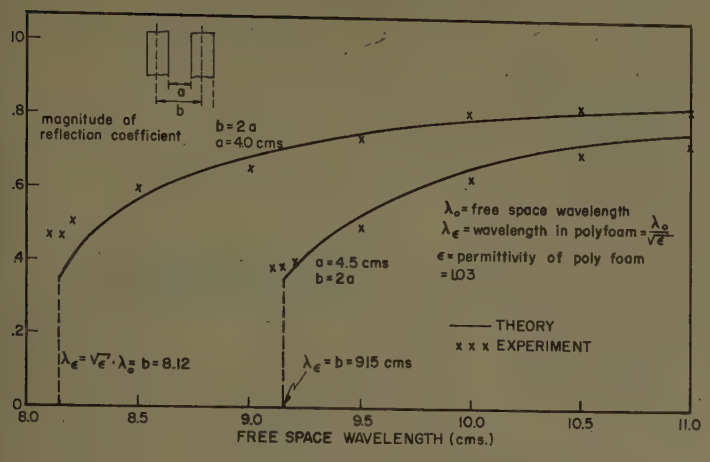

Fig. 6.

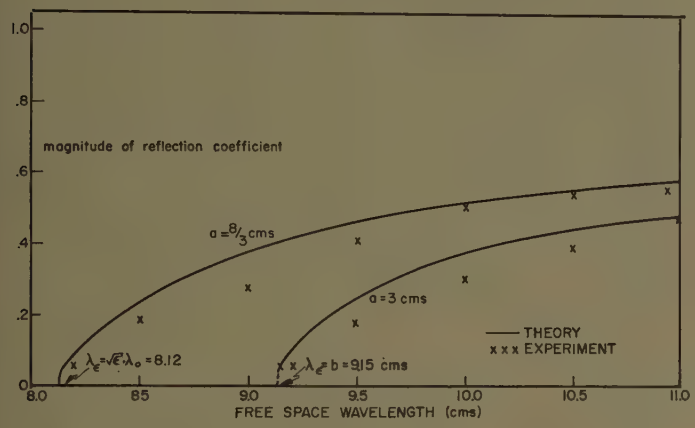

Fig. 7.

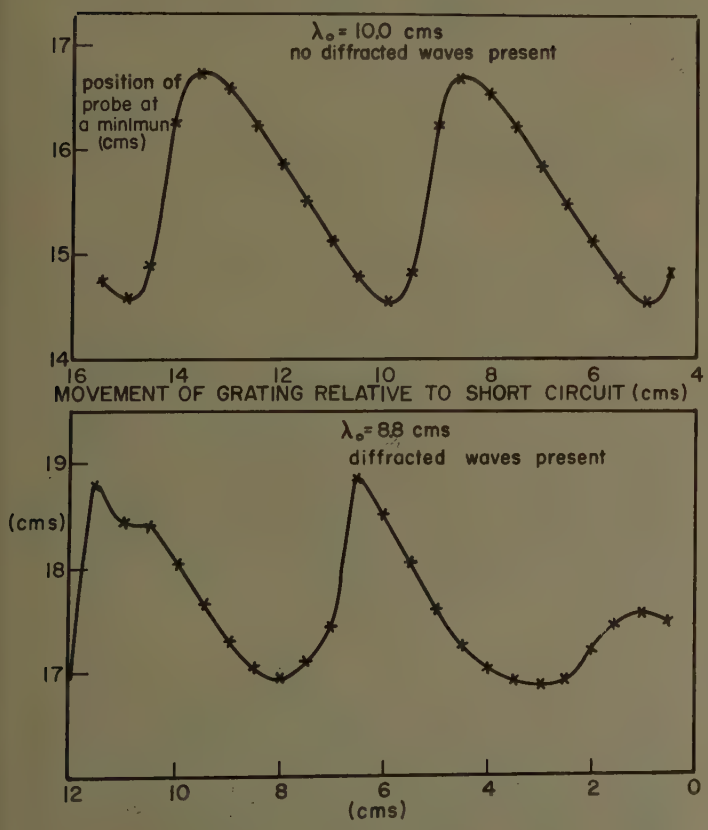

Fig. 8.

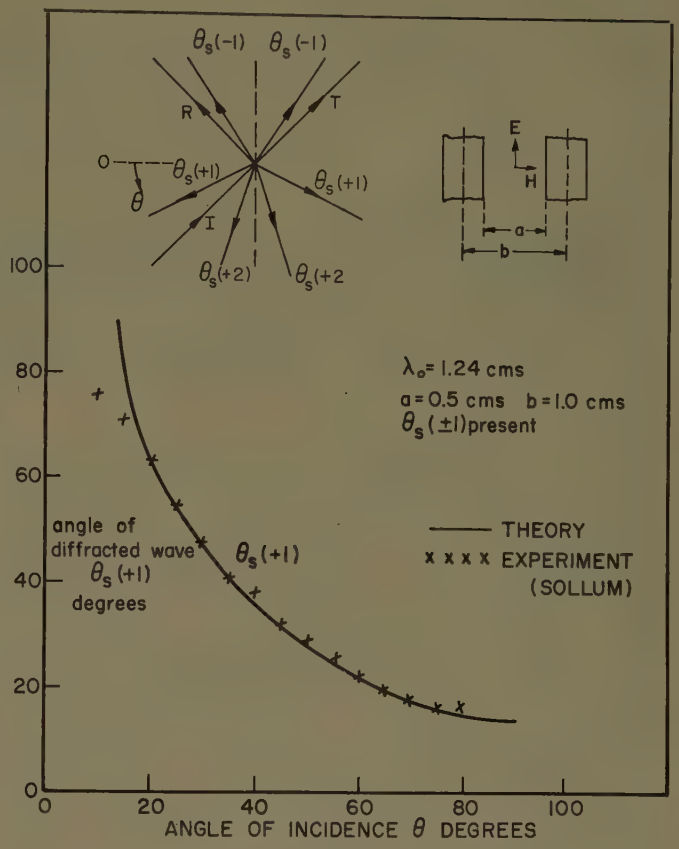

Fig. 9.

computed from the classical grating formula[8]

$$\sin\theta_s = \frac{m\lambda_0}{b} - \sin\theta_i$$

θ_i = angle of incidence

θ_s = angle of emergence of higher-order wave.

Fig. 11 shows a typical power spectrum for which the computation still has to be done. The peak in transmitted power at an angle of incidence off normal is of considerable interest as this shows the beginnings of a phenomena well known for optical gratings, *i.e.*, the series of transmission peaks at various angles of incidence.[23,24]

Comparison Between a Strip Grating and a Semi-Infinite System of Thick Plates

It has been conjectured[7] that the results for a strip grating could be used to compute the reflection proper-

[23] W. C. Meecham, "A Variational Method for the Calculation of the Distribution of Energy Reflected from a Periodic Surface," Eng. Res. Inst., Univ. of Michigan, Ann Arbor, Mich.; November, 1955.

[24] Since the writing of this paper, some work which has a direct bearing on this phenomena has come to the author's attention. Meecham, *ibid.*, has used a variational method to compute the reflection from a blazed grating. A specific anomaly of Wood (*loc. cit.*) is treated and it is clearly evident that a peak in the main reflected wave is associated with the first-order diffracted wave changing to an evanescent condition. Fig. 11 is an excellent experimental illustration of this situation.

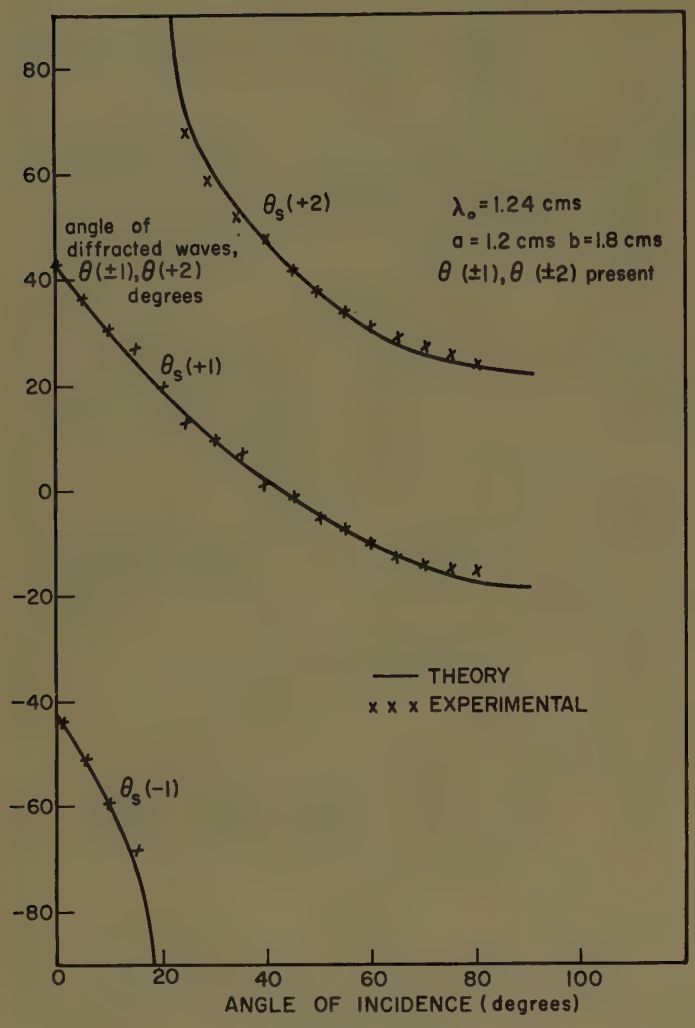

Fig. 10.

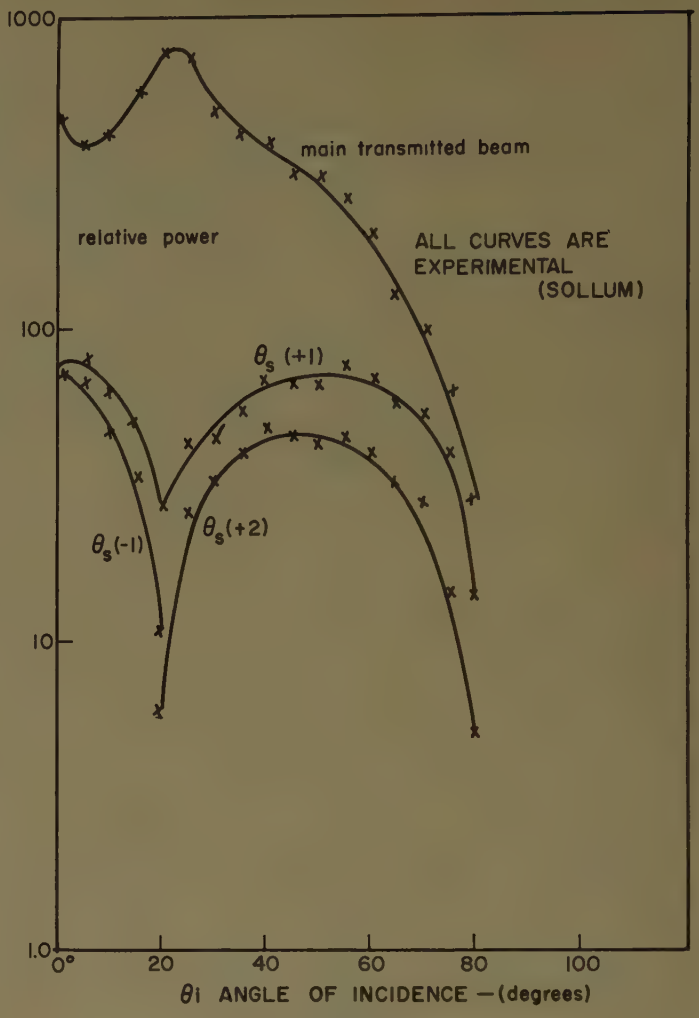

Fig. 11.

ties of a system of thick plates,[6] owing to the identical cross sections. This has been examined in a very general way[6] and no simple relation appears to exist. For instance for $b<\lambda_0$. the admittance of a thick plate system can be written

$$Y_{in} = jB_g + F$$

where B_g is the grating susceptance and F is a complicated function which bears no simple relation to the input admittance of a system of infinitely thin plates. Although the formal separation of the grating susceptance has been achieved, it is quite pointless as the function F requires as much, if not more calculation than the original Y_{in}.

The general conclusion is that the grating results cannot be used to advantage in obtaining numerical results for a system of thick plates. However, owing to the similarity in the free space field structure of the grating and a system of thick plates, the definite possibility does emerge of using a grating to match a parallel plate lens, especially in the wavelength region where the first diffracted wave is present. This would permit such a lens to be operated over a wider range of angle of incidence with less interference from high-order waves, but this will not be pursued any further here.

Conclusion

The variational method has been found to be very useful to obtain the properties of a strip grating. Its accuracy has been verified experimentally for all values of the parameter $(b/\lambda_0)\leq 1$. There is still a definite need for results for arbitrary incidence and in principle the variational method is still applicable. In fact, expressions have been obtained for the grating admittance for any angle incidence and it is hoped that these will be presented later. It would be instructive to compare these with Muller's numerical computations, which, as far as the author is aware, are not yet available.

Acknowledgment

This work was carried out at Imperial College, in partial fulfillment of the requirements for the Ph. D. degree at the University of London, England. The author wishes to acknowledge the assistance of Prof. Willis Jackson and Dr. J. Brown, both formerly of the above college. Thanks are due to Dr. P. H. Sollom who did the measurements for arbitrary incidence.

The Dependence of Microwave Radio Signal Spectra on Ocean Roughness and Wave Spectra*

C. I. BEARD† AND I. KATZ‡

Summary—**This paper is an extension of previous work on reflection of microwaves from an ocean surface. The present analysis, dealing with spectra, is based on data obtained in a one-way *X*-band propagation experiment performed across the Golden Gate, San Francisco. Two paths of 9000 and 15,000 feet were used. To describe the ocean surface, wave gages were mounted on a piling driven into the Golden Gate channel.**

Radio-signal spectra are found to be broader than the ocean-wave spectra and the spectral breadth a function of ocean roughness. The important result of this analysis is the establishment of a linear relationship between ocean roughness and the spectral breadth of the radio signals. Ocean roughness is measured by the product of the standard deviation of the wave height and the grazing angle divided by the radio-wave length. Radio spectral breadths are determined by the frequencies at which each spectrum drops to the 0.9-, 0.8-, 0.7-, 0.5-, 0.25-, and 0.1-power points. The breadths are then expressed as ratios of these frequencies to the frequency of the peak in the simultaneous ocean-wave spectrum.

The analysis now enables one to predict the approximate shape of the spectrum of the radio signal received in a one-way transmission path given only a knowledge of the geometry, radio-wave length, ocean-wave height, and the peak frequency in the ocean spectrum.

Introduction

THIS PAPER is concerned with the propagation of short-wave electromagnetic energy in over-water line-of-sight paths. In general, the aim is to obtain knowledge of the mean value of the signal strength, the amplitude of the fluctuations about the mean and spectra of the fluctuations. A certain measure of progress has been made in a previous paper[1] to predict the mean signal level and the amplitude of its fluctuations from a knowledge of ocean-wave height and geometry. The present paper reports on subsequent analysis along similar lines, but stressing primarily the relationship between ocean-wave spectra and spectra of received radio signals. It will be assumed in this paper that atmospheric inhomogeneities are of minor importance in the spectra since the measurements were made over relatively short paths.

Since the interpretation of the spectra is based on the vector model representation[1] of the process of microwave reflection from the ocean surface, a brief summary of the model is given first. The subsequent section then describes the experimental conditions. A section on the general features of the spectra serves as an introduction for the section on the details of the quantitative relations which were found experimentally. A qualitative vector model interpretation is followed by comparison of results of an approximate theoretical calculation.

The Vector Model

In the formulation of the vector model it is assumed that the radio signal may be represented as the vector sum of a direct signal and a water-reflected signal, each with certain properties. The direct ray, D, is assumed constant in magnitude and phase, whereas the reflected signal is composed of a coherent part, C, whose amplitude and phase are fixed by geometry and surface roughness, and an incoherent part, I, of random amplitude and phase. Except under special conditions, which will be mentioned later, I may be assumed to be the resultant of vectors from a large number of independent random scatterers. The incoherent part, I, may be decomposed into two orthogonal independent vectors each representing a Gaussian process with zero mean. It is convenient to orient these two orthogonal vectors along and normal to C; in addition, their standard deviations and spectra are assumed to be equal. Both C and I are related to geometry and sea conditions by use of the roughness parameter $h\psi/\lambda$, where h is the standard deviation of the water surface, ψ is the grazing angle, and λ the wavelength of the electromagnetic radiation. The quantitative dependence of both C and I on $h\psi/\lambda$ has been presented.[1]

The Golden Gate Experiment

During April, 1953, a propagation experiment was performed by the Applied Physics Laboratory, in conjunction with the Electrical Engineering Research Laboratory of The University of Texas, across the Golden Gate at San Francisco. In the experiment two paths were used as shown in Fig. 1. At one end of the path marked "slope," a transmitter was placed at various heights from 92 feet to 900 feet on the slope of a 900-foot mountain adjacent to the Golden Gate (the twelve sites lie along the line denoted by the numbers 1, 11, and 12 on the map). The signal was received at a point about 85 feet above water on the other side, a transmission distance averaging about 9000 feet. On the other path to Bonita Cove, 15,000 feet long, transmitter heights of 75 feet to 360 feet (denoted by A, B, C, and D on the map) were available. This second path was chosen to obtain a greater variety of conditions, *i.e.*, a different angle to the ocean swells and a different path length. The Golden Gate has an unblocked westerly exposure

* Manuscript received by the PGAP, July 9, 1956; revised manuscript received, October 26, 1956.

† Sylvania Electronic Defense Lab., Mountain View, Calif. Formerly at Appl. Phys. Lab., Johns Hopkins Univ., Silver Spring, Md.

‡ Appl. Phys. Lab., Johns Hopkins Univ., Silver Spring, Md.

[1] C. I. Beard, I. Katz, and L. M. Spetner, "Phenomenological vector model of microwave reflection from the ocean," IRE TRANS. vol. AP-4, pp. 162–167; April, 1956.

to the open ocean and the prevailing swell and wind directions are northwesterly. For the slope path the predominant wave directions varied from southwesterly to westerly.

The transmitting antenna pattern was chosen to minimize illumination of the mountainside and yet to illuminate the water adequately. It was a 12-inch diameter paraboloid, at X band, with an 8° beamwidth at half-power points and side lobes down 24 db. The transmitting antenna was set on tripods at each site and was pointed optically at the receiver. Under these conditions more than 20 Fresnel zones were illuminated within the half-power points.

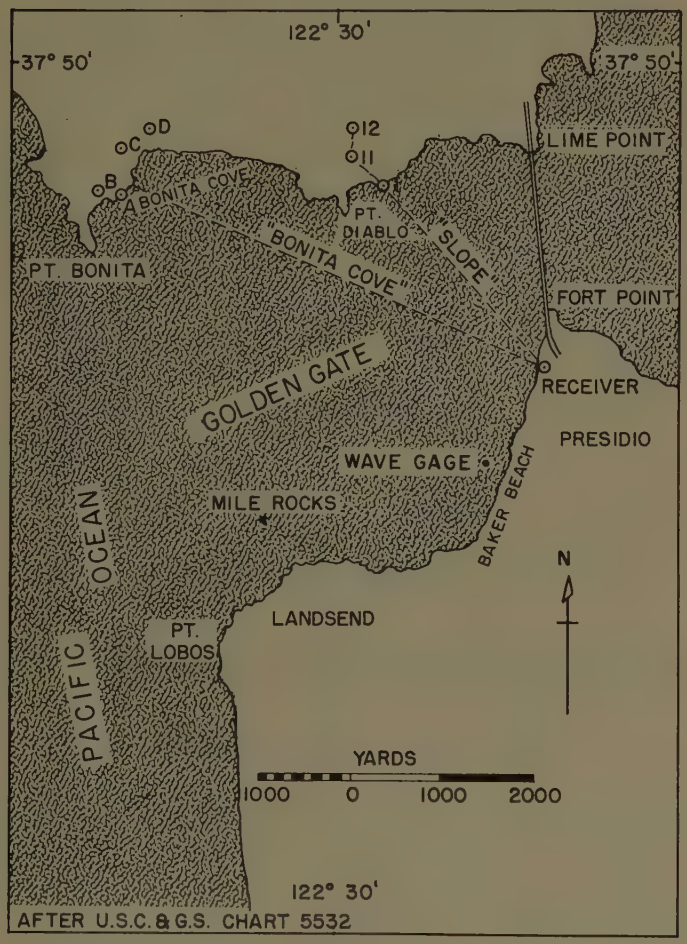

Fig. 1—Map of Golden Gate experiment area.

The receiving antenna was an 18-inch diameter paraboloid with a 5.5° beamwidth between half-power points and side lobes down 30 db; it was placed on an 85-foot high ledge where the ground dropped sharply away in front and to the sides of the antenna. To vary the illumination, this antenna was pointed at angles from zero to 5° above the horizontal. Both vertical and horizontal polarization were used in the experiment but only the vertical polarization spectra are analyzed in this paper.

Ocean-wave heights were measured by three types of gages mounted on a piling driven into the channel in about 35 feet of water off the northern end of Baker Beach.[2] Water-surface fluctuations between 0.3- and 1.1-feet rms were experienced during the course of the experiment.

Of interest in this paper is the method of data reduction and analysis. Ocean-wave heights were recorded on magnetic tape. The radio signals were recorded on Brush strip-chart recorder, then curve followed later in the laboratory to put the information on magnetic tape. Because the fluctuations were of such long periods it was necessary to rerecord twice to obtain a speed-up of about 500. Such speed-up permitted utilization of a harmonic analyzer for obtaining spectra.[3] Tapes were spliced into continuous loops and played into the analyzer as the analyzer frequency was varied. The spectra had a minimum of 38° of freedom corresponding to a 4-minute length of record and a 0.04-cps wide bandpass filter. Many of the wave records were 15 minutes in length with a proportional increase in the degrees of freedom.

General Features of Ocean-Wave and Radio-Signal Spectra

Ocean-Wave Spectra

The observed ocean-wave spectra may be placed in two general classes: single-peaked and double-peaked; spectra are considered to be double-peaked when a second peak is within 3 db of the first maximum. Some spectra show incipient second peaks on the higher frequency side which undoubtedly indicate the presence of wind waves of insufficient power relative to the swell to show up as definite peaks in the spectrum. Figs. 2 and 3 are examples of the single- and double-peaked spectra. Fig. 4 is illustrative of a spectrum in which the presence of wind waves is indicated at about 0.13 cps.

Of the data runs resolved into spectra, there are cases in which significant peaks occur at frequencies as low as 0.065 cps and as high as 0.12 cps. Half-power "bandwidths" of the wave spectra range between 0.03 cps and 0.17 cps.

A useful analytic form for wave spectra developed by Neumann is[4]

$$A^2(f) = f^{-6} \exp -2(g/2\pi fv)^2$$

where $A^2(f)$ is the power spectrum, f the frequency, g acceleration of gravity, and v the wind speed. This expression may be rewritten

$$A^2(f) = f^{-6} \exp (-K/f^2)$$

[2] K. H. Jehn, J. R. Gerhardt, D. F. Metcalf, and S. J. Prosser, "Some Meteorological and Oceanographic Characteristics of the Golden Gate, California, Area," Elec. Eng. Res. Lab., Univ. of Texas, Rep. CM-760; February 26, 1954.

[3] D. B. Staake, "A Low-Frequency Spectrum and Amplitude-Distribution Analyzer," Appl. Phys. Lab., Johns Hopkins Univ., Rep. CM-833; March, 1955.

[4] W. J. Pierson, Jr., "Advances in Geophysics," Academic Press, Inc., New York, N. Y., vol. 2, pp. 140–146; 1955.

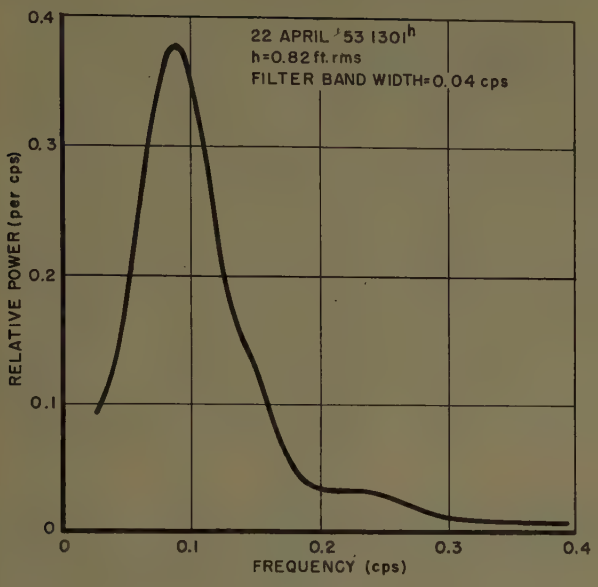

Fig. 2—Example of single-peaked ocean-wave spectrum.

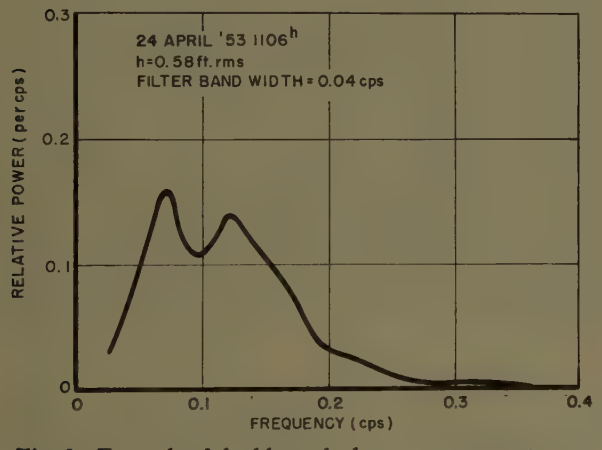

Fig. 3—Example of double-peaked ocean-wave spectrum.

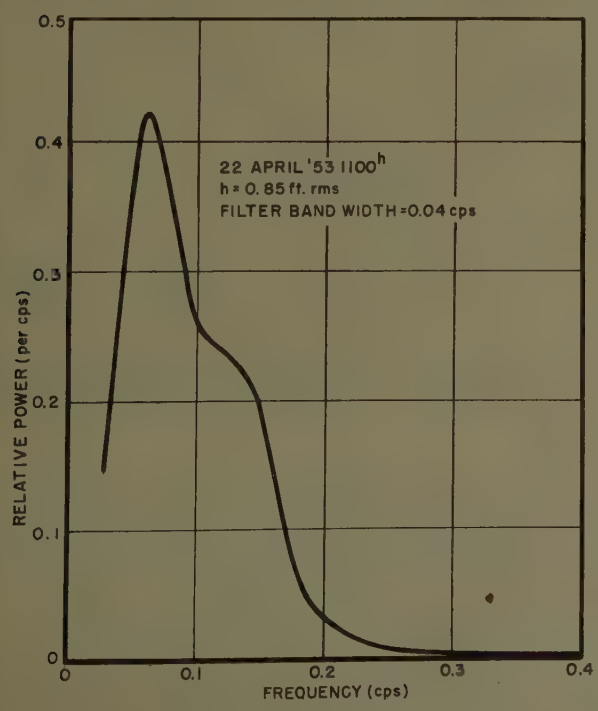

Fig. 4—Example of an ocean-wave spectrum indicating presence of wind waves at about 0.13 cps.

in which only the frequency dependence is explicitly utilized. The maximum of $A^2(f)$ occurs at a frequency $f_{max} = [K/3]^{1/2}$.

The sample single-peaked ocean-wave spectrum in Fig. 2, normalized for unity at the peak, is shown again in Fig. 5 for comparison with its corresponding Neumann spectrum. The Neumann spectrum was "broadened" by computation to simulate its passage through a 0.04-cps bandwidth filter in order to compare it adequately with the observed wave spectrum. It may be seen that the measured spectrum fits the Neumann spectrum except for the somewhat higher energy content at the low frequencies.

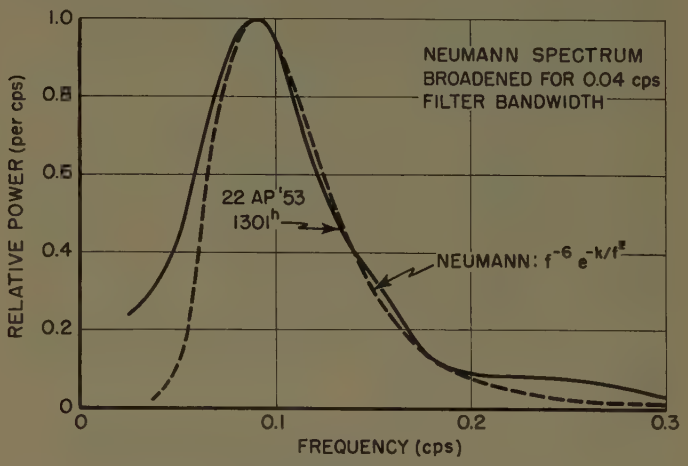

Fig. 5—Comparison of single-peaked ocean-wave spectrum with corresponding Neumann spectrum.

Of the many ocean-wave recordings obtained at the Golden Gate, 24 are used in this analysis. They are divided as indicated below.

1) *Single-Peaked Spectra:* The observed ocean-wave spectra were compared at the half-power levels with broadened Neumann spectra with the following results: 5 of 12 have half-power widths within ± 10 per cent of the corresponding Neumann spectra, 7 of 12 within ± 20 per cent, and 10 of 12 within ± 30 per cent. For some analytical applications, then, it may be adequate to use the Neumann spectrum rather than a measured spectrum when single-peaked spectra are needed.

2) *Double-Peaked Spectra:* In these cases a reexamination of the original strip-chart record discloses two separate easily identifiable "trains" of waves at the frequencies corresponding to the two major spectral components.

A possible mechanism for this type of spectrum is that the swell corresponding to the lower frequency peak comes a comparatively long distance from a generating area where the effective wind speed is V_1. In traversing this distance, the swell may pass through a nearby generating area where local winds of speeds V_2 superimpose a higher frequency set of wind waves, resulting in the higher frequency peak of the spectrum.

Radio-Signal Spectra

Radio-signal spectra are found to be characteristically broader than the wave spectra, half-power points in these spectra extending out to 1 cps or more. In these broader spectra there appear many minor spectral peaks, apparently harmonics of fundamentals in the ocean-wave spectrum. For purposes of analysis, to obtain the equivalent of more degrees of freedom, smoothing by computation has been performed on the radio spectra to simulate passing the signal through a 0.2-cps-wide band-pass filter. A sample radio spectrum is shown in Fig. 6. The original spectrum replotted from the spectrum-analyzer record is shown as a solid line and the smoothed spectrum is dashed. Additional features of radio spectra will be discussed in the next section.

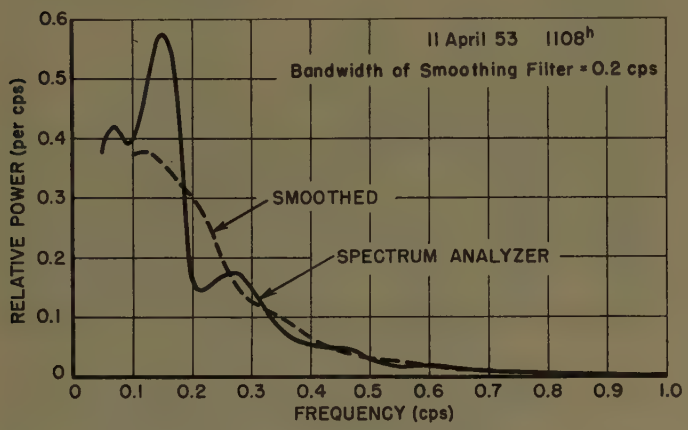

Fig. 6—Sample radio spectrum as obtained from spectrum analyzer (with 0.04-cps filter) and smoothed spectrum (with 0.2-cps filter).

Quantitative Relationships Between Ocean-Wave and Radio-Signal Spectra

It has been demonstrated by the Electrical Engineering Research Laboratory[5] that the peaks in radio spectra generally occur at the same frequency as the peaks in the simultaneous ocean-wave spectra. In the present analysis, it is found that maxima in the radio spectra appear on some occasions at frequencies which are second and possibly third harmonics of the ocean-wave spectra maxima in addition to occurring at the ocean-wave fundamental. The smoothing process, however, blurs the fine structure around the maxima making their positions rather indefinite.

Broadening of the radio-signal spectrum with increasing roughness was quite evident. When runs were made during one day in which the grazing angle, ψ, was progressively increased but wave height, h, was almost constant (yielding increasing $h\psi/\lambda$), the spectra broadened successively. On different days of the experiment runs were made at the same grazing angles but under different wave-height conditions; again broader radio

[5] W. J. McKune and H. W. Smith, "Comparison of Power Spectrum Estimates of Overwater Microwave Signals and Associated Water Waves," Elec. Eng. Res. Lab., Univ. of Texas, Rep. No. 68; May 6, 1953.

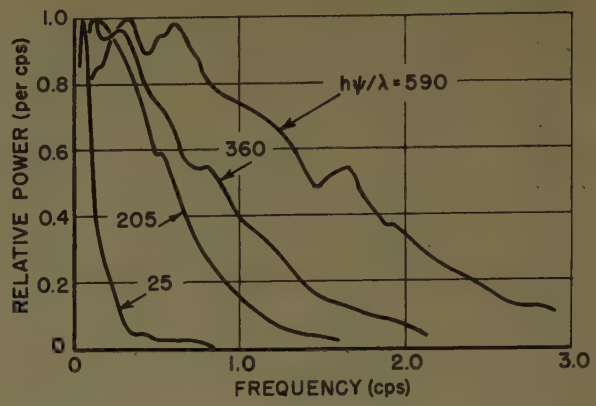

Fig. 7—Radio spectra showing broadening with increasing roughness.

spectra resulted when $h\psi/\lambda$ was larger. Fig. 7 shows four smoothed radio spectra, under conditions of $h\psi/\lambda$ from 25 to 590. The equivalent smoothing filter used to obtain these curves was 0.2 cps wide except for the $h\psi/\lambda = 25$ curve for which the bandwidth was cut in half. For this latter spectrum, where the spectral width is narrower than the filter bandwidth, using an 0.2 cps filter width would have masked the true spectrum; hence a narrower filter was used.

A set of empirical curves has been obtained which indicates the relationship of signal-strength spectra and peak frequencies of ocean-wave spectra to apparent ocean roughness $h\psi/\lambda$. These are shown in Figs. 8, 9, and 10. The ordinate in Fig. 8 is the ratio, f_r/f_w, of the

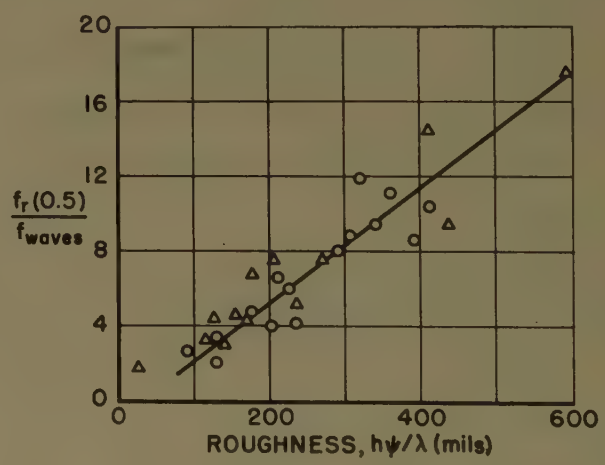

Fig. 8—$f_r(0.5)/f_{waves}$ vs $h\psi/\lambda$. $f_r(0.5)$ = frequency of $\frac{1}{2}$-power point of radio spectrum. f_{waves} = frequency of maximum of wave spectrum. ⊙: Represent ratios when ocean-wave spectra are single peaked. △: Represent ratios when ocean-wave spectra are double peaked.

frequency at which the radio-signal spectrum has decayed to $\frac{1}{2}$ power to the frequency of the lower frequency peak in the ocean-wave spectrum. The frequency at the $\frac{1}{2}$ power point on the radio spectrum is here denoted as $f_r(0.5)$. The circles are values of the ratio f_r/f_w when the ocean-wave spectra are single peaked while the triangles are for double-peaked ocean spectra. The lower frequency peak of the double-peaked spectrum is used to compute the points. In Fig. 9 the 1/10-power frequency

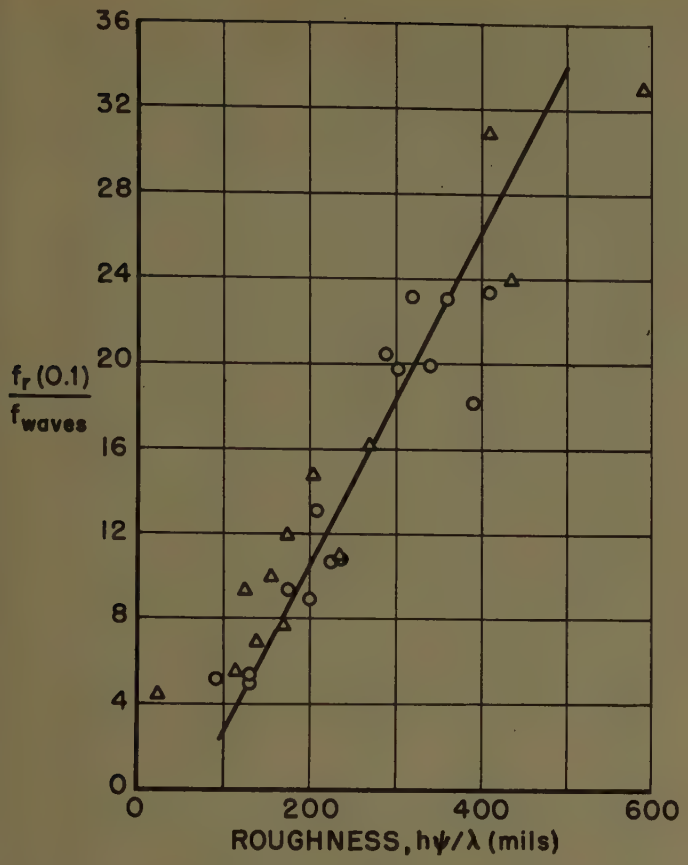

Fig. 9—$f_r(0.1)/f_{waves}$ vs $h\psi/\lambda$. $f_r(0.1)$ = frequency of 1/10-power point of radio spectrum. f_{waves} = frequency of maximum of wave spectrum. ⊙: Represent ratios when ocean-wave spectra are single peaked. △: Represent ratios when ocean-wave spectra are double peaked.

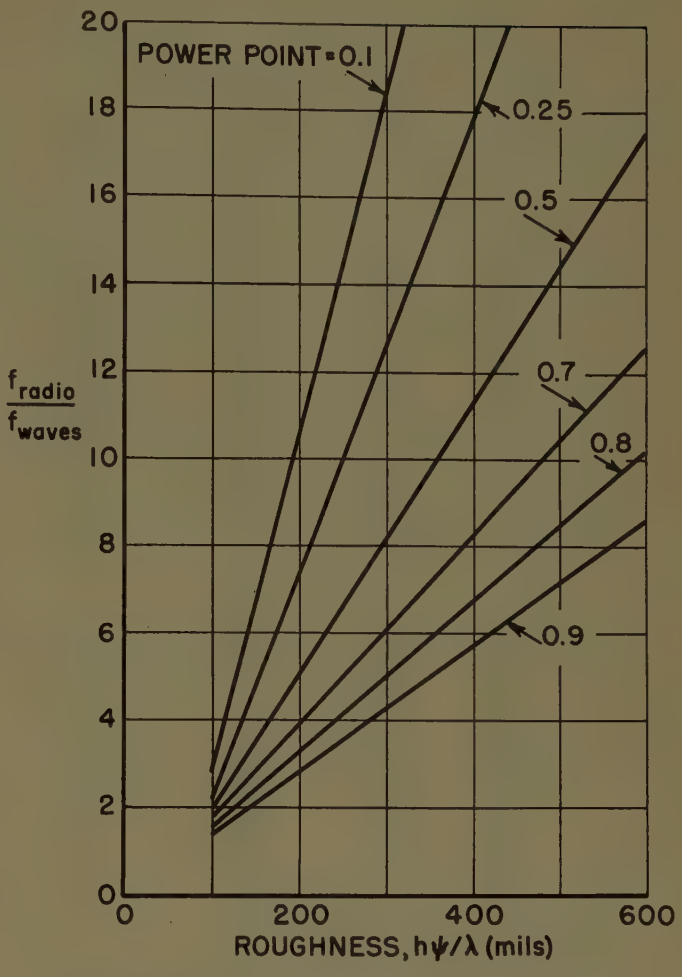

Fig 10—Composite curves of f_{radio}/f_{waves} vs $h\psi/\lambda$ for various power points of the radio spectra from experimental data.

of the radio spectrum is used. In these figures the ½- and 1/10-power frequencies are on the high-frequency side of the peak in the spectrum. The plots in Figs. 8 and 9 giving all the individual data points illustrate the behavior shown by the data for other power levels. The results of such plots for power levels from 0.9 to 0.1 are summarized in Fig. 10, which shows the straight lines fit to the data points for each power level. Data on the values of f_r and f_w for all the runs used in this analysis are given in Table I, on page 188. A discussion of the possible sources of error in the data presented here, including the effects of sample length, representativeness of particular wave spectra, and reliability of the spectra at the low-frequency end, has been reported.[6]

The effect of the parameter $h\psi/\lambda$ overrides the influence of other possible factors:

1) The points for double-peaked wave spectra fall close to those for single peaks when the lower frequency peak, or swell frequency, is used to compute the points. This behavior indicates that the width of the ocean-wave spectrum is of less importance in determining the width of the radio spectrum than the swell frequency.

2) Illumination of the water was varied radically by changing the pointing of the receiving 18-inch-diameter antenna from zero to 5° above the horizontal without changing the spectrum width. Under-illumination of scatterers far from the specular point (by pointing the antenna upwards) should have little effect on the spectra according to the next section on theory which considers only the area near the specular region.

Although the low $h\psi/\lambda$ ends of the lines in Figs. 8, 9, and 10 have been left open, lower limits of the frequency ratios as $h\psi/\lambda \rightarrow 0$ can be specified in the following manner. One assumes that the radio spectrum does not become narrower than the wave spectrum as $h\psi/\lambda \rightarrow 0$. Then for the Neumann wave spectrum the ratio of the upper half-power frequency to the peak frequency is 1.55; the lowest point in Fig. 8 is 1.8 which does not violate the lower limit. For Fig. 9 the Neumann ratio is 2.3 and the lowest point is 4.4. Hence there is no disagreement with this criterion in the curves.

An analytic expression for the shape of the smoothed radio spectra was sought. The portions of the curves above the maxima of the radio spectra, f_m, follow the form $\exp[-k(f_r - f_m)^n]$. Seventy-five per cent of the values of n fall between 1 and 1.5 with an average value

[6] C. I. Beard and I. Katz, "The Dependence of Microwave Radio Signal Spectra on Ocean Roughness and Wave Spectra," Appl. Phys. Lab., Johns Hopkins Univ. Rep. CF-2456; January 17, 1956.

TABLE I

Date April 1953	Time (PST)	$h\psi/\lambda$ (mils)	Wave Spectra	Radio Spectra					
			Frequency of Maximum (cps)	$f_r(0.9)$ (cps)	$f_r(0.8)$ (cps)	$f_r(0.7)$ (cps)	$f_r(0.5)$ (cps)	$f_r(0.25)$ (cps)	$f_r(0.1)$ (cps)
			Single Peak						
11	1328	175	0.090*	0.19	0.21	0.28	0.42	0.63	0.84
11	1339	200	0.090	0.24	0.27	0.30	0.36	0.52	0.80
11	1410	225	0.090*	0.19	0.21	0.38	0.53	0.65	0.96
18	1134	130	0.120	0.18	0.20	0.21	0.25	0.46	0.60
21	1102	210	0.115**	0.38	0.46	0.54	0.76	1.12	1.49
21	1111	235	0.115	0.16	0.20	0.30	0.48	0.90	1.24
21	1444	290	0.100	0.45	0.51	0.56	0.80	1.38	2.04
22	1008	390	0.100	0.52	0.59	0.65	0.86	1.30	1.81
22	1157	305	0.075	0.35	0.42	0.47	0.66	1.05	1.48
22	1218	340	0.080	0.42	0.47	0.52	0.76	1.15	1.59
22	1235	360	0.075	0.36	0.44	0.58	0.83	1.29	1.73
22	1301	320	0.090	0.39	—	0.94	1.06	1.43	2.08
22	1315	410	0.085	0.38	0.47	0.80	0.88	1.44	1.98
23	1458	90	0.105	0.16	0.19	0.22	0.28	0.38	0.54
24	1016	130	0.100	0.19	0.25	0.28	0.34	0.42	0.53
			Double Peak						
11	1034	235	0.085	0.32	0.36	0.39	0.44	0.56	0.92
11	1055	115	0.085***	0.21	0.23	0.25	0.28	0.38	0.47
18	1107	140	0.105	0.18	0.21	0.24	0.32	0.52	0.72
18	1229	170	0.095	0.19	0.26	0.32	0.41	0.59	0.73
22	1100	205	0.075	0.25	0.31	0.38	0.56	0.84	1.10
22	1144	270	0.080	0.39	0.43	0.46	0.61	0.94	1.29
22	1412	410	0.080	0.68	0.78	0.89	1.15	1.86	2.46
22	1448	590	0.090	0.74	0.88	1.22	1.58	2.20	2.95
22	1525	435	0.100	0.54	0.65	0.77	0.94	1.51	2.38
24	1009	125	0.070	0.18	0.20	0.23	0.31	0.50	0.65
24	1041	155	0.080	0.20	0.23	0.27	0.36	0.59	0.80
24	1106	175	0.070	0.17	0.23	0.30	0.47	0.66	0.83
25	1502	25	0.065	0.09	0.10	0.10	0.12	0.20	0.29

* The closest wave spectrum was at 1340–1356^h.
** The closest wave spectrum was at 1111–1115^h.
*** The closest wave spectrum was at 1020–1036^h.

of about 1.25. There appears to be no dependence of n upon $h\psi/\lambda$. The parameter k, however, varies inversely with $h\psi/\lambda$ as given by the approximate relation:

$$k \cong -0.5 + \frac{380}{(h\psi/\lambda)}, \qquad 90 < h\psi/\lambda < 590.$$

Hence, an average expression for 75 per cent of the radio spectra on the high-frequency side of the peak is given by:

$$W(f) \cong \exp -\left[\left(-0.5 + \frac{380}{(h\psi/\lambda)}\right)(f_r - f_m)^{1.25}\right].$$

As $h\psi/\lambda$ increases outside of the limits given above towards infinity, it appears reasonable to assume that k tapers off to zero (rather than to the straight line intercept value of -0.5). Thus as $h\psi/\lambda \to \infty$,

$$W(f) \to 1 - k(f_r - f_m)^{1.25} \to 1,$$

or the spectrum approaches a white-noise spectrum.

The explanation for the spectral broadening with increasing roughness may be found in concepts inherent in the vector model. Earlier work by the Electrical Engineering Research Laboratory[7] has shown that harmonics of the ocean-wave fluctuations are found in the radio spectrum, having been generated by the vertical motion of the ocean surface. Various ratios of fundamental to harmonics were possible. In their treatment the entire surface was assumed to move up and down as a unit, moving the interference pattern past the receiving point. The writers of the present paper conclude that the entire surface can be considered to move as a unit only under the following conditions: The transmission path is parallel to the swell crests with short ranges and beams narrow enough so that the entire illuminated area and important Fresnel zones are contained within one swell wavelength. This case may be achieved across narrow inlets from the sea.

In the more general open-ocean situation, however, waves arrive at a point from various directions, up to $\pm 30°$ is common; this diversity of direction of arrival causes the waves to be short crested. As the Fresnel zones become longer than a few thousand feet, the short crestedness results in the existence of many scatterers

[7] A. H. LaGrone, A. W. Straiton, and H. W. Smith, "Synthesis of radio signals on overwater paths," IRE TRANS., vol. AP-3, pp. 48–52; April, 1955.

within the Fresnel zones. Irregularity of the wave structure as indicated by the width of the frequency spectrum also aids in breaking up the Fresnel zones. Using the vector model as a guide one may interpret the phenomena as follows: Fluctuations in the radio signal are caused by the vector addition to the direct and coherent signal of signals reflected from several or many reflecting areas. The model in its simplest form postulates that there are many independent, random scattering areas. [In the special case of the narrow inlet cited above where the reflecting areas are greater in size than the Fresnel zones, the "incoherent term" loses its randomness and the postulate of the model of many (>5) independent random scatterers is no longer satisfied.] As each small scatterer moves vertically through any height it changes its contribution to the phase of the resultant signal [for example, the phase of the return from a patch near the specular point will vary as $4\pi(h\psi/\lambda)$ as h changes]; if it moves through twice that height in the same time its contribution to the frequency of fluctuation is doubled. Thus as wave height increases one would expect an increased spectrum bandwidth generated by harmonics of all the frequencies in the wave spectrum. Actually minor peaks in the radio spectra have been found which are in harmonic ratios—up to the sixth have been resolved—of the frequency of the peak in the wave spectrum. Since the integrated effect of signals from all the scatterers, especially after being passed through the band-pass filter, might be expected to smear out the effects of individual wave frequencies, this effect was looked into. In many cases it was found that clear-cut trains of waves of 1 to $1\frac{1}{2}$ minute duration of practically constant frequency existed near the time of the data run. The persistence of one-wave frequency would account for the predominance of its harmonics in the radio spectrum. In this picture all the fluctuations are considered to stem from the incoherent portion of reflected energy; the coherent part, and consequently the interference pattern, are fixed by geometry, as stated previously.

Approximate Theoretical Treatment

The qualitative explanation of spectral widening given in the preceding section can be made more quantitative, although still not exact, as follows.

The reflected signal (coherent plus incoherent) from each individual scatterer has been shown by Spetner[8] to be proportional to

$$e^{ikv}(\psi_1 + \psi_2)$$

where $k = 2\pi/\lambda$, v = height of scatterer above mean water level, ψ_1 = grazing angle of incidence from source, and ψ_2 = grazing angle of reflection to receiver.

[8] L. M. Spetner, "An Independent Scatterer Model for Forward Scattering of Microwaves," Appl. Phys. Lab., Johns Hopkins Univ. Rep. CF-2533; July, 1956.

The assumptions involved in this simplified form are:

1) Uniform illumination of the water surface by both transmitting and receiving antennas.
2) Each scatterer has a constant scattering cross section and radiates isotropically.
3) Each scatterer has the same reflectivity.

The total value of reflected signal is obtained by integrating over the area. In order to obtain a solution, it is desirable to assume that the principal contribution is from scatterers near the specular region. One justification for this assumption is that it leads to reasonable results.

The spectrum is obtained by first calculating the correlation function $R(\tau) = \langle I_y(t) I_y(t+\tau) \rangle$, where I_y is the component of I along c. In calculating the averages, use is made of the known Gaussian probability distribution of the water surface. The result Spetner obtains is:[8]

$$R(\tau) \cong \exp\left[(4\pi h\psi/\lambda)^2 \rho_w(\tau) - \gamma\tau\right]$$

where $\rho_w(\tau) = \langle y(t) y(t+\tau) \rangle$ is the correlation function of the water surface and γ is the probability per unit time that a given scatterer disappears.

The power spectrum $W(f)$ of $I_y(t)$ is then computed by the cosine transform relation

$$W(f) = 4 \int_0^\infty R(\tau) \cos \omega\tau d\tau.$$

The integrations were performed numerically taking $\gamma = 0.1$ cps, the predominant wave frequency, and an assumed expression for $\rho_w(\tau)$ of a damped cosine form which decayed to e^{-1} in two water wavelengths.[9] The I_y spectra resulting from these calculations are given in Fig. 11.

Before discussing these I_y spectra it is necessary to consider which spectra should be compared to the observed total-signal spectra. This can be seen by the series expansion of the signal strength, T, derived by Beard, *et al.*,[1] within $\pm 90°$ of maxima of the interference pattern:

$$T \cong D_1 + I_y + \frac{I_x^2}{2D_1}\left(1 - \frac{I_y}{D_1} + \frac{I_y^2}{D_1^2} - \cdots\right) - \frac{I_y^4}{8D_1^3} + \cdots$$

where $D_1 = |\vec{D} + \vec{C}|$.

To the first order of approximation, the spectrum of the fluctuating part of T is that of I_y.

The frequencies of the 0.5-, 0.25-, and 0.1-power

[9] The expression used in the computations was $\rho_w(\tau) = e^{-(bf_w\tau)^2} \cos \omega\tau$. The wave frequency f_w was selected as 0.1 cps and b was chosen as 0.5 to cause a decay to e^{-1} in two periods. For a theoretical derivation of this form of $\rho_w(\tau)$, see Carl Eckert, "The generation of wind waves on a water surface," *J. Appl. Phys.*, vol. 24, pp. 1485–1494; [eq. (49)]; December, 1953.

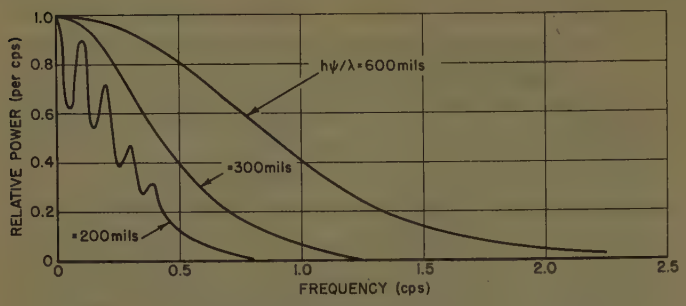

Fig. 11—Power spectra of I_y for $h\psi/\lambda = 200$, 300, and 600 mils calculated from theory.

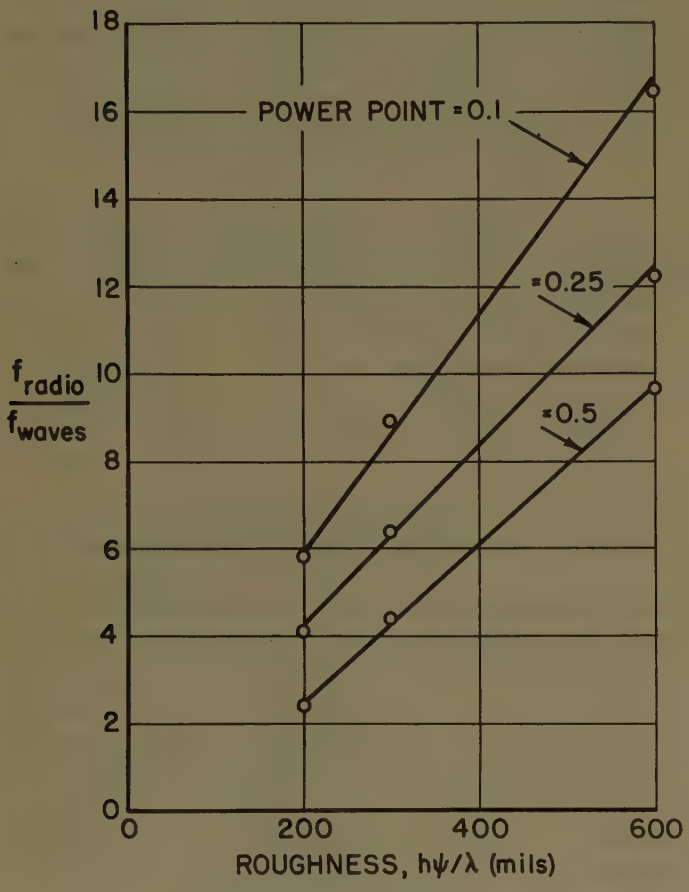

Fig. 12—Broadening of power spectrum of I_y with increasing roughness, as computed from theory.

points of the I_y spectra (each divided by f_w) obtained from Fig 11 are plotted in Fig. 12 vs $h\psi/\lambda$. These plots show the same linear behavior as found experimentally. However, the theory does not predict a continuation of this linear behavior at power levels closer to the spectral peaks. This can be seen by plotting these points from Fig. 11. But since the behavior for these levels is not linear, reliable curves could not be drawn with points at only three values of $h\psi/\lambda$ available.

In addition to this linear broadening with $h\psi/\lambda$, the relative shapes of the calculated I_y spectra are approximately the same (between the 0.1- and 0.5-power points) as the experimental spectra, as shown in Table II.

TABLE II

Ratios	$h\psi/\lambda = 600$		$h\psi/\lambda = 300$	
	Calc.	Exp.	Calc.	Exp.
$\frac{f_r(0.1)}{f_r(0.25)}$	1.35	1.39	1.37	1.38
$\frac{f_r(0.25)}{f_r(0.5)}$	1.27	1.53	1.45	1.49

The ratio

$$\frac{f_r(0.1)}{f_r(0.25)},$$

for example, is actually the ratio

$$\frac{f_r(0.1)/f_w}{f_r(0.25)/f_w},$$

but f_w cancels.

Although the trends agree, the widths' magnitudes of the I_y spectra are only about one-half the experimental widths. This is mainly a result of choice of the wave correlation function.[9] Inspection of the wave correlations determined by the Electrical Engineering Research Laboratory[10] shows that a simple exponential damping $e^{-(b/w\tau)}$ fits better although it is still inadequate.[11] Values of b range from 0.7 to 1.4. With $b=1$, the correlation has decayed to e^{-1} in one water wavelength instead of two as originally assumed. This would widen the spectra by about a factor of two, placing the theoretical spectra in agreement with the experiment.

As will be noted from Fig. 11, the theoretical spectra peak at zero frequency rather than drop towards zero at zero frequency as evidenced by experimental data.[5]

The theoretical calculations were made only for correlation functions corresponding with single-peaked wave spectra. When double-peaked wave spectra occurred, the data indicated that swell frequencies were more important in determining the width of the radio spectra than the higher frequency wind waves. In order to establish the quantitative relative effectiveness of swell vs wind frequencies the next step is to apply Spetner's expression for $R(\tau)$ using correlation functions corresponding to double-peaked wave spectra.

The present simplified theory agrees with the experimental trends of the broadening of the radio spectra with $h\psi/\lambda$ and also of the relative shapes of the radio spectra between the 0.5- and the 0.1-power levels.

[10] F. E. Brooks, Jr., G. P. Dubose, Jr., and C. W. Tolbert, "Preliminary Summary Report of Radio, Meteorological and Oceanographic Data Obtained During 1955 Gulf of Mexico Propagation Tests," Elec. Eng. Res. Lab., Univ. of Texas, Rep. TG-260; January 31, 1956.

[11] There is a wide variation among correlations. The exponentially-damped cosine form above would reasonably describe two, whereas the sin x/x form would describe another correlation. Since the Neumann spectrum fits many observed wave spectra, the cosine transform of this would be a reasonable correlation function to use.

Conclusion

If one assumes a similarity of wave and radio spectral shape on the low-frequency side and that the spectra have primary peaks at the same frequency, there remains only the region on the high-frequency side to be predicted. The graphs of f_r/f_w in Fig. 10 may be used for this purpose. Within limits of accuracy as indicated by the spread of the points in Figs. 8 and 9, one is now in a position to predict the approximate shape of the radio spectrum from a knowledge only of geometry, electromagnetic wavelength, ocean-wave rms height, and the (swell) peak frequency in the ocean-wave spectrum.

Acknowledgment

Grateful acknowledgment is made to Donald P. Rogers for obtaining the spectra which formed the basis for this report, to Ethel P. Fyler for her aid in computations without which the analysis would have been immeasurably more difficult, and to Doris Rubenfeld for the illustrations in this report.

In addition to the part the Electrical Engineering Research Laboratory of the University of Texas played in performing the experiment, we are indebted to them for providing several additional spectra needed to complete the work.

Step Discontinuities in Waveguides*

W. ELWYN WILLIAMS†

Summary—**The method developed by Wiener and Hopf for solving a certain class of integral equations is applied to the problem of a discontinuity in cross section of a rectangular waveguide. We consider the problem of two waveguides of infinite width and different heights joined together with a short step when the only nonvanishing component of the magnetic field is that parallel to the edges of the step. It is assumed that the fundamental mode is incident in the larger channel traveling towards the step. For values of the channel height such that only the fundamental mode is propagated without attenuation, this problem has been treated in the "Waveguide Handbook"[1]; our results are in very good agreement with the results given there. The present analysis is extended to cover the case where the larger channel is capable of supporting the mode above the fundamental without attenuation. Some numerical values are given for the ratio between the reflected and incident energies for various values of the channel and step heights.**

Introduction

PROBLEMS involving discontinuities in waveguides are of great practical importance and a considerable amount of attention has been devoted to them in recent years. The two types of discontinuities that have been most extensively treated for a rectangular guide are the bifurcation of the guide by a semi-infinite plane and a step discontinuity in the guide cross section. The problem of the bifurcation may be solved in terms of known functions by applying the well-known Wiener-Hopf technique for solving integral equations. The methods for solving the problem of a step discontinuity which have appeared in the literature are, however, in no way based on the Wiener-Hopf approach. Two distinct methods have been employed; the first consists of expanding the field components on either side of the discontinuity in terms of the appropriate eigenfunctions for the region considered, and then matching the components across the plane of discontinuity. The second method used is the equivalent static approach as described in the "Waveguide Handbook."[1] Since there is obviously a physical relationship between these two problems it is desirable to solve them both by the same method in order that the solution should display clearly the relationship between them, and this is the object of the present work.

We therefore consider the application of the Wiener-Hopf technique to solve the problem of a step discontinuity in a parallel-plate region (or, equivalently, the coupling of two parallel-plate waveguides of different height). It is assumed that the only nonvanishing component of the magnetic field is that parallel to the edges of the step. It is assumed that the fundamental mode is incident from the larger region on the step, and, initially, that the dimensions of both regions concerned are taken to be such that only the fundamental mode may propagate without attenuation. This restriction is later removed and the case of the larger region being capable of sustaining two nonattenuated modes is treated. The advantage of this method of attack is that it affords a clearer physical picture of the structure of the solution than that obtained by the other methods. In particular, it is possible to separate the reflection coefficient for the fundamental mode into two parts, one of which is expressible in terms of known functions and another which

* Manuscript received by the PGAP, May 17, 1956. The research reported in this article was done at the Inst. of Mathematical Sciences, New York Univ., and has been made possible through support and sponsorship extended by the U. S. Air Force, Air Force Cambridge Res. Center, under Contract No. AF 19(122)-42.

† Inst. of Mathematical Sciences, New York Univ., New York, N. Y.

[1] N. Marcuvitz, "Waveguide Handbook," McGraw-Hill Book Co., Inc., New York, N. Y.; 1951.

may be obtained from the solution of an infinite set of equations. That part of the reflection coefficient which is known exactly is by far the dominant part of the complete expression, and thus the percentage error in determining an approximate value of the reflection coefficient is much less than the corresponding error made in the solution of the equations. The analytic part of the solution may be obtained by simple physical arguments from the known solution of the bifurcation problem and thus the present form of the solution gives a distinct connection between the two types of problems.

For the case in which only the fundamental mode is propagated without attenuation in any of the regions considered, it is possible to compare the present results with those given in the "Waveguide Handbook," which were obtained by the equivalent static method, and the results of both methods show remarkably good agreement. The method used here may be easily extended to solve the problem of a bifurcated waveguide when the material composing one of the bifurcated regions differs in dielectric properties from that of the remainder of the waveguide. The approach may also be used to consider the problem of radiation from a dielectric waveguide, and it is hoped that both of these problems will be treated in future papers. The method can, of course, be applied to the general electromagnetic case since it is known that this problem can be reduced to the solution of two scalar problems,[2] but no attempt is made to consider this more general case. The author has been informed by Prof. N. Marcuvitz that Prof. J. Schwinger has considered the application of the Wiener-Hopf technique to problems similar to the one treated here. An account of his work may appear in a forthcoming book by Marcuvitz and Schwinger.

Statement of the Problem

The waveguide is assumed to occupy the region $-\infty \leq X \leq 0$, $d < y < a$; and $0 \leq x \leq \infty$, $0 < y < a$ (see Fig. 1), where x, y are Cartesian coordinates with their

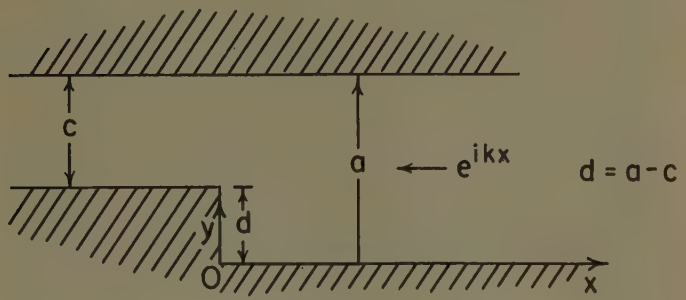

Fig. 1.

origin at O. Oz, the third axis of the system, is not shown, and the solution is assumed to be independent of z. A time variation $e^{i\omega t}$ will be taken as understood throughout the work, and it is assumed that an incident wave e^{ikx} is approaching the step from the right, k being $2\pi/(\text{wavelength})$.

The total magnetic field will be written as $e^{ikx}+\Psi$, and hence a function Ψ is sought which satisfies the following conditions:

$$(\nabla^2 + k^2)\Psi = 0, \tag{1}$$

$$\frac{\partial \Psi}{\partial x} = -ik \text{ on } x = 0, \qquad 0 \leq y \leq d \tag{2}$$

$$\frac{\partial \Psi}{\partial y} = 0 \qquad \text{on } y = a, \qquad -\infty \leq x \leq \infty,$$

$$\text{on } y = d, \qquad -\infty \leq x \leq 0, \text{ and} \tag{3}$$

$$\text{on } y = 0, \qquad 0 \leq x \leq \infty.$$

It is convenient to assume that $k = k_r - ik_i$, where k_i, $k_r > 0$; then the form of the radiation condition for Ψ is $\Psi = O(e^{-ik|x|})$ as $|x| \to \infty$. In order to specify the problem uniquely, a condition has to be imposed on Ψ at the edges of the step.[3] This condition is that Ψ is $O(1)$ as the point of observation approaches $(0, d)$ or $(0, 0)$, while $|\nabla\Psi|$ is $O(r^{-1/3})$ as the point of observation approaches $(0, d)$, and is $O(1)$ in the neighborhood of the origin, here $-r$ is being the distance from the point approached. The above conditions now specify the problem completely and uniquely.

Solution for Ψ

We shall now define a function $\phi(s, y)$ by

$$\phi(s, y) = \int_{-\infty}^{\infty} e^{-sx}\Psi(x, y)dx$$

where s is the complex variable $\sigma + i\tau$. From the assumption on Ψ as $|x| \to \infty$, it is clear that the above integral is convergent for $-k_i < \sigma < k_i$. Hence ϕ is a regular function of s in the region $|\sigma| < k_i$. We also define $\phi_-(s, y)$, $\phi_+(s, y)$ as

$$\phi_-(s, y) = \int_{-\infty}^{0} e^{-sx}\Psi(x, y)dx$$

$$\phi_+(s, y) = \int_{0}^{\infty} e^{-sx}\Psi(x, y)dx.$$

Clearly, from the behavior of Ψ as $|x| \to \infty$, $\phi_-(s, y)$ is a regular function of s for $\sigma < k_i$, and $\phi_+(s, y)$ is a regular function of s for $\sigma > -k_i$. In the region $0 \leq y \leq d$, $\phi_-(s, y)$ is identically zero and hence we have the following equations. For $y \geq d$

$$\frac{d^2\phi}{dy^2} + \kappa^2\phi = 0. \tag{4}$$

For $0 \leq y \leq d$

$$\frac{d^2\phi}{dy^2} + \kappa^2\phi_+ = -ik + sf(y) \tag{5}$$

[2] L. Lewin, "Advanced Theory of Waveguides," Iliffe and Sons, London, England; 1951.

[3] D. S. Jones, "A note on diffraction by edges," *Quart J. Math. and Mech.*, vol. 3, pp. 189, 1950.

where $f(y)=\Psi(0, y)$ and $\kappa=(s^2+k^2)^{1/2}$, and where that branch of the root is taken which reduces to k when $s=0$.

The solution of (5) which satisfies the boundary condition on $y=0$ is

$$\phi_+(s, y) = A\cos\kappa y - \frac{ik}{\kappa}\int_0^y \sin\kappa(y-t)dt + \frac{s}{\kappa}\int_0^y f(t)\sin\kappa(y-t)dt$$

$$= A\cos\kappa y - \frac{ik}{\kappa^2}(1-\cos\kappa y) + \frac{s}{\kappa}\int_0^y f(t)\sin\kappa(y-t)dt \qquad (6)$$

where A is a function of s but not of y.

If primes are taken to mean derivatives with respect to y, then differentiation of (6) and then substitution of $y=d$ in the resulting equation gives

$$\phi_+'(s, d) = -\kappa A\sin\kappa d - \frac{ik}{\kappa}\sin\kappa d + s\int_0^d f(t)\cos\kappa(d-t)dt. \qquad (7)$$

If the value of A from (7) is substituted in (6), then this latter equation may be rewritten as

$$\kappa\sin\kappa d\phi_+(s, y) = -\left\{\phi_+'(s, d) + \frac{ik}{\kappa}\sin\kappa d - s\cdot\int_0^d f(t)\cos\kappa(d-t)dt\right\}\cos\kappa y + \left\{\frac{s}{\kappa}\int_0^y f(t)\sin\kappa(y-t)dt - \frac{ik}{\kappa^2}(1-\cos\kappa y)\right\}\kappa\sin\kappa d. \qquad (8)$$

By definition $\phi_+(s, y)$ is regular for $\sigma>k_i$. Hence, since $\kappa\sin\kappa d$ has zeros in $\sigma>-k_i$, the right-hand side of (6) must vanish for those zeros of $\kappa\sin\kappa d$ in $\sigma>-k_i$. These zeros will be at $s=\kappa_m$ $(m=0, 1, 2, \cdots)$ where

$$\kappa_m = \left(\frac{m^2\pi^2}{d^2} - k^2\right)^{1/2};$$

κ_m is positive when real, and positive imaginary when not real (for k real). It is also easy to show that $R\kappa_m\leq\kappa_i$. Thus, in order that the right-hand side of (8) vanishes for $s=\kappa_m$, the following relations must hold

$$\phi_+'(\kappa_m, d) = (-)^m\kappa_m\int_0^d f(t)\cos\frac{m\pi t}{d}dt, \qquad m\neq 0$$

$$\frac{\phi_+'(ik, d)+ikd}{ik} = \int_0^d f(t)dt.$$

If the expression for $f(t)$ as a Fourier cosine series as obtained from the above expressions is substituted in (8), then application of the well-known results for term by term integration of Fourier series, together with some slight manipulation, yields the following equation for $\phi_+(s, y)$

$$\kappa\sin\kappa d\phi_+(s, y) = -\phi_+'(s, y)\cos\kappa y + \frac{\kappa\sin\kappa d}{s+ik} + \frac{2\kappa s}{d}\sin\kappa d\sum_{n=0}^{\infty} g_m\frac{\cos\frac{m\pi y}{d}}{s^2-\kappa_m^2} \qquad (9)$$

where

$$g_m = \frac{(-)^m\phi_+'(\kappa_m, d)}{\kappa_m} \quad m\neq 0, \qquad g_0 = \phi_+'\frac{(ik, d)}{2ik}.$$

We now consider the region $y\geq d$. The solution of (4) which satisfies the boundary condition on $y=a$ is

$$\phi(s, y) = B\cos\kappa(y-a)$$

where B is a function of s only. Since $\partial\Psi/\partial y$ vanishes on $y=d$ for $-\infty\leq x\leq 0$, $\phi_-'(s, d)=0$ and hence

$$-B\kappa\sin\kappa(d-a) = \phi_+'(s, d).$$

Thus we obtain the following equation for $\phi(s, y)$

$$\phi(s, y) = -\frac{\cos\kappa(y-a)}{\kappa\sin\kappa(d-a)}\phi_+'(s, d).$$

Hence

$$\phi_+(s, d) + \phi_-(s, d) = -\frac{\cot\kappa(d-a)}{\kappa}\phi_+'(s, d). \qquad (10)$$

Substitution for $\phi_+(s, d)$ from (9) into (10) gives

$$\phi_-(s, d) = \frac{\sin\kappa a}{\kappa\sin\kappa c\sin\kappa d}\phi_+'(s, d) - \frac{1}{s+ik} - \frac{2s}{d}\sum_{m=0}^{\infty}\frac{(-)^m g_m}{s^2-\kappa_m^2}. \qquad (11)$$

On writing

$$\frac{\sin\kappa a}{\kappa\sin\kappa c\sin\kappa d}$$

as

$$\frac{N_+(s)}{N_-(s)}$$

it is seen that (11) may be rewritten as

$$N_-(s)\phi_-(s, d) = N_+(s)\phi_+'(s, d) - \frac{N_-(s)}{s+ik} - \frac{2s}{d}N_-(s)\sum_{m=0}^{\infty}\frac{(-)^m g_m}{s^2-\kappa_m^2}.$$

The formulas for $N_+(s)$, $N_-(s)$ are given in the Appendix but a brief summary of their essential properties will be given here. $N_+(s)$ is regular and nonzero in the region

$\sigma > -k_i$; $N_-(s)$ is regular and nonzero for $\sigma < k_i$. Also, as $|s| \to \infty$, $N_+(s) \sim s^{-1/2}$ and $N_-(s) \sim s^{1/2}$.

It is now convenient to rewrite the above equation for $\phi_-(s, d)$ as follows:

$$N_-(s)\phi_-(s, d) + \frac{N_-(s) - N_-(-ik)}{s + ik} + \frac{2s}{d} N_-(s) \sum_{m=0}^{\infty} \frac{(-)^m g_m}{s^2 - \kappa_m^2} - \frac{1}{d} \sum_{m=0}^{\infty} \frac{(-)^m N_-(-\kappa_m) g_m}{(s + \kappa_m)} = N_+(s)\phi_+'(s, d) - \frac{N_-(-ik)}{s + ik} - \frac{1}{d} \sum_{m=0}^{\infty} \frac{(-)^m N_-(-\kappa_m) g_m}{(s + \kappa_m)}. \quad (12)$$

Clearly the left-hand side of (12) is regular for $\sigma < k_i$ while the right-hand side is regular for $\sigma > -k_i$; hence both sides are equal to an integral function in the common strip $|\sigma| < k_i$. This integral function may be determined from examination of the growth of both sides of (12) as $|s| \to \infty$. In order to do this we require the behavior of $\phi_+'(s, d)$ as $|s| \to \infty$ in $\sigma > -k_i$ and the edge condition shows that $\phi_+'(s, d) \sim s^{-2/3}$ as $|s| \to \infty$. The integral function is now easily seen to be zero and we have

$$N_+(s)\phi_+'(s, d) = \frac{N_-(-ik)}{s + ik} + \frac{1}{d} \sum_{m=0}^{\infty} \frac{(-)^m N_-(-\kappa_m) g_m}{s + \kappa_m}. \quad (13)$$

From (13), on substituting $s = \kappa_n$, the following set of equations is obtained to determine the $\phi_+'(\kappa_m, d)$

$$N_+(\kappa_n) a_n = \frac{1}{\kappa_n + ik} + \frac{1}{d} \sum_{m=1}^{\infty} \frac{N_-(-\kappa_m) a_m}{\kappa_m(\kappa_m + \kappa_n)} + \frac{a_0 N_-(-ik)}{2ikd(\kappa_n + ik)}, \quad (n = 0, 1, 2, \cdots) \quad (14)$$

where $a_n = \phi_+'(\kappa_n, d)/N_-(-ik)$.

For the case in which only one mode is propagated without attenuation in both regions of Fig. 1, it is possible to reduce the above set of equations to a real set as follows. We define $L_+(s) = N_+(s)\ (s + ik)$, $L_-(s) = N_-(s)/(s - ik)$. From the formulas for $N_+(s)$ and $N_-(s)$ it is clear that $L_+(\kappa_n)$ is real for $n \geq 1$. Hence (14) may be rewritten as

$$L_+(\kappa_n) a_n = 1 - \frac{1}{d} \sum_{m=1}^{\infty} \frac{a_m L_-(-\kappa_m)}{\kappa_m(\kappa_m + \kappa_n)} (\kappa_m \kappa_n - k^2) - \frac{ik}{d} \sum_{n=1}^{\infty} \frac{a_m L_-(-\kappa_m)}{\kappa_m} - \frac{a_0 L_-(-ik)}{d}. \quad (15)$$

From the asymptotic behavior of $\phi_+'(s, d)$ and $N_-(s)$ it is seen that the terms of the second series in (15) are $O(m^{-13/6})$ as $m \to \infty$; hence this series is convergent.

Putting $n = 0$ in (15), we obtain

$$L_+(ik) a_0 = 1 - \frac{2ik}{d} \sum_{m=1}^{\infty} \frac{a_m L_-(-\kappa_m)}{\kappa_m} - \frac{a_0 L_-(-ik)}{d}. \quad (16)$$

If the value for the series

$$\sum_{m=1}^{\infty} a_m L_-(-\kappa_m)/\kappa_m$$

as obtained from (16) is substituted into (15) then the following system of equations is obtained

$$L_+(\kappa_n) = \frac{1}{2}\left\{1 + a_0 L_+(ik) - \frac{a_0}{d} L_-(-ik)\right\} - \frac{1}{d} \sum_{m=1}^{\infty} \frac{a_m L_-(-\kappa_m)(\kappa_m \kappa_n - k^2)}{\kappa_m(\kappa_m + \kappa_n)}, \quad n = 1, 2, \cdots. \quad (17)$$

Defining a new set of constants c_n for $n \leq 1$ by

$$c_n = \frac{2a_n}{1 + a_0 L_+(ik) - \frac{a_0}{d} L_-(-ik)}$$

it is seen that these will satisfy the following set of equations:

$$L_+(\kappa_n) c_n = 1 - \frac{1}{d} \sum_{m=1}^{\infty} \frac{c_m L_-(-\kappa_m)(\kappa_m \kappa_n - k^2)}{\kappa_m(\kappa_m + \kappa_n)}, \quad (m = 1, 2, \cdots). \quad (18)$$

The set of (18) is real only when the fundamental mode is propagated without attenuation. Finally substitution for a_n into (16) yields the following equation for a_0:

$$\frac{L_+(ik)a_0 - 1 + (a_0/d)L_-(-ik)}{-L_+(ik)a_0 - 1 + (a_0/d)L_-(-ik)} = ig \quad (19)$$

where

$$g = \frac{k}{d} \sum_{m=1}^{\infty} \frac{c_m L_-(-\kappa_m)}{\kappa_m}.$$

Calculation of Reflection Coefficient

In problems involving discontinuities in waveguides, the quantity which is of physical importance is the reflection coefficient. In this section, we calculate this for the fundamental mode when $ka/\pi < 1$.

The reflection coefficient is the residue of $\phi_+(s, y)$ at $s = -ik$ and, from (9), it is given by

$$\frac{\phi_+'(-ik, d)}{2ikd} + 1 + \frac{g_0}{d}.$$

We have from (13)

$$\phi_+'(-ik, d) = \lim_{s \to -ik} \frac{1}{N_+(s)} \left\{\frac{N_-(-ik)}{s + ik} + \frac{1}{d} \sum_{m=0}^{\infty} \frac{N_-(-\kappa_m)\phi_+'(\kappa_m, d)}{\kappa_m(s + \kappa_m)}\right\}$$

and

$$N_+(s) \sim \frac{-a}{2ikdc} \frac{N_-(-ik)}{s + ik} \quad \text{as} \quad s \to -ik.$$

Thus the reflection coefficient R is given by

$$R = \frac{d}{a}\left(1 + \phi_+'\frac{(ik, d)}{2ikd}\right).$$

Substitution in (19) for $\phi_+'(ik, d)$ gives

$$ig = \frac{\dfrac{aR}{d} + \dfrac{L_+(ik)}{L_-(-ik)}\left\{\dfrac{aR}{d} - 1\right\}d}{\dfrac{aR}{d} - \dfrac{L_+(ik)}{L_-(-ik)}\left\{\dfrac{aR}{d} - 1\right\}d}. \qquad (20)$$

For simplicity it is now convenient to introduce the nondimensional expressions $H_+(s)$, $H_-(s)$ defined by

$$H_+(s) = \sqrt{\frac{dc}{a}}\,L_+(s), \qquad H_-(s) = \sqrt{\frac{a}{dc}}\,L_-(s).$$

If this change of notation is made in (20), then, writing α for c/a, we obtain

$$\frac{\dfrac{R}{(1-\alpha)}\left\{1 + \dfrac{H_+^2(ik)}{\alpha}\right\} - \dfrac{H_+^2(ik)}{\alpha}}{\dfrac{R}{(1-\alpha)}\left\{1 - \dfrac{H_+^2(ik)}{\alpha}\right\} + \dfrac{H_+^2(ik)}{\alpha}} = ig. \qquad (21)$$

Eq. (21) may be inverted to give

$$R = \frac{\delta(1 + ig)H_+^2(ik)}{\alpha + H_+^2(ik) - ig(\alpha - H_+^2(ik))} \qquad (22)$$

where δ is written for $1-\alpha$. The expressions in the Appendix clearly indicate that $|H_+(ik)| = 1$ and hence that $H_+(ik)$ may be written as $e^{i\theta}$ (with θ real).

It is instructive to consider the physical significance of the expression defined by (22) when $g=0$. This expression may be derived from physical considerations, as will now be shown. We assume that the step is absent, and superimpose a field Ae^{-ikx} incident from the region $0 \le y \le d$, $x \le 0$ on the original field. This incident field will cause a wave AR_1e^{+ikx} to be reflected back in the negative x direction (R_1 may be calculated by use of the Wiener-Hopf technique) and we thus find that the total velocity component of the potential in the fundamental mode for $y \le d$, $x \le 0$ is

$$AR_1e^{ikx} + e^{ikx} + Ae^{-ikx}$$

and we choose A so that the partial derivative of this expression with respect to x vanishes on the line $x=0$, $0 \le y \le d$. If this is done, then the transmission coefficient for the problem of a wave Ae^{-ikx} incident in the region formerly occupied by the step is seen to agree with the expression of (22) for $g=0$. Thus we see that the expression (22) illustrates the connection which was alluded to in the first section between the bifurcation and the step problems. The assumption $g=0$ of course merely implies that Ψ is constant over the short vertical part of the step. For $ka < \pi$, it is possible to compare the present results with those given in the "Waveguide Handbook," and, since the solution given there is an equivalent circuit formulation, the present results have to be recast in this form. The equivalent circuit is

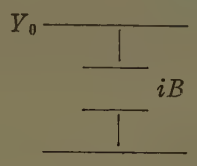

$$\frac{Y_0}{Y_0'} = \frac{1}{\alpha}$$

where Y_0, Y_0' are the characteristic admittances of the two guides and B is purely real. $B/Y_0' = C$ may be expressed in terms of the reflection coefficient R, and we have

$$iC = -\frac{\{(\alpha+1)R + (\alpha-1)\}}{\alpha(R-1)}. \qquad (23)$$

If the expression for R in terms of g is inserted in (23) then we obtain

$$C = \frac{\delta}{\alpha}\left\{\frac{\sin\theta + g\cos\theta}{\cos\theta - g\sin\theta}\right\}. \qquad (24)$$

Inspection of this expression for C shows that it may be obtained by applying the above simple argument for determining the reflection coefficient to the case in which the bifurcation extends a distance $\tan^{-1} g$ to the right of the origin, and we then obtain the exact form of C. Thus the reflection coefficient for the step problem is the same as the transmission coefficient for the bifurcation problem mentioned above, when the bifurcation extends a distance $\tan^{-1} g$ further towards the positive x direction than the original step structure.

Comparison with the Results of the "Waveguide Handbook"

Some simplification will be afforded if (18) is rewritten in dimensionless form by making the substitutions given in the preceding section and defining a new set of constants d_n as $c_n d^{-1/2}$. The following equation is then satisfied by the d_n:

$$H_+(\kappa_n)d_n = \alpha^{1/2} - \alpha\sum_{m=1}^{\infty}\frac{d_m(\mu_m\mu_n - \epsilon^2)}{\mu_m(\mu_m + \mu_n)}H_-(-\kappa_n) \qquad (25)$$

where $\epsilon = kd/\pi$ and $\mu_m^2 = m^2 - \epsilon^2$. The function g may now be written in dimensionless form as $\epsilon f \alpha^{1/2}$ where

$$f = \sum_{m=1}^{\infty} d_m H_-(-\kappa_m)/\mu_m.$$

The formulas are now in the simplest form possible and are suitable for comparison with the results of the "Waveguide Handbook." First of all we shall consider the special case of neglecting all powers of $\epsilon \ge 2$. To this order of approximation it may be shown that for $m > 0$

$$H_+(\kappa_m) = \frac{A^m m!(m(1-\delta)/\delta)!}{(m/\delta)!}$$

where

$$A = \frac{\left(\frac{\delta}{1-\delta}\right)^{(1-\delta)/\delta}}{\delta^{1/\delta}}.$$

The argument of $H_+(ik)$ may be shown to be $\epsilon \log A$, and we thus have

$$\frac{C}{\epsilon} = \frac{\delta}{\alpha}(\log A + \alpha^{1/2} f).$$

The amount of computation involved in this special case is fairly small, since to the present order of approximation the μ_m's reduce to m. Eq. (25) has been solved on the assumption that all the coefficients, apart from the first five, vanished. This gives for $\delta = \frac{1}{2}$ the result C/ϵ $(\epsilon = 0) = 1.556$, while the corresponding result in the "Waveguide Handbook" is 1.364. For $\delta = 0.8$ the present method gives $C/(ka/\pi) = 2.45$ while the value in the "Waveguide Handbook" is 2.48.

In order to test further the accuracy of the present approach, the general expressions developed in the Appendix were used to calculate $H_-(-\kappa_m)$ for certain values of ϵ, and an approximate solution of (25) was obtained. The calculations were carried out for $\epsilon = 4$, $\delta = \frac{1}{2}$; $\epsilon = 0.64$, $\delta = 0.8$; and the values obtained for C were 0.954 and 3.67. The values given in the "Waveguide Handbook" are 0.96 and 3.73. The values of ϵ and δ were chosen so that ka/π ranges from 0 to 0.8; hence if there were any large deviation between our results and those in the "Waveguide Handbook," it would have been evident in the numerical results. It is thus evident that there is very good agreement between both methods, and that the solution of the first five equations is sufficient to give a very accurate answer. In fact, complete neglect of g produces a percentage error of less than 30 in the expression for C while the percentage error in R will of course be considerably less (*i.e.*, a very large error in determining g does not produce an equally large error in the expressions for R and C). This indicates that the assumption of a constant value for Ψ on the vertical step is a fairly satisfactory one.

The Case of $ka/\pi > 1$

We now consider the modifications which have to be made to the above analysis when $ka/\pi > 1$ but kc/π $kd/\pi < 1$. One difference is that there will be a term in Ψ which behaves as $\exp(-i\eta x)$, where

$$\eta = (k^2 - \pi^2/a^2)^{1/2},$$

as $x \to \infty$ and η is now real. The coefficient of $\exp(-i\eta z)$ may be found, after some manipulation, to be

$$-\frac{\cos \pi y}{a} \frac{2\sqrt{2}\epsilon\sqrt{\alpha\delta}}{(\beta+\epsilon)} \cdot \left\{1 - \frac{2i(\epsilon-\beta)}{\delta(1+i\epsilon f\alpha^{1/2})} \sum_{m=1}^{\infty} \frac{e_m(\mu_m + i\epsilon)}{\mu_m - i\beta}\right\} \mathrm{Re}^{i\phi}$$

where $e_m = d_m H_-(-\kappa_m)\mu_m$, $\beta = (\epsilon^2 - \delta^2)^{1/2}$, and

$$\phi = -\left\{S_1(\beta, \delta, 0) + S_1\left(\frac{(1-\delta)\beta}{\delta}, \alpha, 0\right) - S_1\left(\frac{\beta}{\delta}, 1, 0\right) - S_1(\epsilon, 0, 0) - S_1\left(\frac{\epsilon(1-\delta)}{\delta}, 0, 0\right) - S_2\left(\frac{\epsilon}{\delta}, 0, 0\right) - \frac{(\epsilon-\beta)}{\delta}(1 + \alpha \log \alpha + \delta \log S)\right\}$$

and

$$S_N(x, \alpha, \beta) = \sum_{n=N}^{\infty} \left\{\sin^{-1} \frac{x}{\sqrt{(n-\beta)^2 - \alpha^2}} - \frac{x}{n}\right\}.$$

The S_N's are tabulated in the "Waveguide Handbook." The above expressions are now in the most convenient dimensionless form for numerical computation.

Another different feature of the case $ka/\pi > 1$ is that the functions $H_-(-\kappa_n)$ are no longer real and we have

$$H_+(\kappa_m) = \frac{1}{\delta}(\mu_m + i\beta)G_+(\kappa_m)$$

where the G_+'s are real. The equation for the new unknowns e_n defined above is

$$\mu_n e_n H_+^2(\kappa_n) = \alpha^{1/2} - \alpha \sum_{m=1}^{\infty} \frac{e_m(\mu_m\mu_n - \epsilon)^2}{(\mu_m + \mu_n)}. \quad (26)$$

Eq. (26) may be written as two sets of real equations as follows:

$$\frac{\mu_n f_n}{\alpha\delta^2} G_+^2(\kappa_n)(\mu_n^2 - \beta^2) - 2\beta \frac{\mu_n^2 g_n G_+^2(\kappa_n)}{\alpha\delta^2} = \alpha^{-1/2} - \sum_{m=1}^{\infty} f_m \frac{(\mu_m\mu_n - \epsilon^2)}{(\mu_m + \mu_n)}, \quad (27)$$

$$\frac{G_+^2(\kappa_n)\mu_n}{\alpha\delta^2}(\mu_n^2 - \beta^2)g_n + \frac{2\beta\mu_n^2 G_+^2(\kappa_n)}{\alpha\delta^2} f_n = -\sum_{m=1}^{\infty} g_n \frac{(\mu_m\mu_n - \epsilon^2)}{(\mu_m + \mu_n)} \quad (28)$$

where $e_n = f_n + ig_n$.

It is possible to reduce (27) and (28) to two sets of linearly-independent equations, but since in the present case they were solved on the digital computer, there does not appear to be any advantage gained by their reductions. The above equations also have the advantage that they are in a form from which it is fairly simple to estimate the error involved in their solution. It is possible to estimate the error made in solving only a finite number of the above equations. The analysis, which requires the establishing of various inequalities for the functions occurring in the equations, will not be presented here, but it is available in the author's report.[4]

[4] W. E. Williams, "Step Discontinuities in Waveguides," Res. Rep. No. EM-77, Inst. Math. Sci., New York University, New York, N. Y., April, 1955.

Numerical Results

The set of equations occurring for the case $ka/\pi > 1$ was solved by assuming that f_n, $g_n = 0$ for $n > 5$. Since there is no particular physical significance in the actual numerical values of the coefficients f_n and g_n, they have not been tabulated. One quantity which is of particular interest is the reflected energy crossing a plane normal to the x axis which will be proportional to

$$\lim_{x\to\infty} \int_0^a \Psi^* \frac{\partial \Psi}{\partial x}\, dy,$$

where the asterisk indicates the complex conjugate. If the coefficient of $e^{-i\eta x}$, referred to in the foregoing section, is written as $R_1 \cos \pi y/a$, then the above integral may be evaluated to give

$$-ia\{k|R|^2 + \tfrac{1}{2}\eta |R_1|^2\}.$$

Hence the (reflected energy/incident energy) ratio is

$$|R^2| + \frac{\beta}{2\epsilon}|R_1|^2.$$

The two quantities

$$|R|^2,\ |R|^2 + \frac{\beta}{2\epsilon}|R_1|^2 = |R_2|^2,$$

are given in Table I. The numerical values show that the ratio of the reflected energy to the incident energy increases, for constant step height, as the waveguide height decreases. This, of course, was to be expected on physical grounds. The percentage of the reflected energy which is due to the $|R_1|^2$ tends to increase as the waveguide height decreases for constant step height. This percentage is, however, fairly constant, ranging between 19 and 25 per cent for all the values given in Table I.

TABLE I

	$\epsilon=0.9$			$\epsilon=0.8$				$\epsilon=0.7$				$\epsilon=0.6$	
ka/π	1.8	1.6	1.4	1.7	1.6	1.4	1.2	1.6	1.4	1.2	1.1	1.5	1.4
$\|R\|^2$	0.25	0.32	0.41	0.23	0.26	0.34	0.47	0.20	0.28	0.39	0.49	0.17	0.20
$\|R_2\|^2$	0.31	0.40	0.52	0.29	0.33	0.44	0.58	0.25	0.35	0.31	0.63	0.21	0.26

The values obtained for $|R|^2$ were compared with those obtained by assuming that all the coefficients of the set of equations vanish, and the two results were found to differ by only a few per cent in all cases. The difference between the two values obtained for $|R_1|^2$ was greater, but this contributes only a small amount to the total energy. It thus appears that a very good estimate may be obtained for the reflected energy by assuming a constant value of the magnetic field on the step. In all cases the values obtained for f_1 and g_1 did not differ by more than 5 per cent from those obtained by assuming that f_1 and g_1 were the only nonvanishing coefficients.

Appendix

In this appendix, formulas are developed which may be used for computing the functions $N_+(\kappa_m)$. If the same method is employed as that used by Carlson and Heins[5] then it is fairly easily shown that

$$N_+(s) = \frac{1}{(s+ik)}\sqrt{\frac{a}{dc}}\,\frac{P(\delta)}{P\left(\frac{\delta}{1-\delta}\right)P(1)} \cdot \exp\frac{s\{a\log a - c\log c - d\log d\}}{\pi},$$

$N_-(-s)\,N_+(s) = -1$, where

$$P(\delta) = \prod_{n=1}^{\infty}\left\{\left(1 - \frac{\epsilon^2}{\delta^2 n^2}\right)^{1/2} + \frac{s\epsilon}{k\delta n}\right\}\exp\left[-\frac{s\epsilon}{k\delta n}\right].$$

It is not really necessary to retain the exponentials in the above infinite products when the complete expression for $N_+(s)$ is being considered, but they must be retained for evaluating each separate product. For generality we shall consider the evaluation of each of the products separately since products of a similar nature occur in the other problems of diffraction theory and only slight modification of the following analysis will be required to cover other cases.

It is clear from the expressions occurring in the text that we must compute expressions of the form

$$\prod_{n=1}^{\infty}\left\{\left(1 - \frac{k^2a^2}{n^2\pi^2}\right)^{1/2} + \frac{\kappa_m a}{n\pi}\right\}\exp -\left(\frac{\kappa_m a}{n\pi}\right).$$

Though most of the computations involved in this work were carried out on a digital computer it is also possible to obtain fairly convergent expansions in powers of ϵ^2 for the above products. These expansions are convergent for all the powers of ϵ and δ that occur, and have the advantage of being very much more suitable for numerical computation than straightforward multiplication of the terms of the product. In order to obtain the numerical values for a large number of values of ϵ and δ, the digital computer has a distinct advantage over any other form of computer. The program developed for the present problem has also been used for computing infinite products for which the approach used here may not be used (in these products the $n\pi$ in the infinite product was replaced by the nth zero of a Bessel function or of a transcendental equation involving Bessel and Hankel

[5] F. Carlson and A. E. Heins, "Diffraction by a pair of parallel plates," *Quart. Appl. Math.*, vol. 4, pp. 313; 1947.

functions). The following formulas are suitable when not too many values of ϵ and δ are required, and the computations for $ka/\pi<1$ were carried out using these formulas. Expansion of

$$\left(1-\frac{k^2a^2}{n^2\pi^2}\right)^{1/2}$$

and κ_m in powers of ϵ^2, together with some algebraic manipulation, gives the following result for $m\neq 0$

$$\prod_{n=1}^{\infty}\left\{\left(1-\frac{k^2a^2}{n^2\pi^2}\right)^{1/2}+\frac{\kappa_m a}{n\pi}\right\}\exp\left[-\frac{\kappa_m a}{n\pi}\right]$$

$$=\prod_{n=1}^{\infty}\left(1+\frac{m}{\delta n}\right)\exp\left\{-\frac{m}{\delta n}\right\}\exp P_m(\delta)$$

$$=e^{-(jm/\delta)}\left\{\frac{m!}{\delta}\right\}^{-1}\exp P_m(\delta)$$

where $x'_{n'}$ is the factorial function, j is Euler's constant and

$$P_m(\delta)=a_1\epsilon^4+a_2\epsilon^6+a_3\epsilon^8+a_4\epsilon^{10}+a_5\epsilon^{12}$$

where

$$8m\delta^3a_1=-\zeta(3),\quad 48m^3\delta^5a_2=-3m^2\zeta(5)-2\delta^2\zeta(3)$$

$$2^7m^5\delta^7a_3=-5m^4\zeta(7)-3m^2\delta^2\zeta(5)-3\delta^4\zeta(3)$$

$$5\cdot 2^9m^7\delta^9a_4=-35m^6\zeta(9)-140m^4\delta^2\zeta(7)+36m^2\delta^4\zeta(5)-20\delta^6\zeta(3)$$

$$3\cdot 2^{10}m^9\delta^{11}a_3=-63m^8\zeta(11)-35m^6\delta^2\zeta(9)-31m^4\delta^4\zeta(7)-30m^2\delta^6\zeta(5)-35\delta^8\zeta(3)$$

where $\zeta(s)$ is the Riemann Zeta function, *i.e.*,

$$\zeta(s)=\sum_{n=1}^{\infty}\frac{1}{n^s}.$$

The other two products in $N_+(\kappa_m)$ are of the same form as the above with a replaced by c and d respectively, and hence the above formulas can be extended to cover the other two products by replacing δ in the expressions for $a_1\cdots, a_5$ by $\delta/(1-\delta)$ and 1 respectively. These results are valid for $(\epsilon/\delta)<1$ but may be extended to include the case of $1<(\epsilon/\delta)<2$, $\epsilon<1$ as follows.

For $(\epsilon/\delta)>1$ the first term in the above infinite product will be complex, and hence if we consider the integer n as now ranging from 2 to infinity this new product may be treated exactly as before. The $\zeta(s)$ in the formulas for $a_1\cdots, a_5$ should now be replaced by $\zeta(s)-1$.

The case of $m=0$ requires special consideration. In this case the products occurring in $N_+(ik)$ may be written in the form

$$\exp i\left\{\sum_1^{\infty}\left(\sin^{-1}\frac{ka}{n\pi}-\frac{ka}{n\pi}\right)\right\}.$$

The functions occurring in this exponent have been extensively tabulated in the "Waveguide Handbook."

Acknowledgment

The author would like to acknowledge the permission of R. A. Brooker to use the digital computer at Manchester University for most of the computations involved in the text, and also the many helpful suggestions given by D. S. Jones during the period in which the present work was carried out.

The Transient Behavior of the Electromagnetic Ground Wave on a Spherical Earth*

JAMES R. WAIT†

Summary—**Some calculations are presented to show the nature of the transient ground wave radiated from an electric dipole which is situated over a spherical earth. The moment of the dipole is considered to vary with time in a linear manner. It is shown that the departure of the leading edge of the radiation field from a step function form is a consequence of diffraction and loss in the finitely conducting ground.**

* Manuscript received by the PGAP, February 17, 1956; revised manuscript received, October 26, 1956.

† National Bureau of Standards, Boulder, Colo.

Introduction

IT IS THE PURPOSE of the present paper to calculate the transient response of the ground wave due to a suddenly applied current at a source located over a spherical earth. With no subsequent loss of generality, the source can be considered to be an infinitesimal current element whose moment varies with time as a ramp function. Furthermore, the height of the vertical current source, whether it be a lightning channel or a man-made

transient electromagnetic source, can be synthesized by a line distribution of dipole sources. Since the observer, in most practical instances, is at a distance large compared to the height of the column, the radiated field is proportional to the instantaneous value of the surge current integrated over the length of the column.[1]

The extension of the responses calculated for the ramp source to the case of more complicated source functions such as lightning strokes can be calculated by superposition. As mentioned in the preceding paragraph, the analysis will treat only the omnipresent ground-wave pulse. The transient signal propagated via the ionosphere, albeit is the most important component at large distances, is not considered here.

The Steady-State Response

It is desirable to first illustrate the radiation from a harmonic source at very low radio frequencies. With respect to a spherical coordinate system (r, θ, ϕ) the earth's surface is defined by $r=a$ and the source is a radially oriented dipole of moment $P(\omega)$ with a time factor $\exp(i\omega t)$ located at $\theta=0$ and $r=a$. The earth is assumed to be homogeneous with conductivity σ and dielectric constant ϵ. It is convenient to express the field components in terms of a Hertz vector which has only a radial component U as follows:

$$E_r = \left[\beta^2 + \frac{\partial^2}{\partial r^2}\right]\left(\frac{r}{a}U\right) =$$

$$E_\theta = \frac{1}{r}\,\frac{\partial^2}{\partial r \partial \theta}\left(\frac{r}{a}U\right)$$

$$H_\phi = -\,i\epsilon_0\omega\,\frac{\partial U}{a\partial\theta} \qquad (1)$$

where $\beta = 2\pi/$free space wavelength and ϵ_0 is the dielectric constant of free space. Van der Pol and Bremmer[2] have shown that to a good approximation, U, for $r \simeq a$, can be expressed in the following form

$$U = 2U_0 W \qquad (2)$$

where U_0 is the Hertz potential of the primary field and W is the "Watson-type residue series" given by

$$W = (2\pi)^{1/2} X e^{-i(\pi/4+\theta/2)} \sum_{s=0}^{\infty} \frac{e^{-i\tau_s X}}{2\tau_s - 1/\delta^2} \qquad (3)$$

where $X = (\beta a)^{1/3}\theta$ and

$$\delta = -\,\frac{i}{(\beta a)^{1/3}}\,\frac{\beta_1^2/\beta^2}{[(\beta_1^2/\beta^2) - 1]^{1/2}}$$

with

$$\beta_1^2 = \epsilon\mu\omega^2 - i\sigma\mu\omega \simeq -\,i\sigma\mu\omega$$

and $\mu = 4\pi \times 10^{-7}$. The coefficients τ_s are related to the roots of an equation involving Hankel functions of order one third. They have been treated numerically in an extensive manner by Bremmer.[3] Since θ is not a large number, the primary Hertz potential is given by

$$U_0 = \frac{P}{4\pi i\omega\epsilon_0}\,\frac{e^{-i\beta D}}{D} \qquad (4)$$

where $D = a\theta$ is the distance from the source to the observer. Remembering now that E_r is a solution of the wave equation, it can be expressed as

$$E_r = -\,\frac{\dfrac{\partial}{\partial\theta}\left[\sin\theta\,\dfrac{\partial}{\partial\theta}\left(\dfrac{U}{a}\right)\right]}{r\sin\theta} \qquad (5)$$

so that the vertical field E on the surface of the earth is

$$E = [E_r]_{r=a} \simeq -\,\frac{1}{D}\,\frac{\partial}{\partial D}\,D\,\frac{\partial}{\partial D}\,(U) \qquad (6)$$

subject again to θ being small. The fact is now utilized that W is a slowly varying function of D compared to $\exp(-i\beta D)/D$, so that

$$E \simeq \frac{i\mu\omega P}{2\pi D}\left[1 - \frac{i}{\beta D} - \frac{1}{\beta^2 D^2}\right] e^{-i\beta D} W. \qquad (7)$$

For a highly conducting earth, W is near unity at short distances and the terms in powers of $1/D$, $1/D^2$, and $1/D^3$ can be identified as the radiation, induction, and static fields, respectively. It is to be noted that W is a correction factor which accounts for finite ground conductivity and diffraction. It modifies not only the radiation field, but also the induction and static fields at very low radio frequencies.

Using data[4] computed from (7), the amplitude and phase of the field E are plotted as a function of frequency in kilocycles per second in Figs. 1 and 2. The conductivity of the path is that of sea water ($\sigma = 4$ mhos/meter) and the effective earth's radius is taken to be four thirds that of the actual earth radius, to account for normal atmospheric refraction. The amplitude of the fields is normalized so that the radiation field at short distances is the same. In other words, the quantity that is plotted is $2\pi DE/i\mu\omega P$. The curves show clearly the effect of the induction and static fields at lower frequencies and shorter distances. At greater ranges, the relative amplitude drops appreciably as a result of diffraction by the earth's curvature and the phase lag increases consider-

[1] R. B. Morrison, "The variation with distance in the range 0–100 km of atmospheric waveforms," *Phil. Mag.*, vol. 44, pp. 980–986; June, 1953.

[2] B. Van der Pol and H. Bremmer, "The diffraction of electromagnetic waves from an electrical point source round a finitely conducting sphere, with applications to radio telegraphy and the theory of the rainbow," *Phil. Mag.*, vol. 24, pp. 141–175, July, 1937; pp. 825–864, November, 1937; vol. 25, pp. 817–834, June 1937; vol. 27, pp. 261–275, March, 1939.

[3] H. Bremmer, "Terrestrial Radio Waves," Elsevier Publishing Co., pp. 105–106; 1949.

[4] J. R. Wait and H. H. Howe, "Amplitude and Phase Curves for Ground-Wave Propagation in the Band 200 cps to 500 Kc," Natl. Bur. of Standards Circular 574, Washington, D. C.; May 21, 1956.

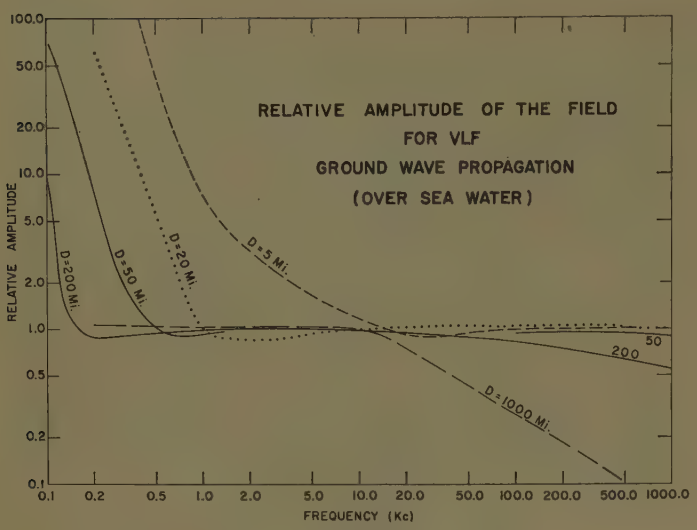

Fig. 1—The amplitude of the ground wave as a function of frequency.

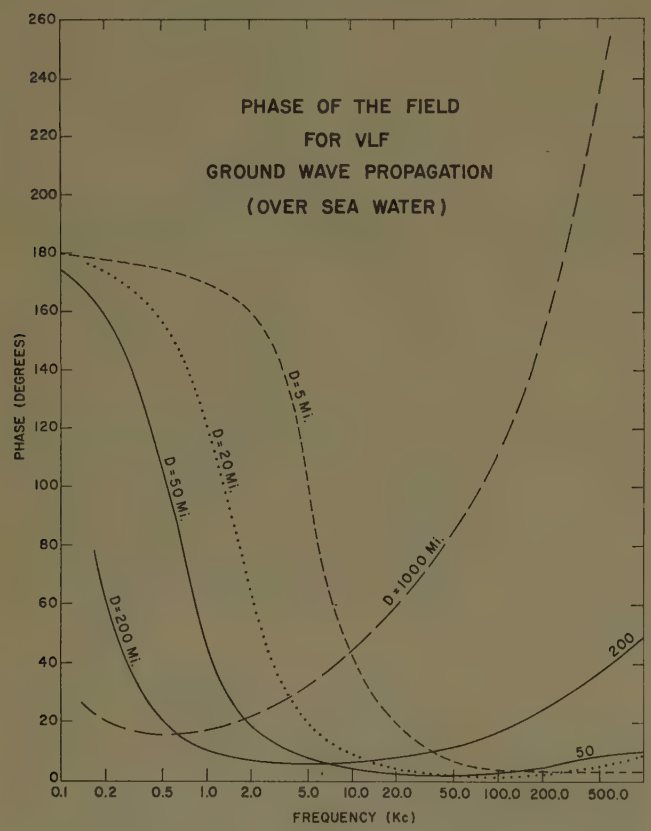

Fig. 2—The phase of the ground wave as a function of frequency.

ably. If the earth were flat and perfectly conducting, so that $W \simeq 1$, the relative amplitude curves would approach unity and the phase would approach zero at the higher frequencies.

The Transient Response

When the moment of the source varies as a function of time, the instantaneous response can be expressed, at least formally, by a Fourier integral, if the appropriate frequency spectrum for the source is employed. For example, if the product of the instantaneous height of the column times the instantaneous current is $p(t)$, then the frequency spectrum $P(i\omega)$ of the source is given by

$$P(i\omega) = \int_0^{+\infty} p(t)e^{-i\omega t}dt, \tag{8}$$

it being assumed that $p(t)=0$ for $t<0$. The field response $e(t)$ is then expressed by

$$e(t) = \frac{1}{2\pi i}\int_{-i\infty}^{+i\infty} E(i\omega)e^{i\omega t}d(i\omega) \tag{9}$$

where

$$E(i\omega) = \frac{i\omega\mu P(i\omega)}{2\pi D}e^{-i\omega D/c}\left[1+\frac{c}{i\omega D}+\frac{c^2}{(i\omega D)^2}\right]W(i\omega) \tag{10}$$

and $c=(\epsilon_0\mu)^{-1/2}=3\times10^8$ meters per sec. The expression $W(i\omega)$ is identical to the W defined in (3) where it is emphasized here that it is a function of $i\omega$. The principle task is to evaluate the contour integral for $e(t)$. The difficulty of this task stems from the complexity of the function $W(i\omega)$ which is in the form of a residues series whose individual terms themselves are rather complicated functions of $i\omega$. In a previous paper[5] a method for evaluating the contour by operational methods was described which was suitable for shorter ranges where the earth could be regarded as nearly flat. The formulation developed there regarded the diffraction by the earth's curvature as a correction to the flat-earth Sommerfeld formula, and consequently, $W(i\omega)$ could be expressed in a more convenient form.

At large distances, where diffraction plays a major role in the analytic behavior of $W(i\omega)$, it seems necessary to evaluate the contour integral for $e(t)$ by numerical means. A method for doing this has been described by the author,[6] which is particularly suitable if the real part of $E(i\omega)$, when plotted on a log ω base, can be approximated by a series of straight line segments. To apply this method, the function $E(i\omega)$ is written

$$E(i\omega) = \sum_{m=1}^{M} A_m \frac{1}{(i\omega)^m} + R(\omega) + iX(\omega) \tag{11}$$

where M is a finite integer and where $R(\omega)$ and $X(\omega)$ are real and have no poles on the real axis of ω. The first term contains the singularities of $E(i\omega)$ on the imaginary axis of $i\omega$ (*i.e.*, on the real axis of ω) that can be introduced by the frequency spectrum $P(i\omega)$ of the source. The coefficients A_m are the residues of these poles. Subject to the restriction that there are no poles of $E(i\omega)$ in the right-hand part of the complex plane of $i\omega$, it follows that

[5] J. R. Wait, "Transient fields of a vertical dipole over a homogeneous (gently) curved ground," *Can. Jour. Phys.*, vol. 34, pp. 27–35; January, 1956.

[6] J. R. Wait, "An approximate method of obtaining the transient response from the frequency response," *Can. Jour. Tech.*, vol. 31, pp. 127–131; March, 1953.

$$e(t) = \sum_{m=1}^{M} A_m \frac{t^{m-1}}{(m-1)!} + e'(t) \qquad (12)$$

where

$$e'(t) = \frac{a}{\pi} \int_0^\infty R(\omega) \cos \omega t d\omega.$$

As shown in the earlier paper,[6] $e'(t)$ can be approximated by

$$e'(t) \simeq \frac{2}{\pi} \sum_{n=1}^{N} B_n [Si(\omega_{n-1}t) - Si(\omega_n t)] t^{-1} \qquad (13)$$

where

$$Si(z) = \int_0^z \frac{\sin x}{x} dx$$

is the sine integral and B_n is the slope of the segment of the $R(\omega)$ curve between the points ω_{n-1} and ω_n and is defined by

$$B_n = \frac{R(\omega_n) - R(\omega_{n-1})}{\log (\omega_n/\omega_{n-1})}. \qquad (14)$$

In applying the above formula it is convenient to take $\omega_0 = 0$ and ω_1 the angular frequency where $R(\omega)$ departs from its static value so as to make $B_1 \simeq 0$. On the other hand, ω_N is taken at a sufficiently large value so as to have $R(\omega_N) \simeq 0$. The number of intervals is chosen so as to obtain the degree of accuracy required. In the present instance, N is taken to be 10.

To illustrate the fundamental character of the transient response, it is considered desirable to choose a source that would give rise to a radiation field on a flat perfectly conducting earth in the form of step function. This is effected by taking the moment $p(t)$ to be a linearly rising current or a "ramp" function at $t=0$. That is

$$p(t) = P_0(t/t_0) \text{ for } t > 0 \qquad (15)$$
$$= 0 \text{ for } t < 0.$$

The frequency spectrum of the source is then given by

$$P(i\omega) = P_0(1/i\omega)^2/t_0. \qquad (16)$$

Using the steady frequency response data[4] of $W(i\omega)$ calculated for frequencies from 200 cps to 500 kc, the approximate method described above is used to calculate the transient response $e(t)$ to the ramp function source. For purpose of presentation, the response is written

$$e(t) = \frac{P_0 \mu_0}{2\pi D t_0} A(t') \qquad (17)$$

where $t' = t - D/c$. On a flat perfectly conducting earth, $W(i\omega) = 1$, and consequently

$$A(t') = 1 + \left(\frac{c}{D}\right)t' + \left(\frac{c}{D}\right)^2 \frac{(t')^2}{2} \text{ for } t' > 0$$
$$= 0 \text{ for } t' < 0.$$

That is, for short times ($t' \ll D/c$) the response is characterized by a step function. For longer times, the terms proportional to t' and $(t')^2$ which are the induction and static fields, respectively, become significant. The response for ground conductivities of 4, 10^{-2}, and 10^{-3} mhos per meter are shown in Figs. 3, 4, and 5, respectively. The departure of the leading edge of the waveform from a step function is a consequence of diffraction and the losses due to the finite ground conductivity. It can be seen that for large distances of the order of 1000 miles, the radiation component of the ground-wave pulse takes the order of 100 microsecs to build up to one half its final value. Since the induction and static fields are present, the response function $A(t')$ actually rises above unity although this is not noticeable at larger distances for times less than one millisecond. The rise time at short distances in the range from 50 to 100 miles is very rapid. At these distances the effect of ground conductivity is more significant and diffraction plays a negligible role. In fact, at a distance of 75 miles the response for an all sea water path ($\sigma \simeq 4$) has risen to about 0.95 at 1.0 microsecond. For the all land paths with conductivities of 10^{-2} and 10^{-3} the corresponding responses at 1.0 microsecond are 0.8 and 0.2 respectively.

The response function $A(t')$ for the conductivities of 10^{-2} and 10^{-3} and for distances of 37 Mi and 75 Mi which are included in Figs. 4 and 5 can be compared directly with those calculated in an earlier paper[5] by an altogether different method. In the previous work, the integrations could be carried out by analytic means for these short distances. The agreement between the two sets of results is good.

Conclusion

While the transient responses were calculated explicitly for a ramp function source, it is not difficult to extend the results to more complicated sources. The response $\bar{e}(t)$ to a source function $p(t)$ can be written in terms of $e(t)$ the response to the ramp function $p_0 t/t_0$ as follows

$$\bar{e}(t) = \frac{t_0}{p_0} \int_0^t e(\tau) g(t-\tau) d\tau \qquad (18)$$

where

$$g(t) = \frac{1}{2\pi i} \int_{-i\infty}^{+i\infty} (i\omega)^2 P(i\omega) e^{i\omega t} d(i\omega).$$

In general, the convolution integral representation for $\bar{e}(t)$ must be evaluated by numerical means. A particular type of source that is convenient to handle by this method is the "tent" pulse. It may be represented in the following way:

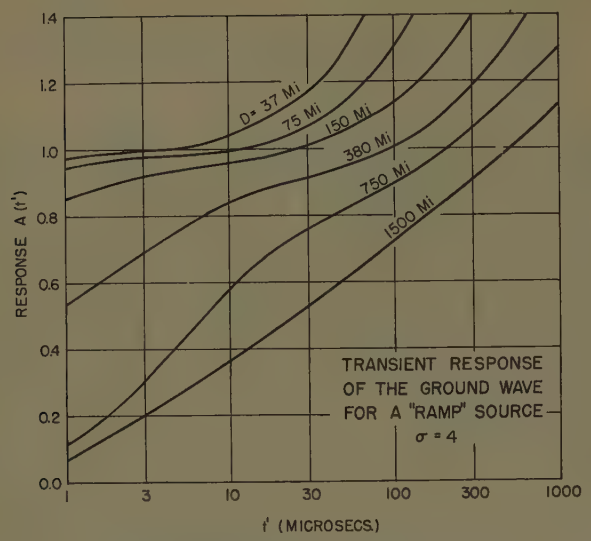

Fig. 3—The transient response of the vertical electric field at various distances *over sea water* ($\sigma=4$) from a source whose moment varies as a "ramp" function.

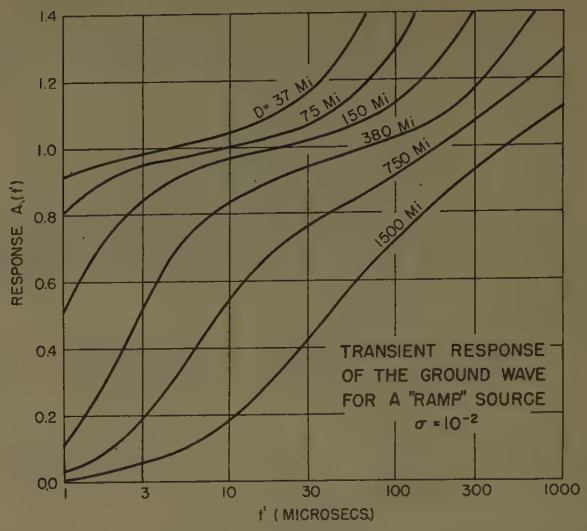

Fig. 4—The transient response of the vertical electric field at various distances *over land* ($\sigma=10^{-2}$) from a source whose moment varies as a "ramp" function.

$$p(t) = \frac{p_0}{t_0}\left[tu(t) - \frac{(t-t_1)t_2u(t-t_1)}{t_2-t_1} + \frac{(t-t_2)t_1}{t_2-t_1}u(t-t_2)\right] \quad (19)$$

where $u(t)=1$ for $t>0$, $=0$ for $t<0$. In this case the moment of the source rises in a linear manner from 0 at $t=0$ to p_0 at t_1 and then decays in a linear manner to 0 at $t=t_2$. The response $\bar{e}(t)$ is then given by

$$\bar{e}(t) = \left\{e(t) - e(t-t_1)\frac{t_2}{t_2-t_1} + e(t-t_2)\frac{t_1}{t_2-t_1}\right\} \quad (20)$$

where it is understood that $e(t_i)=0$ for $t_i<0$.

It is believed that the results in this paper shed some light on the transient behavior of the ground wave. It is hoped that the present analysis can be extended to include the reflections from the ionosphere which would of course mask the ground-wave pulse at longer times.[7]

[7] J. R. Wait and C. Froese, "Reflection of a transient electromagnetic wave at a conducting surface," *J. Geophys. Res.*, vol. 60, pp. 97–103; January, 1955.

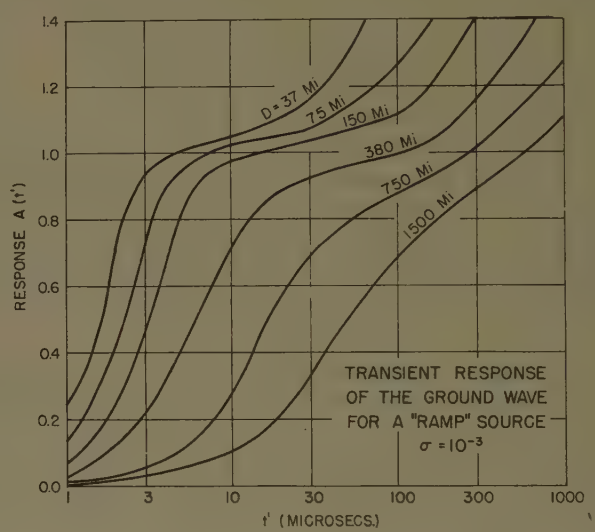

Fig. 5—The transient response of the vertical electric field at various distances *over land* ($\sigma=10^{-3}$) from a source whose moment varies as a "ramp" function.

Acknowledgment

I would like to thank A. Glenn Jean for suggesting this problem and for his continued interest. I am also indebted to Mrs. Anabeth Murphy and Miss Loris Perry for their assistance with the calculations.

An Experimental Investigation of the Diffraction of Electromagnetic Waves by a Dominating Ridge*

J. H. CRYSDALE†, J. W. B. DAY†, W. S. COOK‡, M. E. PSUTKA†, AND P. E. ROBILLARD†

Summary—**The diffraction of electromagnetic waves by a dominating tree-covered ridge north of Ottawa has been the subject of an experimental investigation. The measurements were made at 173, 493, and 1785 mc using both horizontally and vertically polarized radiation. The measurement period extended from late in the winter until early in the summer of 1955. The bulk of the experimental data consists of the results of height-gain and azimuth-gain measurements. Estimates of diffraction loss have been deduced from these results for the component of the radiation which was not reflected by the terrain between the ridge and the terminals of the experimental circuits. These deduced experimental diffraction losses exceed the predictions of Fresnel-Kirchhoff knife-edge diffraction theory, the discrepancies increasing with increasing frequency. There was no evidence of either a pronounced polarization dependence or a pronounced seasonal dependence.**

Introduction

THE EXPANDING use of nonoptical communication circuits at vhf and uhf has revived interest in the diffraction of electromagnetic waves by terrain irregularities such as hills, ridges, and mountains. In general, the geometrical and electrical characteristics of obstructions of this type preclude rigorous analyses and predictions of diffraction loss are often based on the Fresnel-Kirchhoff diffraction theory.[1] While this theory has the advantage of relative simplicity, it does not take into account such significant parameters as the radii of curvature at diffracting edges, the composition of the obstruction, and the polarization of the radiation. Nevertheless, it has been concluded for several of the circuits previously investigated that the diffraction losses deduced from experimental results are in good agreement with the values predicted by the Fresnel-Kirchhoff theory.

The purpose of this paper is to describe and present the results of an experimental investigation of the diffraction of electromagnetic waves by a dominating ridge north of Ottawa. This ridge constitutes a portion of the southern boundary of the Precambrian Shield and is heavily wooded, the trees being primarily of the deciduous type.

Experimental Method

The bulk of the experimental data consists of the results of height-gain and azimuth-gain measurements on two obstructed circuits traversing the ridge and on the line-of-sight circuits between a site on the top of the ridge and the terminals of the obstructed circuits. These measurements were made at three widely separated frequencies in the vhf and uhf bands (173, 493, and 1785 mc), using both horizontally and vertically polarized radiation. In order to investigate the possibility of seasonal effects, the measurement period extended from late in the winter until early in the summer of 1955. At the beginning of the period, the terrain was covered with snow. At the end of the period, the foliage was well advanced toward maturity.

The locations of the experimental sites and the salient topographical features are indicated in Fig. 1.

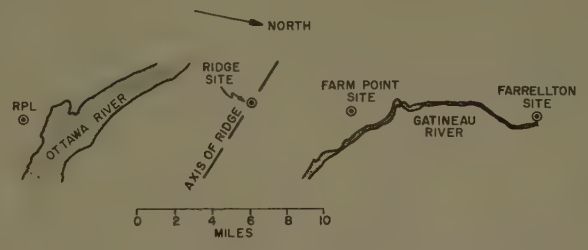

Fig. 1—Locations of the experimental sites.

One site was located to the south of the ridge at the Radio Physics Laboratory (RPL). Two sites were located to the north of the ridge, one near the village of Farm Point and the other near the village of Farrellton. The site on the top of the ridge was visible from the other three sites. Due to the restrictions imposed by the nature of the terrain and the availability of roads, it was not possible to find suitable sites which would lie exactly in a common vertical plane.

The vertical profiles of the obstructed circuits are presented in Figs. 2 and 3.[2] The terrain to the south of

* Manuscript received by the PGAP, August 31, 1956; revised manuscript received, December 19, 1956. This paper is based on RPL project rep. 34-0-3 (dated December 30, 1955) and represents work carried out under project PCC No. D48-38-03-21. Some of the results were presented in papers delivered at the 1955 Fall URSI meeting, Gainesville, Fla., December 15–17, 1955, and at the Canadian IRE Conv., Toronto, Ontario, October 1–3, 1956.

† Radio Physics Lab., Defence Res. Board, Ottawa, Canada.

‡ Federal Electric Corp., Streator, Ill., Formerly at the Radio Physics Lab., Defence Res. Board, Ottawa, Canada.

[1] A fairly complete bibliography of the previous theoretical and experimental work is contained in the following recent papers.

R. S. Kirby, H. T. Dougherty, and P. L. McQuate, "Obstacle gain measurements over Pike's Peak at 60 to 1046 mc," PROC. IRE, vol. 43, pp. 1467–1472; October, 1955. (It should be pointed out that sections of references 1, 7, and 8 of this paper were criticized by J. H. Crysdale, PROC. IRE, vol. 43, p. 627; May 1955. See also PROC. IRE, vol. 43, p. 874; July, 1955.)

K. A. Norton, P. L. Rice, and L. E. Vogler, "The use of angular distance in estimating transmission loss and fading range for propagation through a turbulent atmosphere over irregular terrain," PROC. IRE, vol. 43, pp. 1488–1526; October, 1955.

Some later work is presented in the paper by G. W. Swenson, Jr., "VHF diffraction by mountains of the Alaska range," PROC. IRE, vol. 44, pp. 1049–1050; August, 1956.

[2] Figs. 2 and 3 are based on the 31 G/5 West Half and 31 G/12 West Half 1:50,000 topographical sheets published by the Army Survey Establishment, Dept. of Natl. Defence, Ottawa, Canada. These profiles have been drawn for an effective earth radius equal to 4/3 true earth radius in order to compensate for tropospheric refraction.

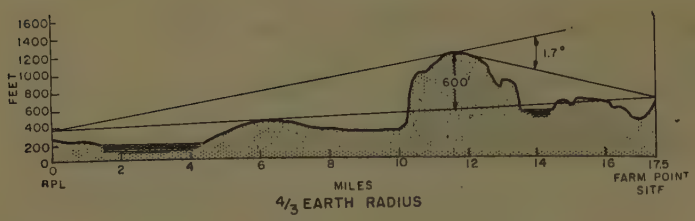

Fig. 2—Vertical profile of the RPL-Farm Point circuit.

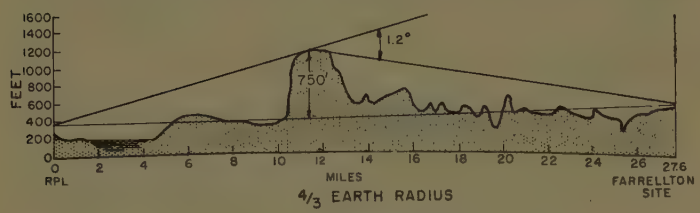

Fig. 3—Vertical profile of the RPL-Farrellton circuit.

the ridge is mainly gently rolling farm land. In contrast, the terrain to the north is more rugged and relatively heavily wooded.

Antenna height and azimuth angle were continuously variable at the sites to the south and north of the ridge due to the use of path testing towers.[3] The RPL tower was located on the roof of the laboratory, where its base was approximately 110 feet above the level of the Ottawa River. At Farm Point and Farrellton, the bases of the towers were located at ground level. Height and azimuth angle information was transmitted automatically and recorded simultaneously with the received signal levels. The antennas at the Ridge Site were mounted in fixed positions on a 50-foot scaffold tower.

Directional antennas were used at each of the experimental frequencies. Yagis, with gains of 10 db relative to an isotropic radiator, were used exclusively at 173 mc. At 493 mc, RCA Victor directional antennas (15 db) and a corner reflector (10 db) were employed. The antennas for the measurements at 1785 mc consisted of dipole-disk fed paraboloidal reflectors (24 db) and pyramidal horns (15 and 21 db). Except where stated otherwise, each antenna was mounted for horizontal beaming of the maximum in the main lobe of the free space antenna pattern. The vswr's at the terminals of the antennas were maintained at less than 1.1. Solid dielectric cables (RG-8 and RG-17) were used as transmission lines at the two lower frequencies. At 1785 mc, where the attenuation of solid dielectric cables was excessive, $\frac{3}{4}$ inch diameter Heliax cable[4] was employed.

The transmitters for the measurements on the obstructed circuits and on the optical RPL-Ridge circuit were located at RPL. These transmitters and the receivers at the other sites were modified components of commercial communications systems. Signal generators at the Ridge Site served as transmitters on the Ridge-Farm Point and Ridge-Farrellton optical circuits. All transmitters were operated unmodulated cw in order to facilitate power measurement and calibration. Power levels were monitored continuously at the transmitter output terminals. In addition, frequent measurements of absolute power were made at the output terminals of the transmission lines to the antennas. The receiving systems were calibrated at the input terminals to their transmission lines. All power meters and bridges were calibrated against one bridge which served as a standard.

[3] The towers used were the type described in a paper by R. D. Campbell, "Path testing for microwave radio routes," *Elec. Eng.*, vol. 72, pp. 571–577; July, 1953.

[4] Manufactured by the Andrew Corp., Chicago, Ill.

Experimental Results

Experimental results were obtained on the obstructed RPL-Farm Point circuit and its associated optical circuits from late in March until May 24, and on the obstructed RPL-Farrellton circuit and its associated optical circuits from May 25 until the end of June.

A number of experimental curves which illustrate some of the features of the results will now be presented and discussed. In general, the curves shown have been plotted in terms of a parameter Δ which represents the difference in decibels between experimental transmission loss and predicted free space transmission loss, assuming the experimental antenna gains for the calculation of the latter quantity. The sign of Δ is defined to be such that positive values correspond to signal levels in excess of the predicted free space levels.

In the results which follow, each height-gain curve represents the average of at least one run made by raising the antenna and one made by lowering the antenna. Similarly, each azimuth-gain curve is the average of at least one clockwise and one anticlockwise measurement.

Height-Gain Measurements

The results of some of the height-gain measurements at 493 mc are summarized in Figs. 4 and 5. The curves in Fig. 4 represent the results of measurements in which antenna height was varied at RPL while the signal level was recorded simultaneously at the Ridge and Farm Point Sites. Each of these pairs of curves have been superimposed for best fit in the region of minimum transmission loss. "Antenna height" refers to height above the base of the appropriate path testing tower. Some experimental curves obtained by varying antenna height at Farm Point are presented in Fig. 5. The measurements of Figs. 4 and 5(a) were preceded by the adjustment of RPL and Farm Point antenna azimuth angles for maximum received signal with the RPL antenna at the 59-foot level and the Farm Point antenna at the 112-foot level. For the measurements in Fig. 5(b), the Farm Point antenna was reoriented in azimuth at the 112-foot level for maximum received signal on the Ridge-Farm Point circuit.

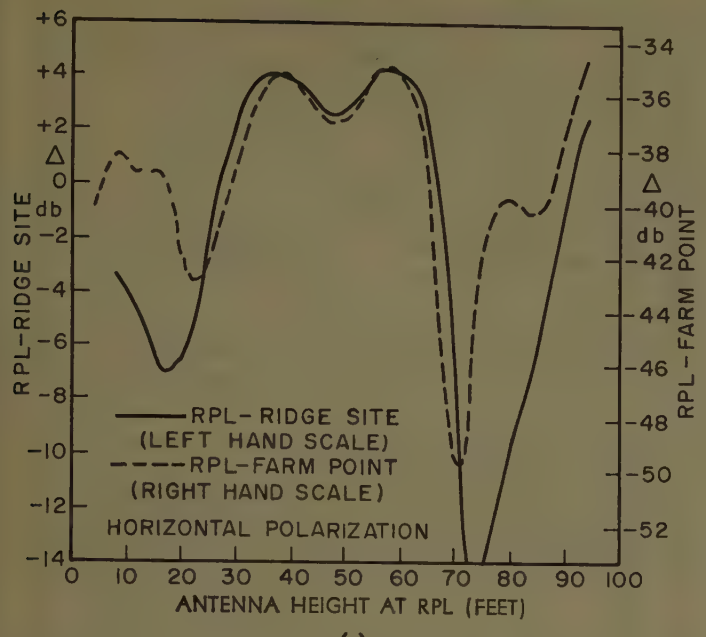

(a)

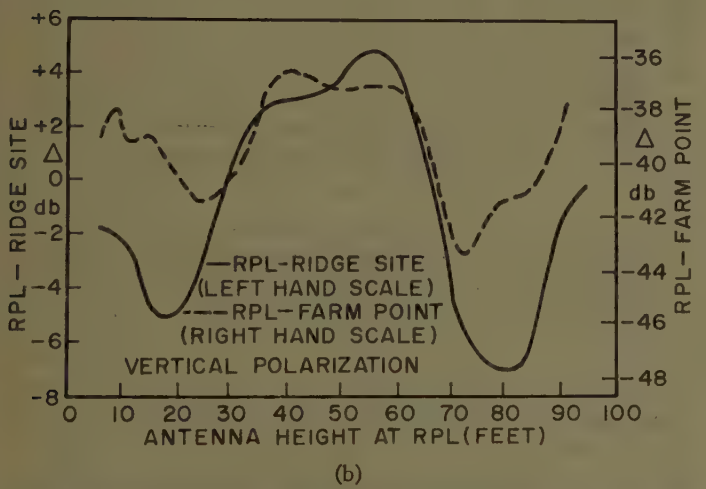

(b)

Fig. 4—Results of some height-gain measurements at 493 mc. In these measurements, antenna height was varied at RPL and the received signal recorded simultaneously at the Ridge Site and Farm Point. The Farm Point antenna was at the 112-foot level.

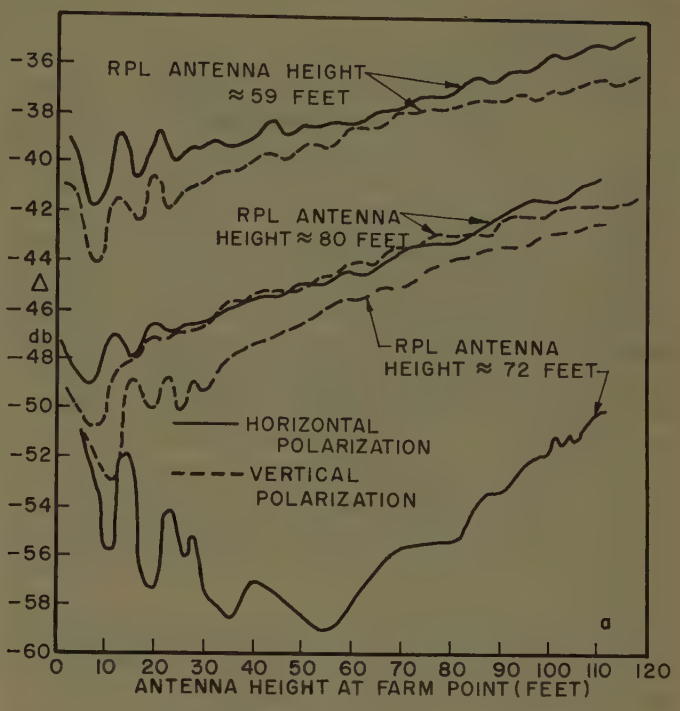

(a)

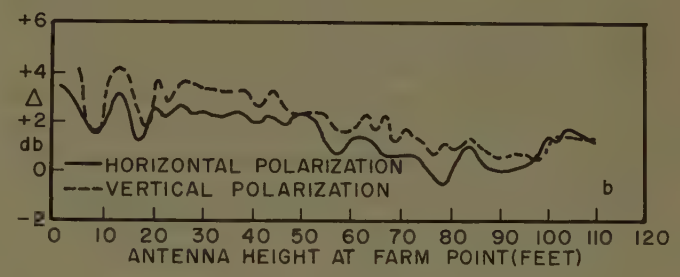

(b)

Fig. 5—Results of some 493 mc height-gain measurements in which antenna height was varied at Farm Point. (a) RPL transmitting. (b) Ridge Site transmitting.

It will be noted that each pair of height-gain curves in Fig. 4 is characterized by strong similarities but with some differences in detail. In particular, the maxima and minima were less pronounced on the obstructed circuit than on the optical circuit. Among the possible explanations for this are the following:

1) It is probable that the greater effective obstruction heights associated with the radiation reflected by the terrain between RPL and the ridge would result in the diffraction losses for this radiation being greater than for the unreflected radiation.
2) Additional regions of stationary phase might be expected to result from the nonuniform nature of the ridge. Such regions could make substantial contributions to the total signal level, particularly with the RPL antenna at heights for maximum destructive interference between the components of the direct diffracted signal.

In addition, some of the differences between the curves in each pair may be due to differences in the effective reflection coefficients resulting from the fact that the sites were not located in a common vertical plane. It is evident that the effective reflection coefficient of the terrain between RPL and the ridge for horizontal polarization was greater than for vertical polarization.

The height-gain curves in Fig. 5(a) were plotted from measurements obtained with the RPL antenna at two heights which produced maximum signal at Farm Point and at one height which gave minimum signal. Except for the result obtained using horizontal polarization with the RPL antenna at the height for minimum signal, the average levels are characterized by a similar approximately linear increase with Farm Point antenna height. In contrast, average signal levels for the Ridge-Farm Point circuit [Fig. 5(b)] actually decreased slightly with Farm Point antenna height. From these results it has been concluded that the variation of average levels on the obstructed circuit with Farm Point antenna

height was probably due to the ridge itself and not to the terrain between the ridge and Farm Point.

The striking differences in Fig. 5(a) between the shape of the curve for horizontal polarization with the RPL antenna at the height for minimum signal and the shapes of the other curves is probably a consequence of the polarization difference of the effective reflection coefficients of the terrain between RPL and the ridge. For vertical polarization, the magnitude of this coefficient evidently was sufficiently small that the direct diffracted signal predominated even when the RPL antenna was at a height associated with maximum destructive interference between the components of the direct diffracted signal. For horizontal polarization, however, it appears that the magnitude of this coefficient was sufficiently large that other mechanisms, such as propagation via secondary regions of stationary phase, made a significant contribution to the total signal level when the RPL antenna was at this height.

All of the curves in Fig. 5 are characterized by essentially similar fine structure. Antenna tilt measurements and an analysis utilizing the height separations between adjacent maxima and minima suggest that this structure was due to interference between the direct radiation and radiation reflected by the brow of the hill on which the Farm Point Site was located.

From the results presented in Figs. 4 and 5, it has been concluded that the terrain between RPL and the ridge made a much greater contribution to the total transmission loss for the obstructed circuit than did the terrain between the ridge and Farm Point. The corresponding experimental results indicate that this conclusion also applies at the other two frequencies. There were greater effects due to the terrain to the north of the ridge in the results of the measurements utilizing the Farrellton Site.

The height-gain results in Fig. 5 suggest a strong dependence of the diffraction loss on Farm Point antenna height. Such a dependence was evident also in the corresponding results at 173 and 1785 mc. On the other hand, it was concluded from the height-gain measurements on the RPL-Farrellton circuit that the diffraction losses for this circuit were not characterized by a marked dependence on Farrellton antenna height. Evidence of a strong diffraction loss dependence on RPL antenna height is not present in any of the height-gain results for either of the obstructed circuits with antenna height varying at RPL. (Fig. 4, for example.)

Azimuth-Gain Measurements

The azimuth-gain measurements included measurements in which 1) the azimuth angle of the transmitting antenna at RPL was varied and the signal level recorded simultaneously at the Ridge Site and at the site in operation to the north of the ridge, and 2) the antenna at the site in operation to the north of the ridge was rotated with RPL and the Ridge Site alternately

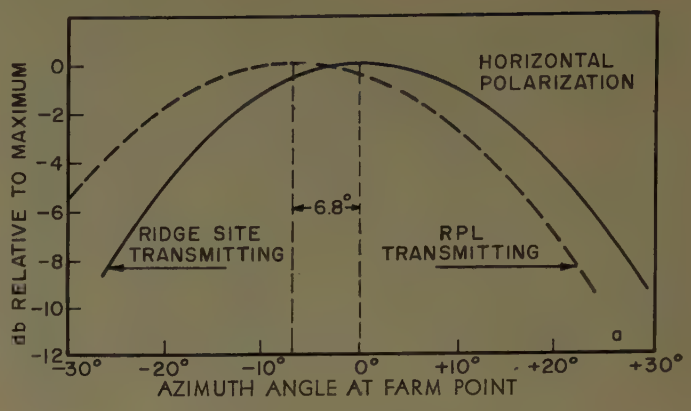

(a)

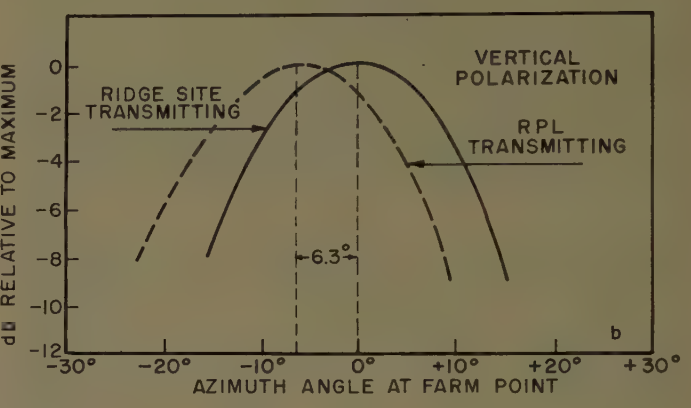

(b)

Fig. 6—Results of some azimuth-gain measurements at 493 mc. For each polarization, azimuth angle is measured from the direction for maximum signal on the Ridge-Farm Point circuit. RPL antenna height≈59 feet; Farm Point antenna height≈112 feet. At Farm Point, true azimuth of RPL relative to the Ridge Site ≈ −6.6°.

transmitting. Some results of measurements of the latter type are presented in Fig. 6. For these measurements, the RPL antenna was at a height which gave maximum signal at Farm Point (see Fig. 4). Prior to the measurements, the antennas at RPL and the Ridge Site were oriented for maximum received signal at Farm Point. It will be noted that the shapes of the individual curves in each pair are quite similar. In addition, the displacements of the maxima are approximately equal to the azimuth of RPL relative to the Ridge Site. Exact equality would be expected for a uniform horizontal knife-edge if the reflecting surfaces between the terminals and the obstruction were uniform and horizontal.

Some azimuth-gain measurements were made also with the RPL antenna at heights which yielded minima at the site in operation to the north of the ridge. Illustrative results are contained in Fig. 7. Their most significant feature is the shift in the azimuth angle for maximum signal on horizontal polarization with the RPL antenna at the height for minimum signal. This shift tends to substantiate the explanation previously advanced for the anomalous shape of the corresponding height-gain curve in Fig. 5(a).

The results presented in Figs. 6 and 7 suggest that, on 493 mc, the direct diffracted signal predominated at

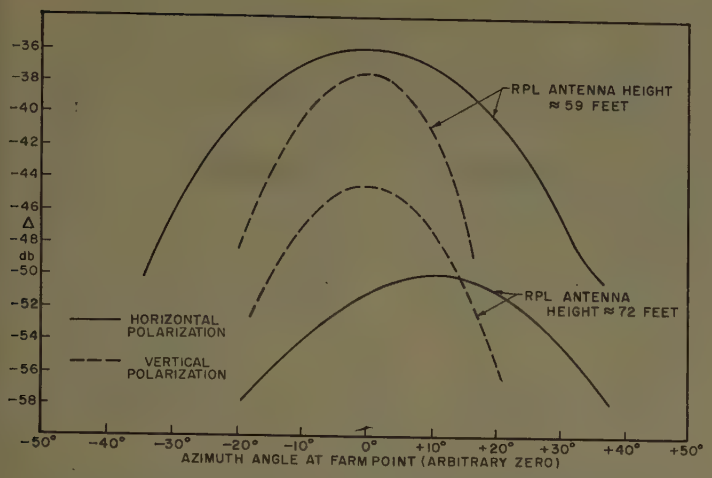

Fig. 7—Some results of 493-mc azimuth-gain measurements with the RPL antenna at a height for maximum signal at Farm Point (≈59 feet) and at a height for minimum signal (≈72 feet). Farm Point antenna height≈112 feet.

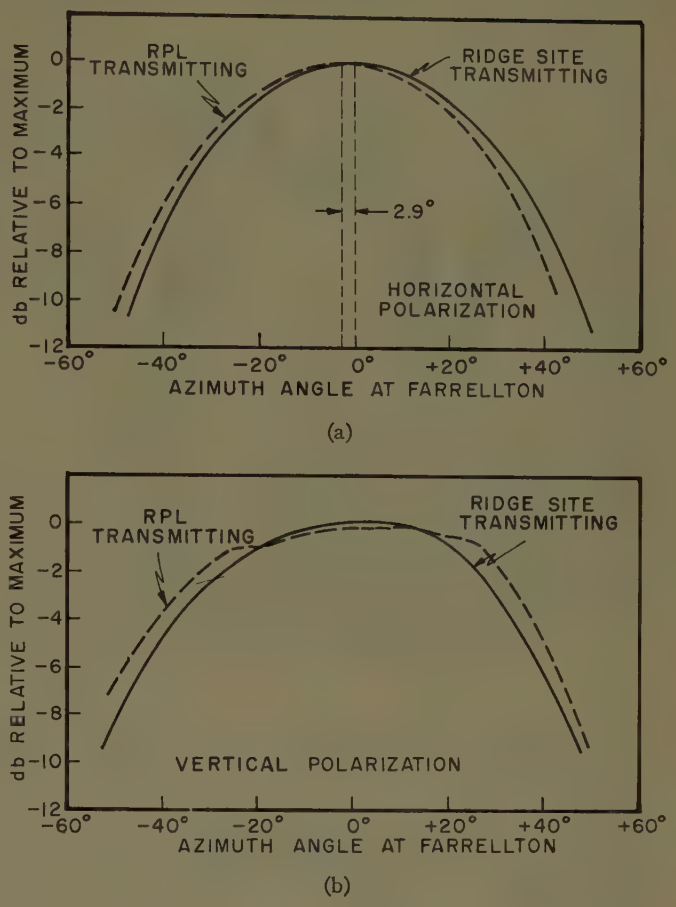

Fig. 8—Some results of 173-mc azimuth-gain measurements on the RPL-Farrellton circuit. At Farrellton, true azimuth of RPL relative to Ridge Site≈ −3.2°.

Farm Point when the RPL antenna was at a height for minimum transmission loss. This was not necessarily the case, however, when the RPL antenna was at heights which resulted in destructive interference between the components of the direct diffracted signal. Similar conclusions for the RPL-Farrellton circuit at this frequency and for both circuits at 1785 mc were deduced also from azimuth-gain measurements. Unfortunately, the situation was not so simple at 173 mc. At this frequency, the contributions of lateral multipath propagation were greater, particularly on vertical polarization. Fig. 8 illustrates the results obtained. For these measurements, antenna heights at RPL and Farrellton were those which resulted in minimum transmission loss. In the results for horizontal polarization, there are only minor differences in the shapes of the curves, and the displacement of the maxima is approximately equal to the true azimuth of RPL relative to the Ridge Site. With vertical polarization, there is evidence of considerable distortion in the result for the obstructed circuit. This distortion appears to be a flattening relative to the free space pattern. Similar 173-mc azimuth-gain measurements on the RPL-Farm Point circuit at equivalent antenna heights also indicated only slight distortion with horizontal polarization but considerable distortion with vertical polarization.

Temporal Effects

Most of the height-gain measurements were repeated on different days in order to investigate their reproducibility and the possibility of seasonal effects. Fig. 9, on page 208, is a representative example of the diagrams which were obtained from the superposition of these sets of experimental curves. April 4 was typical of winter conditions; the Ottawa River was frozen over and the terrain was covered with more than a foot of snow. During the next few days the snow melted and the ice broke up in the river. Shortly afterwards, the buds began to open on the deciduous trees and by the end of the first week in May the leaves were well advanced toward maturity. Undoubtedly some of the differences between the various experimental curves are due to experimental error and to atmospheric conditions. However, it seems reasonable to conclude that there is no evidence of a pronounced seasonal effect.

A few short-term fading recordings were made also. Some results are given in Fig. 10. For these measurements, the antenna at RPL was placed alternately at a height which produced maximum signal at Farm Point and at a height which yielded minimum signal. When the RPL antenna was at the former height, fixed attenuation was inserted between the receiver and its transmission line. There was no observable fading in the received signal with the RPL antenna at this height. The fading with the RPL antenna at the height for minimum signal may have been a consequence of the antiphased relationship between the direct and ground reflected radiation. With this relationship, a small change in path phase difference could result in a large relative increase in signal level. It is possible also that tropospheric scatter may have made a significant contribution to the total signal level with the RPL antenna at this height.

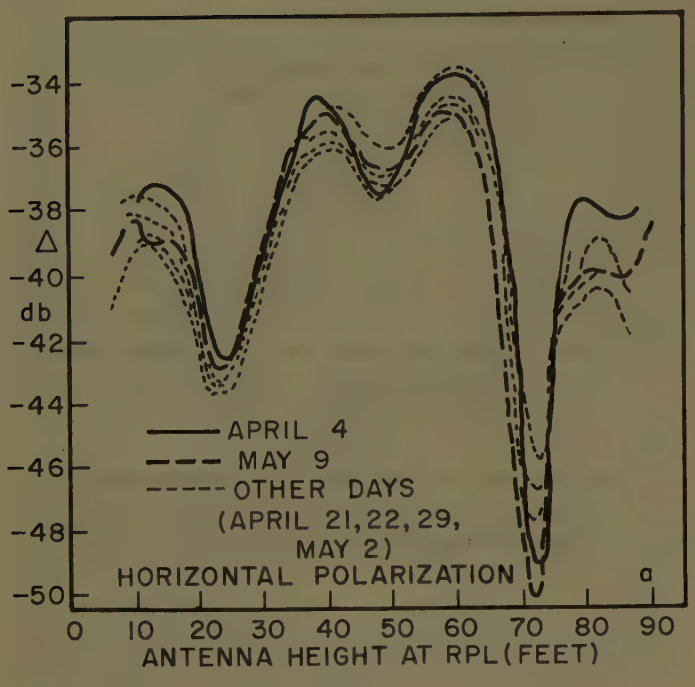

(a)

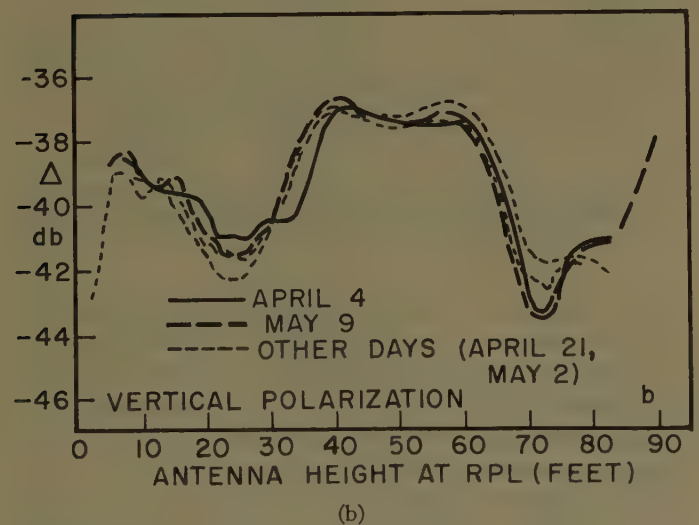

(b)

Fig. 9—Consolidated plot of 493-mc height-gain results obtained on the RPL-Farm Point circuit with antenna height varying at RPL and Farm Point antenna height≈112 feet. Measurements preceded by optimization of azimuth angles with RPL antenna height≈59 feet and Farm Point antenna height≈112 feet.

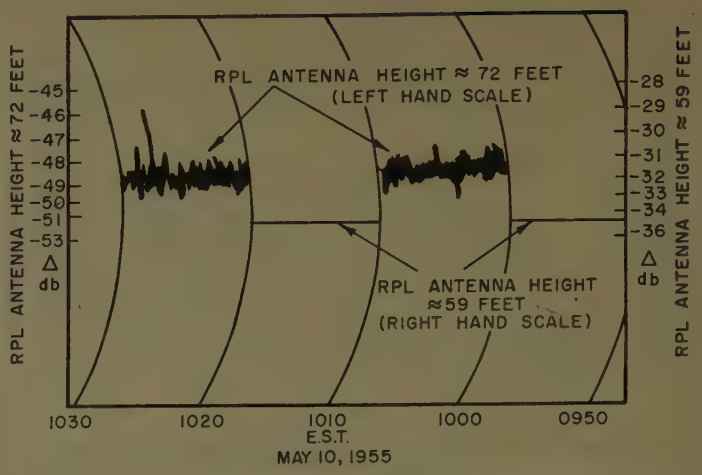

Fig. 10—Results of some short-term fading measurements at 493 mc on the RPL-Farm Point circuit. Horizontal polarization. RPL antenna alternately at a height for maximum signal at Farm Point (≈59 feet) and at a height for minimum signal (≈72 feet); Farm Point antenna height≈112 feet.

Diffraction Loss

Let L_D denote the diffraction loss of the component of the radiation which is not reflected by the terrain between the terminals of a singly obstructed circuit and the obstruction. In this section, estimates of L_D for the present circuits are deduced from the experimental results and then compared with the values predicted by knife-edge theory.

The condition which must be satisfied in order that L_D be essentially independent of antenna characteristics is that these characteristics be sufficiently uniform in the directions corresponding to the significant portions of the associated regions of stationary phase on the obstruction. In general, this condition would be most readily satisfied by obstructions which are characterized by only one such region. Examples are knife-edges and paraboloidal cylinders.

The widths of the theoretical first Fresnel zones on the ridge and the angles which they subtend at the terminals have been calculated for the present circuits on the assumption that the ridge can be regarded as a horizontal knife-edge inclined at an angle of 60° to each of the two vertical planes which contained the terminals. The results of these calculations and the minimum antenna beamwidth at each frequency are contained in Table I, opposite. It is evident that the angles subtended by the theoretical first Fresnel zones are considerably less than the antenna beamwidths. Consequently, it is concluded that the uniformity condition would be satisfied with respect to intensity by the knife-edge model if the antennas were beamed toward the centers of these zones. It would appear that the uniformity condition with respect to polarization was automatically satisfied by the essentially linear nature of the antennas. The phase characteristics of the antennas were not investigated. Nevertheless, it will be assumed that the free space equiphase surfaces were spherical over the significant range of directions.

The rotation measurements have revealed the existence of regions of stationary phase which are inconsistent with the knife-edge model. However, except for 173 mc on vertical polarization, these additional regions appear to have made significant contributions to the total signal level only when the antenna heights were such that there was considerable destructive interference between the components of the direct diffracted signal. Consequently, although it is possible that the single

TABLE I

THEORETICAL FIRST FRESNEL ZONES ON THE RIDGE AND ANTENNA BEAMWIDTHS

Frequency	Length of First Fresnel Zone		Angles Subtended at Terminals by First Fresnel Zone				Minimum Antenna Beamwidth (At 3-db Points)
			RPL-Farm Point		RPL-Farrellton		
	RPL-Farm Point	RPL-Farrellton	At RPL	At Farm Point	At RPL	At Farrellton	
173 mc	790 feet	1040 feet	0.64°	1.25°	0.84°	0.60°	50°
493 mc	470 feet	615 feet	0.38°	0.75°	0.50°	0.36°	18°
1785 mc	250 feet	325 feet	0.20°	0.39°	0.26°	0.19°	9°

regions of stationary phase postulated by the knife-edge model were actually composed of a number of regions not resolved by the antennas, the rotation measurements appear to justify reduction of the data in terms of the knife-edge model and comparison of the deduced experimental diffraction losses with the theoretical losses predicted by knife-edge theory, except at 173 mc on vertical polarization.

One of the major problems in the analysis of the experimental results was the elimination of the effects of the terrain between the terminals and the obstruction. In the extension of knife-edge theory which has been proposed for the inclusion of these effects,[1] additional "rays" are postulated, each "ray" being characterized by an appropriate diffraction loss and phase shift. However, if the differences between the diffraction losses and phase shifts associated with the various "rays" are sufficiently small, the "multi-ray" expression reduces approximately to a "one-ray" expression in which the effects of the intervening terrain are simply intensification or weakening of the "ray" which would exist in the absence of this terrain. If this simplification is valid and if the antennas are beamed toward the center of the region of stationary phase on the obstruction without cross-polarization loss, then

$$\Delta \approx -L_D + G_t + G_r \qquad (1)$$

where Δ and L_D are as previously defined, and G_t and G_r represent the effective increases in the directivities of the antennas toward this region of stationary phase due to the terrain between the terminals and the obstruction. Eq. (1) is least accurate at antenna heights corresponding to maximum destructive interference between the direct and ground reflected radiation. At these heights, Δ is most sensitive to the differences between the diffraction losses and phase shifts associated with the various "rays."

In the analysis of the experimental data, (1) was assumed to describe the effects of the intervening terrain under the required experimental conditions in the vicinity of antenna heights corresponding to minimum transmission loss. It is unlikely that a less approximate extension of knife-edge theory would be applicable at other heights because of the increased importance of the secondary regions of stationary phase on the ridge. For the measurements which were used in the analysis, the antennas actually were beamed horizontally instead of toward the top of the ridge. However, this probably did not cause significant error as the vertical angles involved were considerably less than the antenna beamwidths. (See Figs. 2 and 3, also Table I; for each circuit, the sum of the vertical angles was approximately equal to the angle of diffraction.)

The parameters G_t and G_r in (1) were identified with the appropriate Δ curves for the optical circuits. Consequently, some error resulted from the lack of exact coincidence of the reflection areas associated with the various obstructed and optical circuits. However, it is thought that the ensuing errors in the deduced values of L_D are of the order of 1 db at the most. Additional error is a likely consequence of the absence of a path-testing tower at the Ridge Site. Such a tower would have permitted the evaluation and elimination of the effects of the terrain in the vicinity of this site. Fortunately, the shapes of several of the height-gain curves obtained on the optical circuits are such that estimates can be deduced of the values of Δ that would have resulted in the absence of reflection by the intervening terrain. (See, for example, the appropriate curves in Figs. 4 and 5.) In each case, the maximum difference of the deduced value from the free space value of $\Delta \approx 0$ db is of the order of 2 db or less. Undoubtedly, some of these differences are due partially to experimental error.

Knife-edge theory predicts that the assumption of identical diffraction losses for the direct and reflected radiation would yield values of L_D that are too large. The error would increase with increased magnitudes of the effective reflection coefficients. In principle, it should be possible to estimate this error by comparison of the depths of the minima in the height-gain curves for the optical and obstructed circuits. However, as has already been pointed out, lateral multipath was an important contributor to the transmission loss for the present circuits in the vicinity of the minima. In addition, these regions were probably extremely sensitive to the differences in the effective reflection coefficients. Nevertheless, the height-gain curves have been examined on the assumption that the filling of the minima

was due entirely to differences in diffraction loss. For those results which were susceptible to analysis (Fig. 4, for example), it has been concluded that the error in L_D would be of the order of 2 db. While this may be a reasonable estimate of the error, no attempt has been made to correct the values deduced on the basis of (1) because of the uncertainty of the relative contributions to the minima.

In the application of (1), the displacement between the scales on the left- and right-hand sides of the results typified by Fig. 4 was taken to be equal to L_D minus the terrain gain G_t or G_r, as appropriate, for the terrain to the north of the ridge. The magnitude of the latter factor, which in no case was greater than 1 db, was deduced from the height-gain results in which antenna height was varied at Farm Point or Farrellton, as appropriate. Additional corrections, none of which exceeded 1 db, were made to compensate for the differences in the height-gain curves obtained on different days. The deduced values of L_D and the values predicted by knife-edge theory are contained in Table II. The tabulated experimental values of L_D for the RPL-Farm Point circuit are respectively the minimum and maximum values for the range of antenna heights investigated at the latter site. (See discussion in connection with Fig. 5 and the comments with respect to the dependence of L_D on antenna height at RPL and Farrellton.)

TABLE II

Experimental and Theoretical Diffraction Losses

Frequency (mc)	Circuit	L_D(db)		
		Experimental		Theoretical
		Horizontal Polarization	Vertical Polarization	
173	RPL-Farm Point	27–31	{31–36}*	21
	RPL-Farrellton	25	{30 }	
493	RPL-Farm Point	39–45	41–47	25
	RPL-Farrellton	41	40	
1785	RPL-Farm Point	49–>57	48–54	31
	RPL-Farrellton	47	50	

* The significance of these values is conjectural. See discussion in the text.

The theoretical values of L_D were determined from Bullington's nomogram[5] with the effective obstruction height being taken as 600 feet for the RPL-Farm Point circuit and 750 feet for the RPL-Farrellton circuit. (See Figs. 2 and 3.) The increases in the theoretical losses which result from the assumption of true earth radius instead of 4/3 earth radius are approximately 0.2 db for the RPL-Farm Point circuit and 0.5 db for the RPL-Farrellton circuit.[6] It will be noted that at each frequency knife-edge theory predicts identical diffraction losses on both circuits, to the nearest decibel. This is due to the fact that the greater distance from the ridge to the Farrellton site approximately compensated for the larger effective obstruction height. With regard to the variation of L_D with antenna height, the derivatives of the theoretical knife-edge losses are −0.5 db/100 feet at RPL and −1.0 db/100 feet at Farm Point for the RPL-Farm Point circuit, and −0.7 db/100 feet at RPL and −0.5 db/100 feet at Farrellton for the RPL-Farrellton circuit.[6]

Consideration was also given to the possibility of applying Rice's theory of diffraction by a parabolic cylinder[7] to the experimental circuits. In addition to the difficulties associated with the boundary conditions, it was concluded that the effective radius of curvature at the top of the ridge was far greater than can be tolerated by the approximate Rice theory. [The restriction $rh^{-2} \gg 1$ associated with Rice's eq. (2.10) is not satisfied.]

Comparison of the deduced experimental diffraction losses suggests that there is no evidence of a pronounced polarization dependence at either 493 or 1785 mc. It is unlikely that comparison is valid at 173 mc because of the substantial lateral multipath experienced at this frequency with vertical polarization.

From a comparison of the experimental and theoretical diffraction losses, it is seen that the predictions of knife-edge theory were optimistic. The discrepancies increase with increasing frequency, ranging from a minimum of only 4 db at 173 mc to a minimum of 16 db at 1785 mc. An interesting feature of the results is that, in general, at each frequency the differences between the experimental values of L_D associated with each circuit are relatively small; knife-edge theory predicts that there would be no difference.

Conclusion

The measurements reported show that simple knife-edge theory can result in rather erroneous predictions of diffraction losses associated with obstructed circuits.

Since simple knife-edge theory is of scalar nature, it predicts identical diffraction losses for both horizontal and vertical polarization. In accordance with this prediction, the experimental diffraction losses are not characterized by a marked polarization dependence.

Acknowledgment

The authors are indebted to G. Hough and C. Lemyre for assisting with the final phase of experimental measurements and analysis of experimental data.

[5] K. Bullington, "Radio propagation at frequencies above 30 megacycles," Proc. IRE, vol. 35, pp. 1122–1136, October, 1947. (Fig. 8.) It can be shown that this nomogram may be applied directly even though the equivalent knife-edge is not normal to the straight line joining the terminals.

[6] The asymptotic formula for the Fresnel integral was used in these calculations since the theoretical diffraction losses are sufficiently large that they are given to a good approximation by the use of this formula. The asymptotic formula predicts that the derivatives of L_D with respect to obstruction and antenna heights are independent of frequency.

[7] S. O. Rice, "Diffraction of plane radio waves by a parabolic cylinder," *Bell Sys. Tech. J.*, vol. 33, pp. 417–504; March, 1954.

A Helical Line Scanner for Beam Steering a Linear Array*

LOUIS STARK†

Summary—**A new type of antenna beam scanner which uses the phasing principle for beam steering a linear array is described. The scanner consists of a bank of helical line trombone phase shifters which provide a variable delay circuit for each element of the linear array. The circuits are ganged mechanically by connecting the slides of the trombone phase shifters to a lever arm drive. Short helix sections concentric with the main lines are used to couple the slide of each trombone phase shifter to the main helical lines.**

Measurements of phase characteristics, insertion loss, and vswr of the trombone phase shifters have been carried out. Isolation between phase shifting circuits has also been measured. Radiation studies were conducted using a ten-element scanner in conjunction with a vertical slot array antenna having ten bays. Patterns showing beam scanning out to 52° from broadside are included.

Phasing Principle for Beam Steering

THE DEVICE to be described makes use of the phasing principle in antenna theory in order to vary the angle of beam formation from a fixed linear array. The method is to excite the elements of the array with voltages which are phase retarded uniformly in going from one element to the next. In this way contributions from the individual elements reinforce on a wave front which makes some angle θ with the array. The direction of beam formation is normal to the line of reinforcement. The phasing principle is illustrated in Fig. 1. It is seen from the figure that the beam angle θ

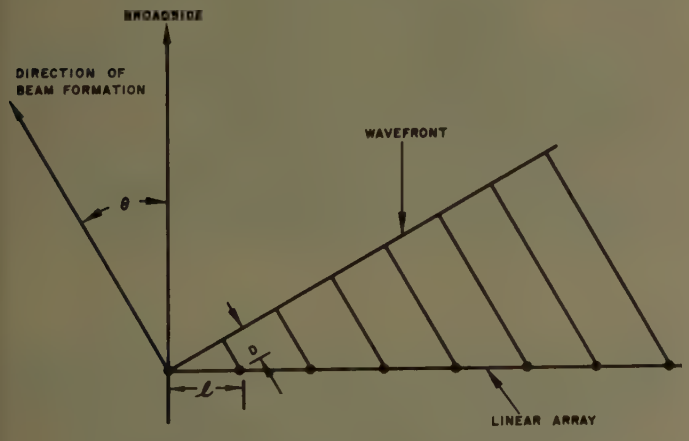

Fig. 1—Phasing principle for beam scanning.

measured from broadside is given by

$$\sin\theta = D/l$$

where

l = element spacing in inches

D = incremental delay between elements, in inches of free space delay.

Principle of Operation of Scanner

The helical line scanner is a ganged arrangement of phase shifters providing channels with delays D, $2D$, $3D$, $\cdots$, with the number of channels equal to the number of radiators. The incremental delay is variable by mechanical means. The scanner is placed between a suitable power distribution network and the radiating elements.

Each of the phase shifting channels is a helical line phase shifter.[1] A trombone configuration is employed, and the slide is electromagnetically coupled to the helical lines by means of coupled helixes as shown schematically in Fig. 2. By design, each of the short coupled

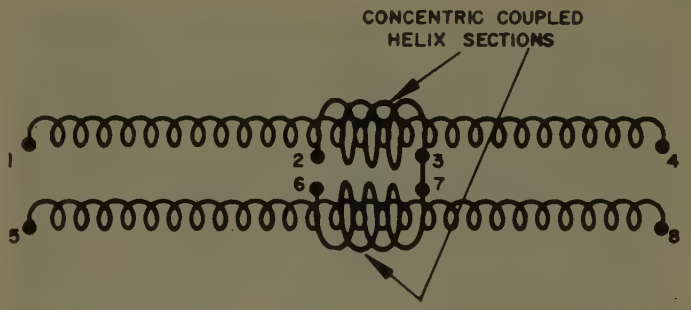

Fig. 2—Schematic drawing of helical line trombone phase shifter.

helixes behaves as a directional coupler which is unity coupled to the main line.[1,2] Thus, a signal incident from terminal 1 is completely transferred to terminal 3, and terminals 2 and 4 are not excited. The signal crosses the bridge to terminal 7 and is completely transferred to the output terminal, no. 5. Similarly, terminals 6 and 8 are not excited. This ideal performance is realized very well in practice. Ordinarily, only a few helix turns are required for the coupled helixes, and performance is good over a broad frequency band.

Displacement of the coupled helix and bridge assembly varies the phase delay between the input and output terminals. If the wavelength on the main helixes is λ_H and if the free space wavelength is λ, a displacement of Δ inches changes the electrical length of the channel by $d = 2(\lambda_0/\lambda_H)\Delta$ inches of free space delay. The reduced wavelength along the main helixes results in a relatively rapid delay change with mechanical displacement. The helix wavelength is reduced from the free space wavelength approximately by the helix wind-up factor. In practical designs this factor may range from 10 to 20.

* Manuscript received by the PGAP, August 27, 1956. The research reported here was supported jointly by the U. S. Army, Navy, and Air Force under contract with Mass. Inst. Tech. and performed under subcontract with M.I.T.

† Hughes Aircraft Co., Culver City, Calif.

[1] L. Stark, "A Helical Line Phase Shifter for Ultra-High Frequencies," M.I.T. Lincoln Lab., Tech. Rep. no. 59, February 4, 1954.

[2] R. Kompfner, Bell Telephone Labs., Memo. for File MM-53-150-8; March, 1953.

Since terminals 4, 2, 6, and 8 are not excited in the arrangement of Fig. 2, a complementary channel can be provided by bridging across terminals 2 and 6 and using terminals 4 and 8 for the second input and output. This channel is isolated from the first, and the incremental phase delay of one channel increases as it decreases in the other.

Description of an Experimental Ten-Element Scanner

A bank of five complementary phase shifting pairs was constructed to form a ten-element scanner. The two members of a pair were used to feed radiating elements on opposite sides of the center of a ten-element antenna array. Each pair of phase shifters was identical with the next. A mechanical drive which positioned the slides correctly with respect to one another was provided by a lever-arm drive pivoted at one end of the bank. The scanner is shown in Fig. 3. This design is for the 400–500-

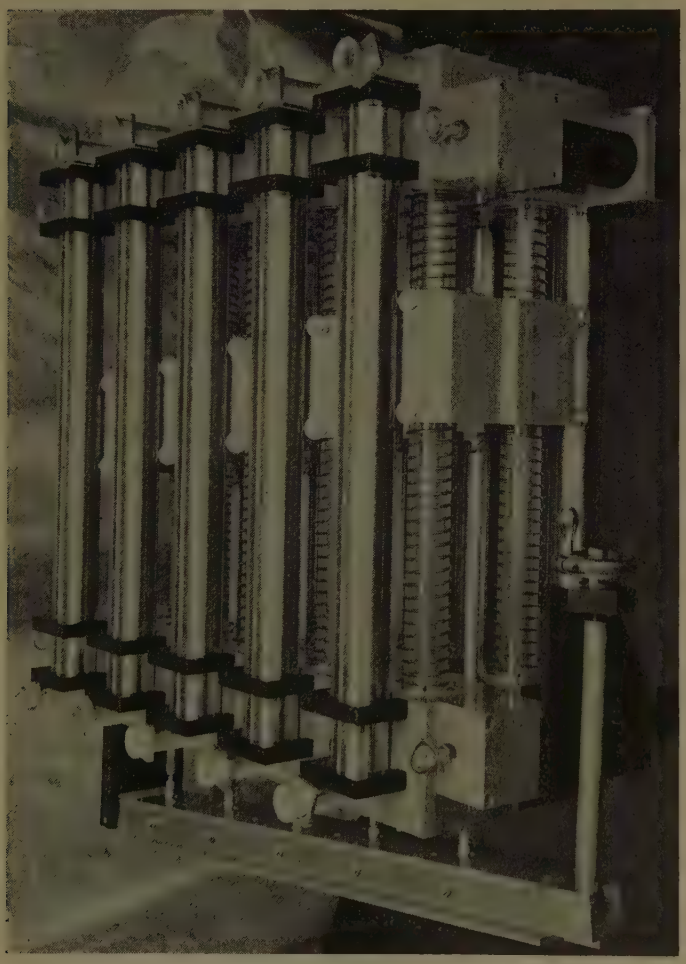

Fig. 3—Helical line phasing unit assembly.

mc range. Fig. 4 shows schematically the phase delays through the various channels when the incremental delay is D. Some of the details of construction are shown in Figs. 5 and 6. Fig. 5 shows the electrical abstraction of a phase-shifting pair. The outer conductors of the coax

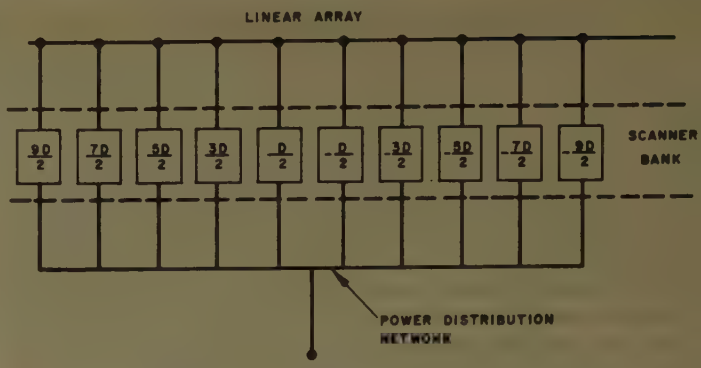

Fig. 4—Delays through phase shifters when incremental delay is D.

Fig. 5—Electrical abstraction of phase shifting pair.

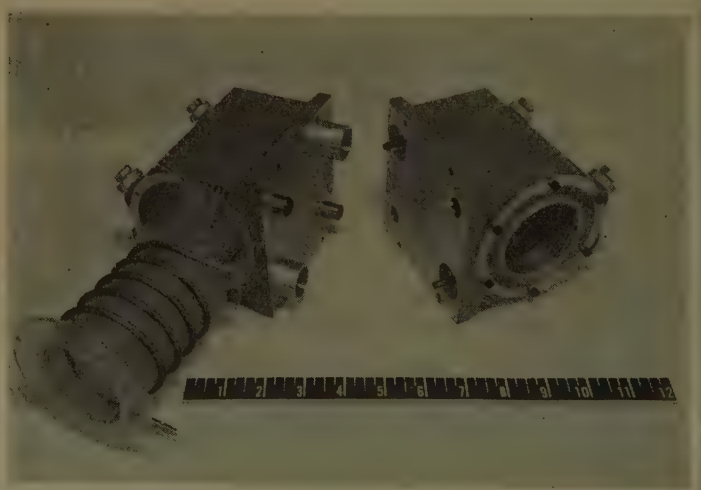

Fig. 6—Slide assembly.

terminal lines and the shields around the short helixes have been removed in this figure. Coupled helixes were employed at the input and output terminals to increase the breakdown power of the coax-helix transitions.[3] The coupled helix design allows pressurization of the transition region and larger physical spacing between critical parts than if a direct connection were made between the coax line and inner helix. Fig. 6 shows the construction of one of the slides.

Scanner Tests

Certain tests were performed on the scanner before radiation testing was carried out. These tests were concerned with the following parts of the design and performance.

1) Phase delay vs slide displacement characteristic of the variable delay channels.
2) VSWR looking into a channel with matched load on output.
3) Cross coupling between channels.
4) Channel insertion loss.

The results of some of these tests are summarized below.

Phase Characteristic

A typical measured phase characteristic is plotted in Fig. 7. This plot shows the additional path length introduced into a delay channel when the slide is displaced a given amount. The additional path length is given in equivalent inches of free space delay. The departure from a linear characteristic corresponds to a $\pm 5°$ phase error at the measuring frequency, 460 mc. The slope of the delay characteristic is 25.5 inches of free space delay per inch of displacement.

Input VSWR of a Delay Channel

The mismatch looking into a channel was measured when this channel and the complementary channel were terminated in a matched load. The results are shown in Table I. The reflections arise from three sources: the input terminal, the output terminal, and the bridge junction in the slide. The resultant mismatch thus depends on both the component reflections and the electrical length between them. The component mismatch at one of the terminals is shown in Fig. 8. This relatively low vswr is the result of some impedance compensation in the coax terminal lines. No compensation was used in the bridge junctions.

It is believed that most of the nonlinearity in the phase delay characteristic is due to the effect of the above reflections.

[3] In Stark, *loc. cit.*, the breakdown power for a similar type of design was reported to be 350-kw peak pulse with 6-microsecond pulses.

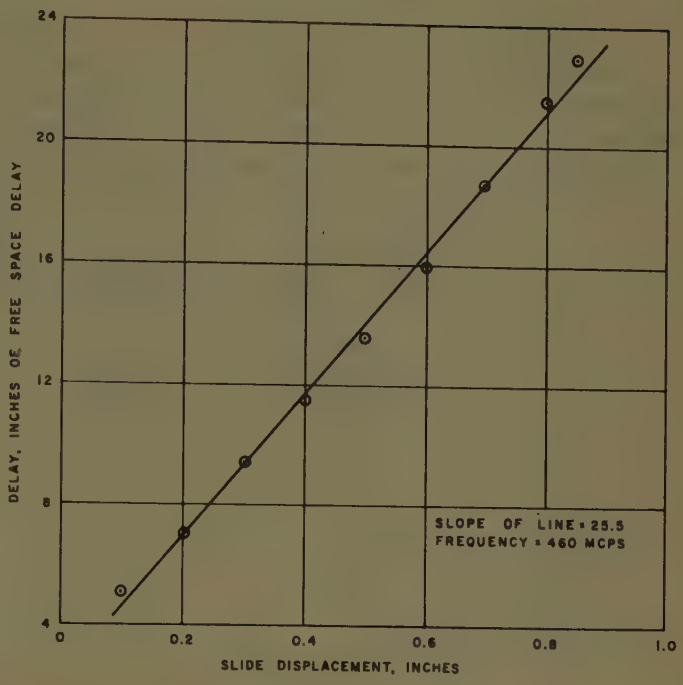

Fig. 7—Phase characteristic.

TABLE I

VSWR Looking Into a Phase-Shifting Channel

Frequency, mc	VSWR at Bridge Position				
	0.0 inch	0.25 inch	0.50 inch	0.75 inch	1.0 inch
400	1.89	2.35	1.90	1.45	1.15
420	1.43	1.33	1.66	2.10	1.78
440	1.29	1.47	1.63	1.56	1.30
460	1.34	1.35	1.42	1.32	1.10
480	1.38	1.39	1.20	1.15	1.36
500	1.64	1.02	1.09	1.67	1.56

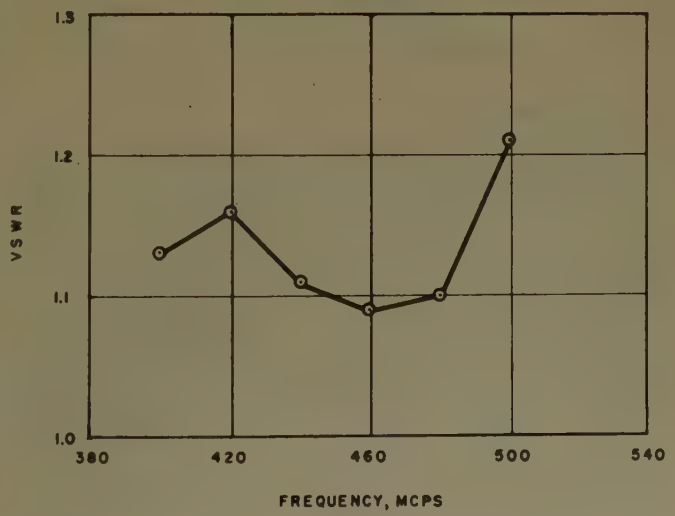

Fig. 8—Compensated vswr of coax-helix transition at phase-shifter terminal.

Cross Coupling

Cross coupling between complementary channels was measured over the band 400–500 mc. Matched bolometers were placed on the output terminal and on the two cross-coupled terminals. The relative power levels measured are shown in Table II. The numbering of the terminals is shown in Fig. 9. Cross coupling is down more than 22 db at terminal 1 and more than 18 db at terminal 2. Cross coupling between complementary channels is attributed primarily to the performance of the coupled helix sections.

TABLE II

CROSS COUPLING BETWEEN PUSH AND PULL CHANNELS

Frequency, mc	Signal Level Below Input	
	At Terminal 1, db	At Terminal 2, db
400	25.2	18.2
410	30.7	26.2
420	37.1	30.1
430	30.0	23.5
440	22.5	18.3
450	30.5	20.1
460	25.3	23.0
470	22.3	22.5
480	26.7	36.2
490	28.5	34.0
500	32.3	34.4

It arises because the energy is not completely transferred between the concentric helix sections and because the directivity is not infinite.

Coupling between channels which are not complementary but which are physically side by side was also measured. The coupling was too small to be measured with the apparatus and was less than −50 db.

Fig. 9—Numbering of terminals for data of Table II.

Insertion Loss

The insertion loss through a channel was measured with the scanner arm in the broadside position. In this position the bridge was 13 inches from both the input and the output ends of the main helixes. The loss was measured to be 0.5 db. The rate at which the loss changed with displacement of the slide was also measured, and this result is plotted in Fig. 10. From the slope of this curve it can be concluded that substantially all the insertion loss is due to attenuation along the helix and that radiation loss is small.

Measurements of attenuation loss along helixes by Peter[4] show the optimum wire diameter-to-pitch ratio to be 0.33. In the design described here this ratio was 0.28. The conductor loss should be reduced by approximately 15 per cent if the optimum ratio were employed.

[4] R. W. Peter, J. A. Ruetz, and A. B. Olson, "Attenuation of wire helices in dielectric supports," *RCA Review*, vol. 13, pp. 558–572; December, 1952.

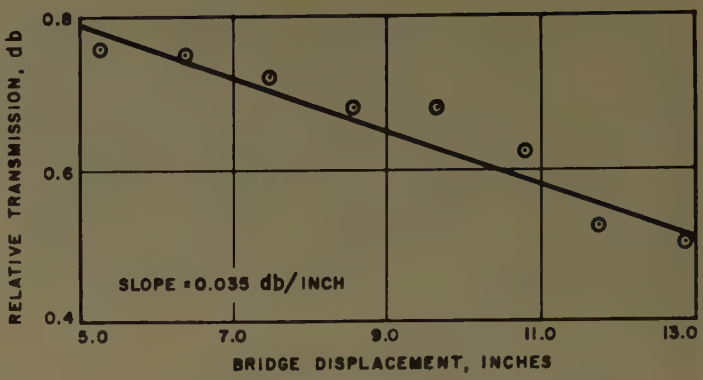

Fig. 10—Rate of loss change with slide displacement.

RADIATION TESTS

For antenna radiation pattern studies the scanner was connected to an array two elements vertical by ten elements horizontal. The elements of the array were vertical full-wave slots in a conducting sheet spaced a quarter wavelength in front of a reflecting plane. Partitions were placed between the vertical pairs of slots, forming ten cavities. A harness feed connected the members of a vertical pair electrically. The horizontal spacing of the slots was a half wavelength at 437 mc, and the array measured 6 feet by 11.2 feet.

A branching coaxial line network was used to distribute the power from the central input terminal to the ten delay channels. A schematic diagram showing the connections is shown in Fig. 11, opposite. Hybrid-T junctions were used to obtain the power splits, and by this method the power distribution was rendered insensitive to the impedance mismatch of the radiating elements or of the scanner. The branching network of hybrids provided a 3-db drop in excitation at the ends of the array for slightly reduced sidelobe levels.

Some typical radiation patterns are shown in Fig. 12(a) and12(b), p.216. Fig. 12(a) shows a run of patterns taken at 439 mc with the beam at broadside and at angles of 13, 27, 43, and 52° off broadside. The displacement of the scanner arm corresponding to these angles was 0.60 inch, 1.20, 1.80, and 2.10 inches measured at the slide farthest from the pivot point. The amount of slide travel available in this scanner was approximately twice as much as was required for these studies. The broadening of the beam which occurred as the beam was scanned from broadside was in accordance with the reduced projected aperture.

The above patterns are representative of the results obtained over the frequency range 410–480 mc. The maximum sidelobe level was less than 14 db below the main beam as the beam was scanned from broadside. The sidelobe level on broadside was −18.5 db. It was observed that the use of hybrid-*T* junctions in the power distribution network had a definite effect in reducing the

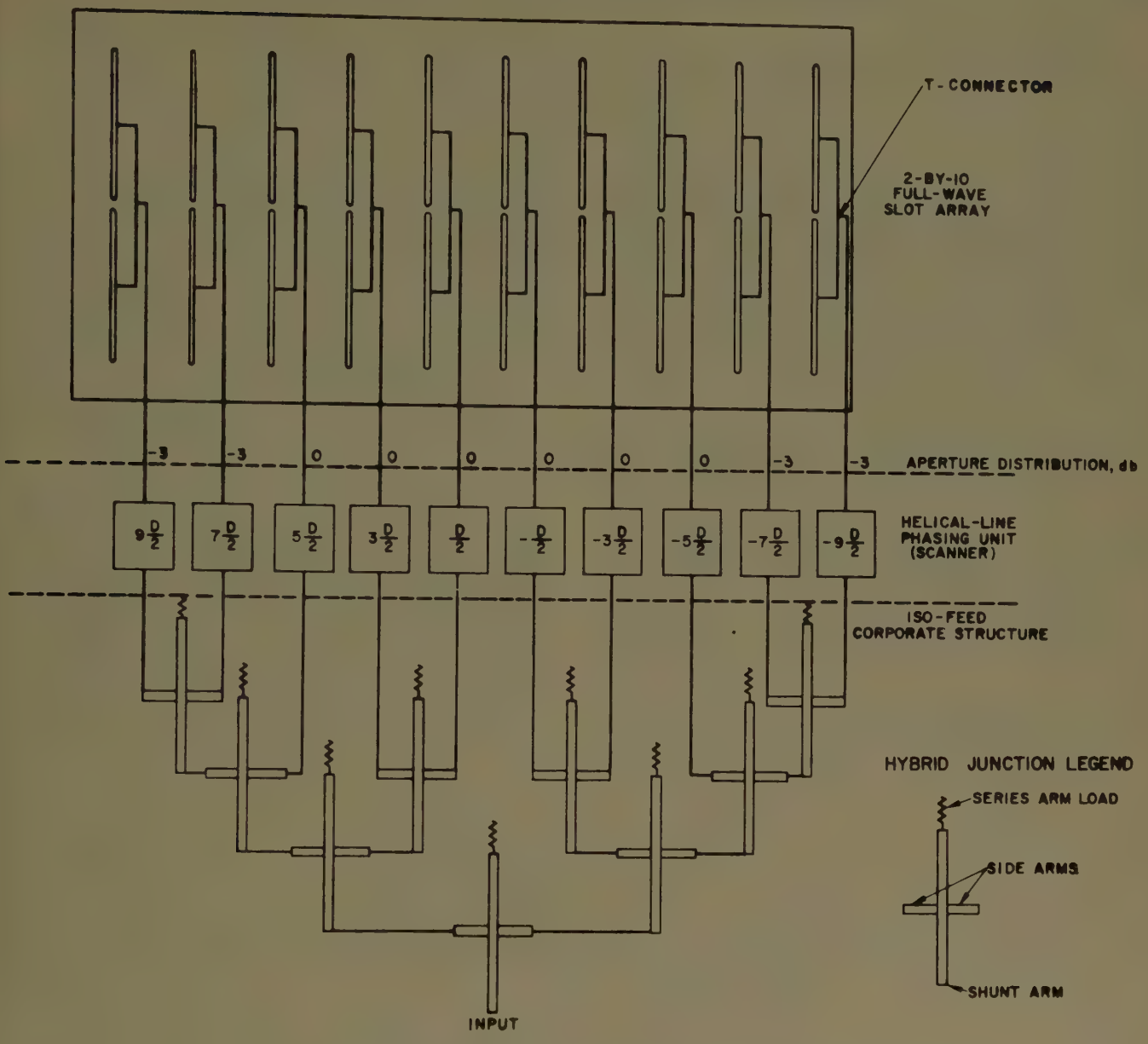

Fig. 11—Schematic diagram of beam-steerable antenna system.

sidelobe level when the beam was off broadside. A typical comparison of patterns taken with and without the effect of the hybrids is shown in Fig. 12(b). For this comparison the effect of the hybrids was removed by removing the matched loads from the series arms of the hybrid T's.

Very little beam steering with changes in frequency was noticed. This fact was attributed to a property of the helical line delay circuits, which is that the equivalent length of free space delay in each circuit is independent of frequency. Each phase-shifting circuit behaved like a long-fixed length of coax line.

Conclusion

A new type of scanner for beam steering a linear array has been constructed and tested. Radiation tests demonstrating beam scanning out of 52° from broadside were carried out. With a feed system giving a −18.5-db sidelobe level on broadside, the sidelobe level remained less than −15 db in the range to 45° and less than −14 db out to 52°. The beam broadening which occurred with scan was in accordance with the reduced projected aperture of the antenna.

The use of hybrid-T junctions in the feed system was found to be an essential factor in maintaining reduced sidelobe levels.

Acknowledgment

The mechanical designs of the scanner, the feed, and the antenna used for these studies were carried out by P. J. Servaas.

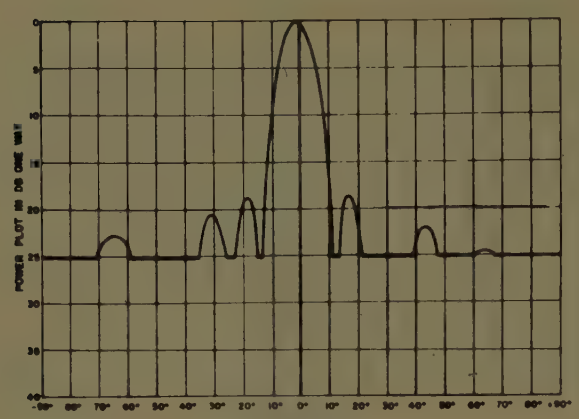

broadside

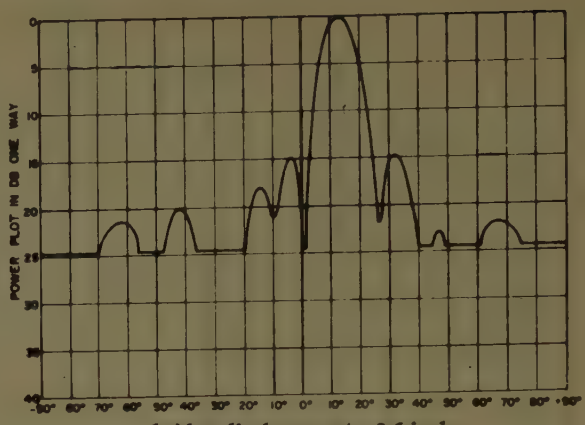

bridge displacement = 0.6 inch

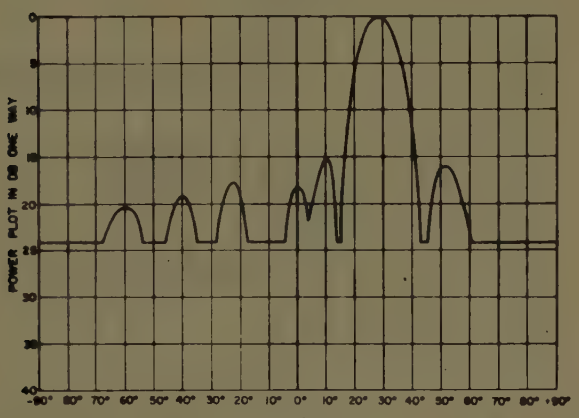

1.2 inches

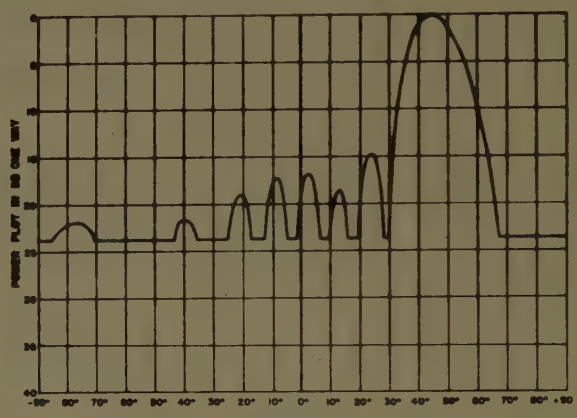

1.8 inches

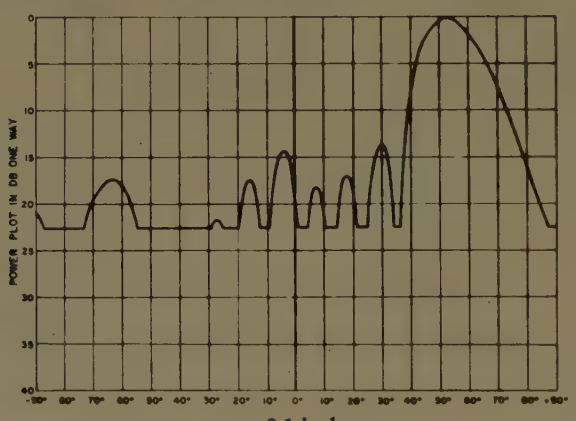

2.1 inches

(a)

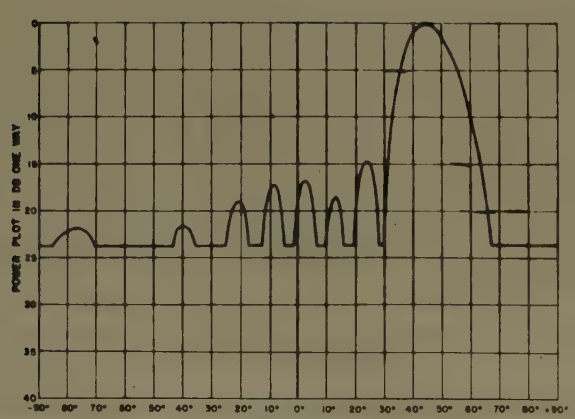

with hybrids

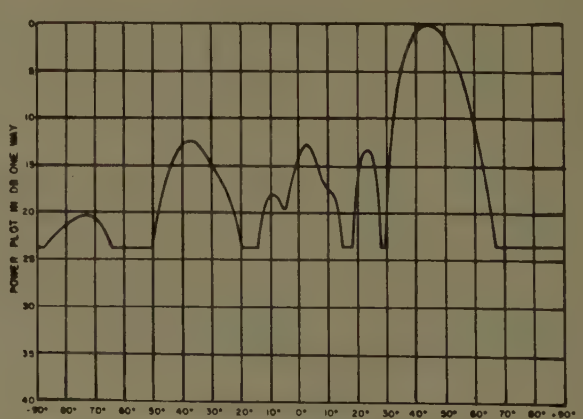

without hybrids

(b)

Fig. 12—(a) Radiation patterns showing beam scanning at a frequency of 439 mc. (b) comparison of radiation patterns with and without hybrids.

A Simple Solution to the Problem of the Cylindrical Antenna*

JESSE G. CHANEY†

Summary—**It is recognized that the variational solution of the cylindrical antenna does not minimize $|Z_{in}-Z_0|$, as implied by Storer; but yields a minimax of the impedance function. Furthermore, the variational solution may be interpreted as simply placing two currents in parallel upon the antenna, following which, the solution for the magnitudes of the currents and for the driving point impedance may be found by elementary circuit analysis. Consequently, a first-order solution by the generalized circuit is found by postulating a linearly-attenuated traveling wave to be superimposed upon the sinusoidal standing wave. The results show excellent correlation with other theoretical and measured results for both the driving point impedance and the current distribution along the antenna.**

Introduction

BROADLY SPEAKING, it may be stated that the calculus of variations in the theory of functions of real variables serves as a tool for discovering certain physical laws. The integrand of a definite integral is perturbed by adding to it a parameter times a function of the independent variable, subject to the condition that the function vanishes at both limits of the integration. The physical laws are obtained by requiring the first derivative of the perturbed integral with respect to the parameter to vanish. Perhaps the most useful laws are those for which the integral is made a minimum by the value of the parameter thus obtained.

Recently, the calculus of variations has been applied to many physical problems set up in terms of analytic functions of a complex variable. In particular, Storer[1] and Tai[2] have used it in obtaining a first-order solution to the symmetrically driven straight cylindrical antenna.

In agreement with Storer,[3] if

$$W = f(z) = U(x, y) + jV(x, y)$$

is analytic, and if W_0 is a constant, using the Cauchy-Riemann equations, it is not difficult to show that setting

$$\frac{\partial}{\partial x}|W - W_0| = 0, \qquad \frac{\partial}{\partial y}|W - W_0| = 0,$$

is equivalent to setting

$$\frac{dW}{dz} = 0,$$

or that the first term of a Taylor's expansion of the function vanishes.

However, by taking the second derivatives and using the Cauchy-Riemann equations in connection with the standard tests for maxima and minima of functions of two variables,[4] it can be shown that $|W-W_0|$ is neither a maximum nor a minimum when the first derivative with respect to z vanishes. That is, if Z_0 is the true input impedance of an antenna, and if $Z(\epsilon_r+j\epsilon_i)=Z(\epsilon)$ is an impedance obtained by using $I(\epsilon, x)=I(x)+\epsilon\eta(x)$ as an approximation to the true current distribution function $I(x)$, the requirement

$$\frac{dZ(\epsilon)}{d\epsilon} = 0$$

does not minimize $|Z-Z_0|$, as implied by Storer,[5] but merely yields a minimax[6] for the value $\epsilon=\epsilon_0$ found by solving the above equation.

Physical Significance of Variational Method

The variational method postulates the generalized Kirchoff's law,[7]

$$\frac{j30}{k}\int_{-l}^{l} I(x')G(x', x)dx' = Z_0 I(0)\delta(x) \qquad (1)$$

in which

l = the half length of the antenna

a = the radius of the antenna

$$K = \frac{2\pi}{\lambda}$$

$$G(x', x) = \left(\frac{d^2}{dx^2} + k^2\right)\frac{e^{-jkr(x'-x)}}{r(x'-x)}$$

and $\delta(x)$ is the Dirac delta impulse function.

The driving point impedance is then chosen in the form

$$Z_0 = \frac{j30}{kI^2(0)}\int_{-l}^{l}\int_{-l}^{l} I(x)I(x')G(x', x)dx'dx. \qquad (2)$$

It has been shown[8] that this form, using the approximate Green's function with $r=[(x-x')^2+a^2]^{1/2}$ yields the same result as that obtained by using the exact Green's function.

* Manuscript received by the PGAP, April 26, 1956. This paper is a revision of Tech. Rep. No. 15, U. S. Naval Postgraduate School, Monterey, Calif., January, 1956.

† Dept. of Electronics, U. S. Naval Postgraduate School, Monterey, Calif.

[1] J. E. Storer, "Variational Solution to the Problem of the Symmetrical Antenna," Cruft Lab., Harvard Univ., Cambridge, Mass., Tech. Rept. No. 101; 1950.

[2] C. T. Tai, "A Variational Solution to the Problem of Cylindrical Antennas," Stanford Res. Inst., Stanford, Calif., Tech. Rep. No. 12; 1950.

[3] Storer, *op. cit.*, pp. 7–8.

[4] E. B. Wilson, "Advanced Calculus," Ginn and Co., New York, N. Y., pp. 114–115; 1912.

[5] Storer, *op. cit.*, p. 8.

[6] Wilson, *op. cit.*, p. 115.

[7] Tai, *op. cit.*, p. 4.

[8] C. T. Tai, "A new interpretation of the integral equation formulation of cylindrical antennas," IRE TRANS., vol. AP-3; pp. 125–127, July, 1955.

The current function is perturbed by choosing

$$I(x, A) = I(x) + \epsilon\eta(x) = I_0[f(x) + A\eta(x)]. \quad (3)$$

If A_0 is a root of $dZ_0(A)/dA = 0$, the impedance is found to be[9]

$$Z_0(A_0) = 30\frac{V_{11}V_{22} - V_{12}^2}{f^2(0)V_{22} - 2f(0)\eta(0)V_{12} + \eta^2(0)V_{11}} \quad (4)$$

with

$$V_{11} = \frac{j}{k}\int_{-l}^{l}\int_{-l}^{l} f(x)f(x')G(x', x)dx'dx$$

$$V_{12} = \frac{j}{k}\int_{-l}^{l}\int_{-l}^{l} f(x)\eta(x')G(x', x)dx'dx$$

$$V_{22} = \frac{j}{k}\int_{-l}^{l}\int_{-l}^{l} \eta(x)\eta(x')G(x', x)dx'dx. \quad (5)$$

By simple algebraic manipulation, (4) may be converted into

$$Z_{in} = \frac{Z_{11}Z_{22} - Z_{12}^2}{Z_{11} + Z_{22} - 2Z_{12}} \quad (6)$$

with

$$Z_{11} = \frac{j30}{kI^2(0)}\int_{-l}^{l}\int_{-l}^{l} I_1(x)I_1(x')G(x', x)dx'dx$$

$$Z_{12} = \frac{j30}{kI_1(0)I_2(0)}\int_{-l}^{l}\int_{-l}^{l} I_1(x)I_2(x')G(x', x)dx'dx$$

$$Z_{22} = \frac{j30}{kI_2^2(0)}\int_{-l}^{l}\int_{-l}^{l} I_2(x)I_2(x')G(x', x)dx'dx, \quad (7)$$

in which it is assumed that neither $I_1(0)$ nor $I_2(0)$ is zero.

Eq. (6) is recognized as the solution of the mesh equations,

$$\begin{aligned} Z_{11}I_1(0) + Z_{12}I_2(0) &= V_0 \\ Z_{21}I_1(0) + Z_{22}I_2(0) &= V_0. \end{aligned} \quad (8)$$

The current distribution becomes

$$I(x) = \frac{V_0}{I_1(0)}\frac{Z_{22} - Z_{12}}{Z_{11}Z_{22} - Z_{12}^2}I_1(x) + \frac{V_0}{I_2(0)}\frac{Z_{11} - Z_{12}}{Z_{11}Z_{22} - Z_{12}^2}I_2(x). \quad (9)$$

Suppose that $I_2(0) \neq 0$ with $I_1(0) = 0$. Let

$$\zeta_{11} = \lim_{x\to 0}\frac{I_1^2(x)Z_{11}}{I_{01}^2}, \qquad \zeta_{12} = \lim_{x\to 0}\frac{I_1(x)Z_{12}}{I_{01}}.$$

Then (6) and (9) become, respectively

$$Z_{in} = Z_{22} - \frac{\zeta_{12}^2}{\zeta_{11}}, \quad (10)$$

and

$$I(x) = \frac{V_0}{\zeta_{11}Z_{22} - \zeta_{12}^2}\left(\frac{\zeta_{11}}{I_2(0)}I_2(x) - \frac{\xi_{12}}{I_{01}}I_1(x)\right), \quad (11)$$

in which I_{01}^{-1} is a normalizing factor.

From (6), (8), and (9), it becomes evident that the vanishing of the first term in the Taylor's expansion of the perturbed current simply yields the physical information that two currents have been postulated to exist in parallel along the antenna. From (10) and (11), it becomes further evident that for singular cases one current becomes the *feed current* with the other parasitically excited.

This recognition greatly simplifies the variational theory of cylindrical antennas. In fact, the statement might be ventured that the variational method is not a distinct method *per se*. Any scheme for finding the self and mutual impedances of the two postulated current distributions may be used. Since $|Z_{in} - Z_0|$ is not minimized, there is no *a priori* reason for assuming that the driving point impedance computed by a method with a vanishing first term in its Taylor's expansion is any more accurate than that computed from the parallel circuit with the self and mutual impedances being computed by any recognized method.

First-Order Solution by the Generalized Circuit

For two straight currents, the mutual impedance by generalized circuit[10] scheme is given by

$$Z_{12} = \frac{j30}{k}\int_{-l}^{l}\int_{-l}^{l}\mathrm{Re}\left[\frac{F_1(\gamma)f_2(x')^*}{f_1(0)f_2(0)^2}\right]\cdot\left[\frac{\partial^2}{\partial x^2} + k^2\right]\frac{e^{-jkr_{12}}}{r_{12}}dxdx', \quad (12)$$

in which the operator Re takes the real part of the product of one current by the complex conjugate of the other current. The current functions are normalized at the driving point. In case the current functions are different and at least one of them is not real, the reciprocity theorem requires the use of only the real part of the current product.

It is possible to show that the results obtained with the approximate Kernel are the same as those obtained when the exact Kernel is used in (12).

For a relatively low-loss transmission line, Tai[11] approximated the current distribution function by

$$I(x) = I_0[\sin\beta(l - x) - j\alpha(l - x)\cos\beta(l - x)] \quad (13)$$

from which he chose his pair of currents. The current on a lossy line also may be written

$$I(x) = I_0[e^{\alpha z}\sin\beta(l - x) - je^{\alpha l}\sinh\alpha[(l - x)e^{j\beta(l-z)}] \approx I_0[\sin\beta(l - x) - j\alpha e^{\gamma l}(l - x)e^{-j\beta z}]. \quad (14)$$

[9] Tai, Rep. No. 12, *op. cit.*, p. 11.

[10] J. G. Chaney, "A critical study of the circuit concept," *J. Appl. Phys.*, vol. 22, pp. 1429–1436; December, 1951.

[11] Tai, Rep. No. 12, *op. cit.*, p. 12.

To the writer, this arrangement intuitively seems preferable to that of (13). Hence, the current pair is chosen as

$$I_1(x) = I_{01} \sin k(l - |x|)$$
$$I_2(x) = I_{02}\alpha(l - |x|)e^{-jk|x|}. \quad (15)$$

The self impedance Z_{11} is then the well-known zero-order solution by the classical induced emf method.[12] For the others,

$$Z_{22} = \frac{j30}{k}\int_{-l}^{l}\int_{-l}^{l}\left(1 - \left|\frac{x}{l}\right|\right)\left(1 - \left|\frac{x'}{l}\right|\right) \cdot e^{jk(|x|-|x'|)}\left(\frac{\partial^2}{\partial x^2} + k^2\right)\frac{e^{-jkr_{12}}}{r_{12}}\,dx\,dx' \quad (16)$$

$$Z_{12} = \frac{j30}{k \sin k}\int_{-l}^{l}\int_{-l}^{l}\left(1 - \left|\frac{x}{l}\right|\right)\sin k(l - |x'|) \cdot \cos kx\left(\frac{\partial^2}{\partial x^2} + k^2\right)\frac{e^{-jkr_{12}}}{r_{12}}\,dx\,dx'. \quad (17)$$

It is not necessary to take the real part in (16) because it is a self impedance and the two current functions are identical. The resulting formulas are listed in the Appendix for $ka \ll 1$, $2a \ll l$.

The current distribution along the antenna then becomes

$$I(x) = \frac{V_0}{Z_{11}Z_{22} - Z_{12}^2}\left[\frac{Z_{22} - Z_{12}}{\sin kl}\sin k(l - |x|) + (Z_{11} - Z_{12})\left(1 - \left|\frac{x}{l}\right|\right)e^{-jk|x|}\right]. \quad (18)$$

Asymptotic Values

It is of interest to examine the asymptotic values of the current and of the impedance.

$$\text{For } \Omega = 2\ln\frac{2l}{a} \to \infty$$

$$Z_{11} = Z_{12} \to -j\,60\Omega \cot kl, \quad Z_{22} \to -j\frac{60}{kl}\Omega, \quad Z_{in} \to Z_{11},$$

and

$$I(x) \to \frac{V_0}{Z_{11}\sin kl}\sin k(l - |x|) = j\frac{V_0}{60\Omega}\frac{\sin k(l - |x|)}{\cos kl}.$$

For $kl \ll 1$,

$$Z_{11} = Z_{12} = Z_{22} \to 20(kl)^2 - j\frac{60}{kl}(\Omega - 2 - 2\ln 2)$$

and

$$I(x) \to \frac{V_0}{Z_{11}}\left(1 - \left|\frac{x}{l}\right|\right)$$

with $Z_{in} \approx Z_{11}$.

[12] S. A. Schelkunoff, "Electromagnetic Waves," D. Van Nostrand Co., New York, N. Y., p. 373; 1947.

For $kl \approx n\pi$, $n = 1, 2, 3, \cdots$,

$$Z_{in} = Z_{22} - \frac{\zeta_{12}^2}{\zeta_{11}}$$

and

$$I(x) = \frac{V_0}{\zeta_{11}Z_{22} - \zeta_{12}^2}\left[\zeta_{11}\left(1 - \left|\frac{x}{l}\right|\right)e^{-jk|x|} - \zeta_{12}\sin k(l - |x|)\right]. \quad (19)$$

From (19), it is seen that the attenuated traveling wave becomes the *feed current*, and that the standing wave becomes parasitically excited.

Thus asymptotically, this method is equivalent to the induced emf method with the removal of the singularities.

Results

Some values of the driving point impedance computed by this method (Tables I and II) were plotted on curves

TABLE I

kl	$\Omega = 10$	$\Omega = 15$
	Z_{in}	Z_{in}
$\pi/2$	$83.0 + j41.8$	$77.5 + j42.3$
2.2	$493 + j304$	$360 + j654$
2.6	$883 + j94$	$1282 + j1101$
2.9	$633 - j492$	$2513 - j349$
π	$372 - j493$	$1345 - j1447$
$3\pi/2$	$78.3 + j15.0$	$92 + j2$
5.1	$178 + j104$	$288 + j287$
5.6	$586 + j63$	$871 + j683$
6.0	$340 + j262$	$1699 - j130$
2π	$332 + j263$	$1094 - j904$

TABLE II

Ω	$kl = \pi/2$	$kl = \pi$
	Z_{in}	Z_{in}
10	$83.0 + j41.8$	$372 - j493$
12	$79.8 + j42.0$	$683 - 837$
15	$77.5 + j42.3$	$1345 - 1447$
22	$75.6 + j42.3$	$3797 - j3463$

by Tai[13] (Figs. 1 and 2) for comparison with values computed by the King-Middleton, the variational, and the Schelkunoff methods. They show excellent correlation with the other methods, being very close to the results of Tai with perhaps about as many of the excursions being on the Schelkunoff side of the curves, as on the King-Middleton side of the curves.

For $\Omega = 10$ and $\Omega = 15$, the current distribution was computed for comparison with the sinusoidal current and with the current computed by King and Harrison[14]

[13] Tai, Rep. No. 12, *op. cit.*, Figs. 4–5.

[14] R. King and C. W. Harrison, Jr., "The distribution of current along a symmetrical center-driven antenna," Proc. IRE, vol. 31, pp. 548–656; October, 1943.

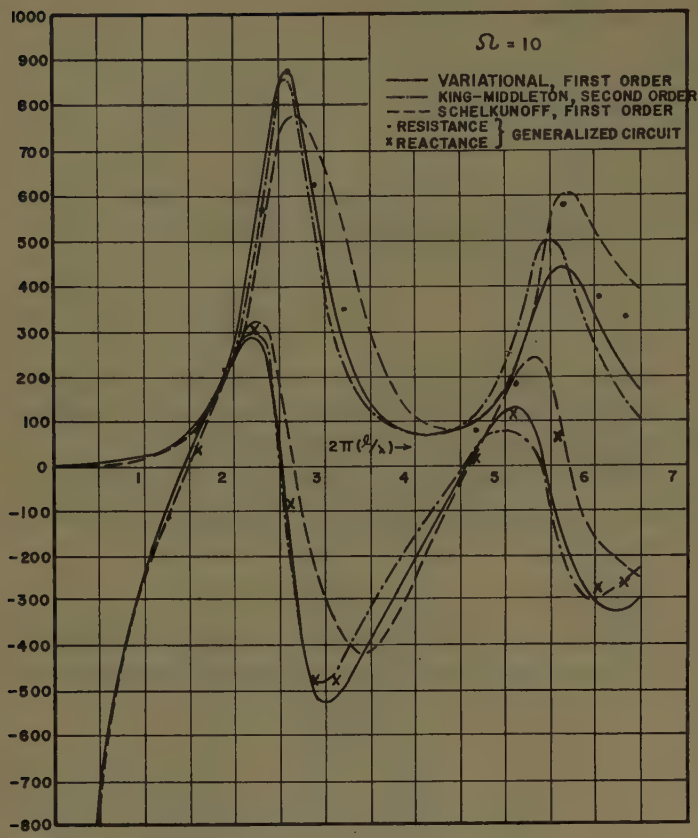

Fig. 1.

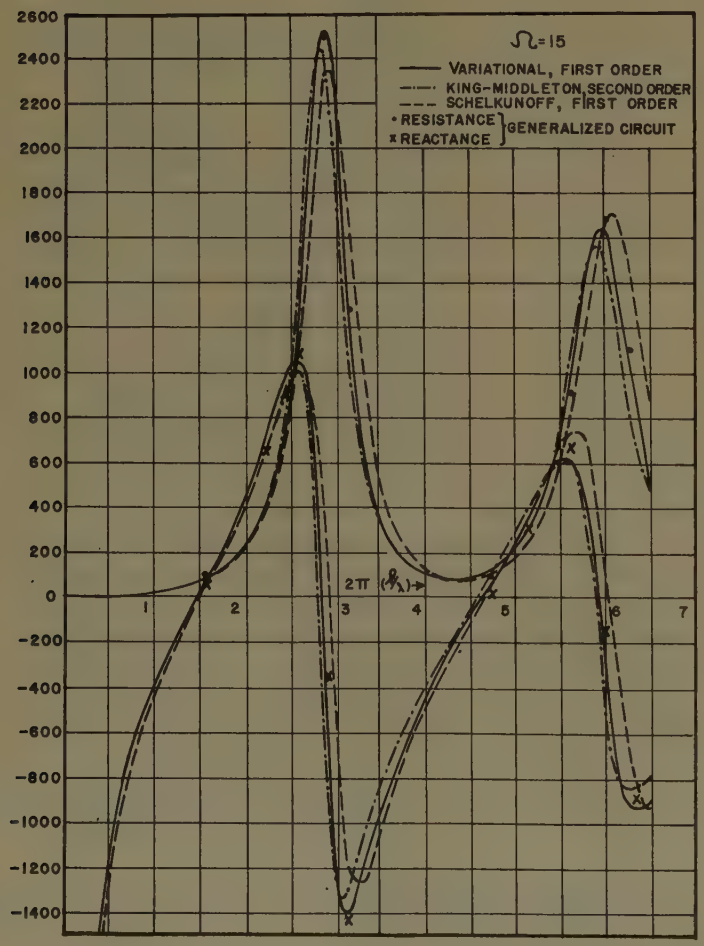

Fig. 2.

from a first-order solution of the Hallén integral equation (Figs. 3 and 4). In view of the known discrepancies existing in the King-Harrison method, good correlation is indicated.

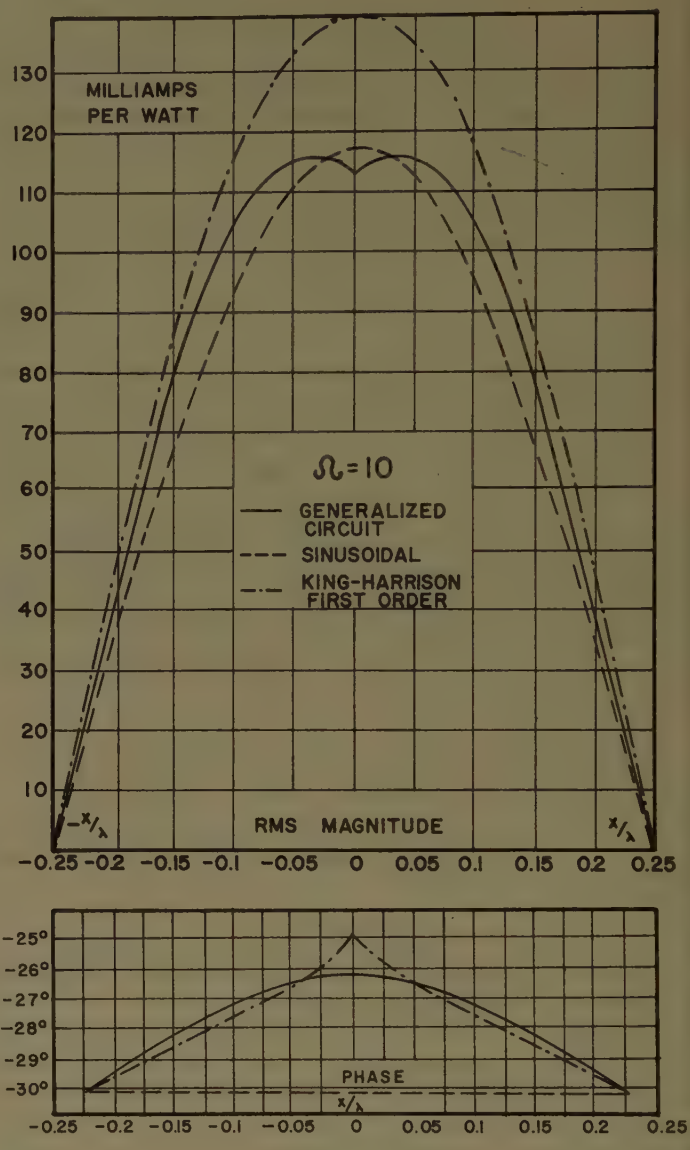

Fig. 3.

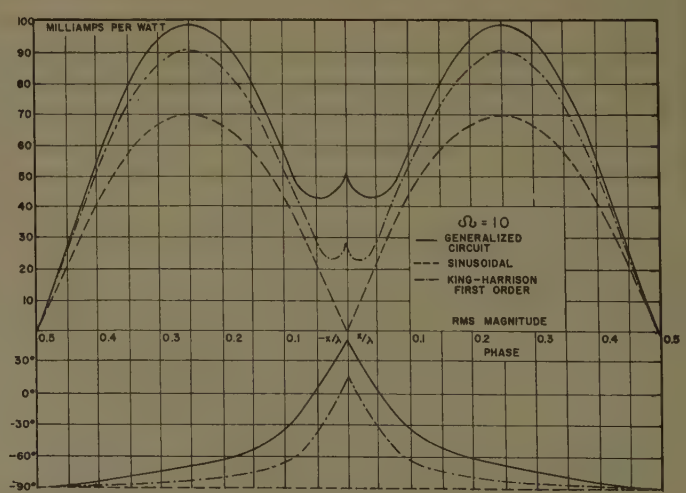

Fig. 4.

These computed values were also compared with the measured values of Barzilai[15] and of Morita.[16] Excellent correlation exists between the computed and measured results. The curves by Morita showed a comparison of the measured values with values computed by the King-Middleton first-order solution. The values by the generalized circuit first order show better correlation to the measured values than do those by the King-Middleton first-order method.

Conclusion

The comparative simplicity of the method of obtaining the first order generalized circuit solution, together with the excellent correlation with other solutions and with published measurements, should justify its introduction into the already crowded group of antenna theories.

It is believed that the simplicity of the method will greatly facilitate the teaching of the theory of the cylindrical antenna.

The method is being extended to the case of the receiving antenna.

It should be pointed out that this is not a variational method, but that the variational method as previously presented becomes a special case of this method because the current functions were real.

Appendix

$$Z_{11}\sin^2 kl = 60cin2kl \quad 30\sin 2kl(2si2kl - si4kl) + 30\cos 2kl(2cin2kl - cin4kl)$$
$$+ j\{60si2kl - 30\sin 2kl(\Omega - \ln 4 + cin4kl - 2cin2kl) + 30\cos 2kl(2si2kl - si4kl)\}$$

$$Z_{12}\sin kl = 60\cos kl(si4kl - 2si2kl) + 60\sin kl(cin4kl - cin2kl) + j\Big\{60\cos kl(\ln 4 - \Omega + 1 - cin4kl + 2cin2kl)$$
$$+ 60\sin kl(si4kl - si2kl) + \frac{15}{kl}(3\sin kl + 2\sin 2kl - \sin 3kl)\Big\}$$

$$Z_{22} = 60cin2kl - 30 + \frac{30}{kl}(\sin 2kl - 2si2kl)$$
$$+ \frac{15}{(kl)^2}[1 + 2cin2kl + \cos 2kl(2cin2kl - 2cin4kl - 1) + 2\sin 2kl(si4kl - si2kl)]$$
$$+ j\Big\{60\,si2kl - \frac{30}{kl}(2\Omega + 2 - \cos 2kl - 2cin2kl)$$
$$+ \frac{15}{(kl)^2}[2si2kl + \sin 2kl(2\ln 4 + 1 + 2cin2kl - 2cin4kl) + 2\cos 2kl(si2kl - si4kl)]\Big\}$$

$$six = \int_0^x \frac{\sin t}{t}\,dt, \qquad cix = \int_\infty^x \frac{\cos t}{t}\,dt,$$

$$cinx = \int_0^x \frac{1 - \cos t}{t}\,dt = \ln \gamma x - cix, \ln \gamma = 0.5772\cdots$$

[15] G. Barzilai, "Experimental determination of the distribution of current and charge along cylindrical antennas," Proc. IRE, vol. 37, pp. 825–829; July, 1949.

[16] T. Morita, "The Measurement of Current and Charge Distributions on Cylindrical Antennas," Cruft. Lab., Harvard Univ., Cambridge, Mass., Tech. Rep. No. 66, Figs. V-4, V-6; 1949.

Acknowledgment

The writer expresses his thanks to Capt. William J. Schreier, U.S.M.C., for lettering and inking the drawings.

Investigations with a Model Surface Wave Transmission Line*

G. GOUBAU† AND C. E. SHARP†

Summary—**This paper summarizes the results of experimental studies conducted with a scale model of a surface wave transmission line (swt line) for long-distance transmission. The purpose of the experiments was to determine the effect of supports, bends, and sags on the transmission loss of such a line. Also, the coupling between parallel identical lines has been measured and compared with the theory.**

Formulas and other information are given which may be applied to the design of a swt line for long-distance transmission.

Introduction

THE FEASIBILITY of employing surface wave transmission lines (swt lines) for the transmission of wide-band signals over long distances has been under study at the Signal Corps Engineering Laboratories for several years. The results indicate that bandwidths of 100 mc or more are readily obtained with a relatively simple and economical installation. The most favorable operating frequency range is between 100 and 300 mc. The practical lower-frequency limit is determined by the extension of the field, and the upper limit by the size of the conductor necessary to obtain low attenuation.

The first experiments with a swt line for long-distance transmission were made with a line having a segmented conductor of the type used for high-tension lines (HH-cable manufactured by General Cable Co.) of 1.42-cm diameter with a polyethylene coating 0.34-cm thick (Fig. 1). This line was installed along a road and supported from crossarms of telephone poles by slings of nylon cord. The results of these experiments, which have been published,[1] demonstrated the feasibility of long-distance transmission by swt lines; however, there was considerable discrepancy between the loss calculated under idealized assumptions, *i.e.*, without bends, supports, etc. and the actual measured loss. The calculated transmission loss at 200 mc, for instance, was 3 db/mile, while the measured loss was about 6 db/mile.

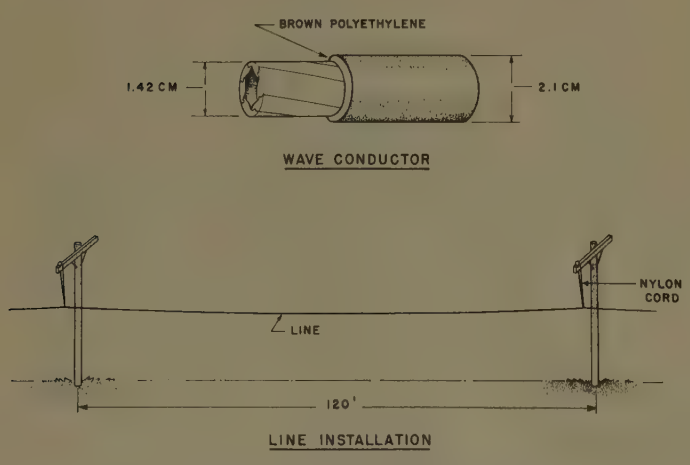

Fig. 1—Experimental surface wave transmission line for long-distance transmission.

There are several reasons for this discrepancy between the calculated and the measured loss. First, the conductor used had increased resistivity because of its segmental structure; the interlocking joints between the segments form spirals, and since the current associated with the surface wave is axially directed, it is affected by the contact resistance of these joints. Second, there was an additional loss due to the fact that the line was not ideally straight. There were sags between the suspension points, and bends at the points of support. Besides, there were bends in the horizontal plane since the line followed the curves of a road. Third, the field of the surface wave was intercepted by the line supporting nylon strings, the telephone poles, and the crossarms. The currents induced in such obstacles also result in an increase in transmission loss.

These various loss-increasing factors have been investigated individually, not just to explain the discrepancy between the measured and calculated losses on the 2 mile line, but mainly to obtain information leading to a better and more efficient construction. Unfortunately the amount of loss caused by the interlocking joints of the line conductor could not be determined since it was found that the loss increased with time. A temporary increase in the tension applied to the cable would bring the loss back to the lower value. However, after a period of several weeks the loss would again increase appreciably. Apparently the movements of the line by the wind affected the joints between the segments. Thus, it was concluded that a solid conductor should be used in future line constructions.

Since experiments with the 2-mile line were inconvenient for physical reasons, it was decided to continue the investigations of the loss factors with a one-tenth scale model. The procedures used for the investigations with the scale model and the conclusions derived from these measurements are given as follows.

Scaling Considerations

If, in any electromagnetic transmission system, the dielectric constant and permeability of all materials were

* Manuscript received by the PGAP, February 15, 1956; revised manuscript received, January 12, 1957.

† Signal Corps. Eng. Labs., Fort Monmouth, N. J.

[1] G. Goubau, C. E. Sharp, and S. W. Attwood, "Investigation of a surface wave line for long distance transmission," IRE TRANS., vol. AP-3, pp. 263–267; August, 1952.

independent of frequency, and if there were no dielectric, magnetic, or conductivity losses, then scaling of all physical dimensions and the wavelength by the same factor would leave the field structure unchanged. The loss of such an idealized system would be only radiation loss, which is independent of the scaling factor.

The dielectric constant and permeability of the materials used for the construction of a swt line are practically independent of the frequency and therefore need not be considered in the scaling procedure. Dielectric loss factor and conductivity loss follow different scaling laws. Fortunately their effect on the field distribution around the line is negligibly small. They only cause a gradual decrease of the field intensity along the line and behave like a uniformly-distributed attenuation which is equivalent to a concentrated attenuation inserted at one end of a lossless line. Since the line is supported at intervals of many wavelengths and these intervals vary phasewise at random, the losses caused by each bend, sag or support can be considered individually. The total loss in db is therefore the sum of the losses of the individual discontinuities. The loss at each discontinuity is determined only by the cross-sectional field distribution and not by the attenuation of the wave along the line. Therefore, scaling of dielectric loss factor and conductivity of the line material is not required. The dielectric losses in the line supporting structures need not be considered too, because the polarization currents in these structures cause primary radiation losses. Thus, a geometrically scaled model will suffice to obtain information about the transmission losses which are effected by bends, sags, and the line supporting structures.

Description of the Model Line

The model line was constructed for operation in a frequency band centered at 2000 mc. Assuming the operating frequency of the full-size line to be 200 mc, the scaling factor with respect to the frequency was therefore 10. A length of about 528 feet simulated a 1-mile section of a full-scale line. The supporting poles were 12 feet apart corresponding to a scaling by a factor ten of the average span of 120 feet between telephone poles. The average height of the model line poles above ground was about 5 feet. The height of the line above the ground is of no consequence provided it is in the order of wavelengths. The model line poles were $1\frac{3}{4}$ inches square. Compared to actual size telephone poles, the thickness of the model poles corresponded to a scaling factor of about 5 rather than 10. The oversize diameter was chosen to emphasize the effect of the poles for measuring purposes. The crossarms used on the model line poles corresponded to the scaling factor 10. The nylon cord used for the slings which supported the model line at each cross-arm had a diameter of 0.03 inch; with the scaling factor 10 applied, this permits a 0.3-inch cord for a full-size line having a breaking strength of more than 1000 pounds. Most of the measurements were conducted with a wire having a conductor diameter of 0.051 inch (No. 16 B&S) with a coating of brown polyethylene of 0.034 inch in thickness; the ratio between the diameter (d_0) of the coated conductor and the diameter d_i of the uncoated conductor was therefore 2.35. A ratio d_0/d_i of slightly above two is a good compromise between the copper and dielectric losses of the line, and the auxiliary losses due to bends, supports, etc.

Effect of Supports

The simplest and most satisfactory means for supporting long swt lines from telephone poles are slings of nylon cord as shown in Fig. 1. Although this method may seem unconventional for supporting transmission lines it has considerable merit. The cord is relatively inexpensive compared to other kinds of supports considered, and in the form of a sling it provides a simple way to obtain good alignment of the swt line. The alignment in the horizontal plane is effected by gravity, and in the vertical plane by adjusting the length of the nylon slings. This type of support also tends to equalize the line tension between adjacent spans and therefore the line can be kept under a higher average tension, thus reducing the amount of the undesired sag between supports. An additional advantage is that very little material is introduced into the field surrounding the line.

In order to determine, with the model line, the amount of loss due to the nylon cord slings, the supporting cord cross section was varied by placing two or more slings in parallel. When the cross-sectional area of a support is doubled, then the total polarization current is also doubled. The result is that the amplitude of the radiated field is increased by a factor two and the radiated power by a factor four. Tripling the supporting cross section, by placing three slings in parallel, causes nine times the radiation loss of a single sling. When two slings were added at each point of support the measured increase in line loss was approximately 0.2 db. Therefore the single sling supports caused $\frac{1}{8}$ of 0.2 db or about 0.025-db loss. Since the radiation loss is independent of the scaling factor, this same amount of loss is produced by the supporting nylon sling of a 1-mile section of a correspondingly scaled full-sized line, and of course, this loss is negligible.

Effect of Poles and Crossarms

Since the poles have a larger cross section than the cross arms, and in practice the distance from the latter can be made sufficiently large, only the effect of the poles was considered. For an approximation, one can assume that the loss is proportional to the square of the maximum radial electric field strength at the axis of the pole. With this simplifying assumption, and the further assumption that the diameter of the pole is small compared to the wavelength, the following formula has been

derived for the loss L_p which is ca sed by a single pole:

$$L_p = \frac{A}{Z}\left[\frac{F}{\lambda^2}\,\frac{\gamma}{k}\,H_1^{(1)}(\gamma D)\right]^2 db. \qquad (1)$$

Z = impedance of the line, defined as the quotient of the propagated power divided by the square of the current in the conductor.

$H_1^{(1)}$ = Hankel-function of first order and first kind.

$$\gamma = \sqrt{h^2 - k^2}\,.$$

$h = 2\pi/\lambda_0$; λ_0 = wavelength of the surface wave.

$k = 2\pi/\lambda$; λ = free space wavelength.

D = distance of the pole axis from the center of the wire.

F = cross-sectional area of the poles.

A = empirical constant. The value of A is dependent on the dielectric constant of the pole.

The constant A for the model poles (redwood) was found to be 1.0×10^5. Since the diameter of the model poles was not small compared to the wavelength, A for full-scale poles may be somewhat different.

Fig. 2 shows the measured and calculated loss per

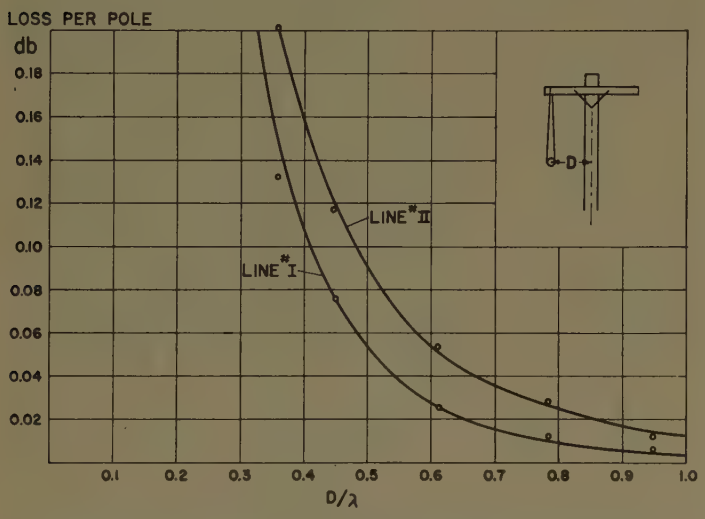

Fig. 2—Loss due to a pole as a function of the distance D of the line from the pole. The cross-sectional area of the model poles is 3 square inches, the frequency is 2000 mc. Dimensions of the lines: Line No. I, Polyethylene insulation, $d_0 = 0.120$ inch, $d_i = 0.051$ inch and Line No. II Polyethylene insulation $d_0 = 0.130$ inch, $d_i = 0.102$ inch. (d_0 = outer diameter of insulated wire, d_i = diameter of wire without insulation.)

pole as a function of the distance (D) from the axis of the pole to the center of the conductor (measured in wavelengths). The cross-sectional dimensions of the lines and the poles used for the model line are given with the figure. The curves were calculated with (1) for $A = 1.0\times10^5$. The points shown along the curves are the measured points. The poles have little effect on the loss of line No. I if their distance from the line exceeds $\frac{3}{4}\lambda$. If the data for Line No. I are applied to a full-size line with a pole spacing of 120 feet, the loss due to the poles will be found to be less than 0.5 db/mile if the poles are at least $\frac{3}{4}\lambda$ from the line. Actually the loss would be less than expected from Fig. 2 because the poles of the model line were oversize.

Effect of Bends

A bend in a swt line radiates like an infinitely long V antenna.[2] The radiation loss from a bend increases with the square of the deflection angle, provided this angle is small (less than 10°). For larger angles the relation between deflection angle and radiation loss is more complex. If the bend is not too great, that is if less than 10 per cent of the energy is radiated, the radiated power N_r can then be determined with the following formula:

$$N_r = 30II^*\left[\frac{u^2 + \sin^2\theta}{u\sin\theta}\ln\frac{u+\sin\theta}{u-\sin\theta} - 2\right] \text{Watt}$$

where

$$u^2 = h^2/k^2 - \cos^2\theta; \qquad \theta = \alpha/2. \qquad (2)$$

α is the deflection angle at the bend, I is the current in the line. The symbols h and k are explained under (1). The formula can be greatly simplified if $\theta = \alpha/2$ is very small, then

$$N_r = 10II^*\frac{\alpha^2}{\delta v/c} \text{ Watt } (\alpha \text{ in radians}). \qquad (3)$$

$\delta v/c$ is the reduction in phase velocity of the surface wave with respect to free space velocity c.

It is interesting to note that the radiation loss of a bend is little dependent on the frequency and mainly determined by the ratio between outer diameter d_0 of the dielectric coated conductor and the diameter d_i of the plain conductor. This is illustrated by the curves in Fig. 3, opposite, which show the calculated radiation loss of bends with small deflection angles as a function of d_0/d_i, for $\lambda/d_i = 50$ and $\lambda/d_i = 500$. The radiation loss within the frequency range of 1 to 10 changes by less than 10 per cent.

Fig. 4 shows the radiation loss of bends for two different lines. The curves were calculated; the points indicate the measured values. The dimensions of the lines are shown in the figure. The agreement between the calculated and measured loss is very good for deflection angles below 30° that is, as long as the radiation loss is considerably less than 1 db. In the case of a line with a thinner dielectric layer, the same loss would occur at a smaller angle, and the theoretical curve would deviate earlier from the measured points.

The fact that the radiation loss of a bend increases approximately with the square of the angle of deflection, suggests a method for reducing this loss. If a single bend is replaced by two bends of half the deflection angle, each of these smaller bends would have one fourth the loss of a single bend, and together they would have one

[2] G. Goubau, "Bends in Surface Wave Transmission Lines," Signal Corps Eng. Lab. Tech. Memo. No. M-1597; August, 1956.

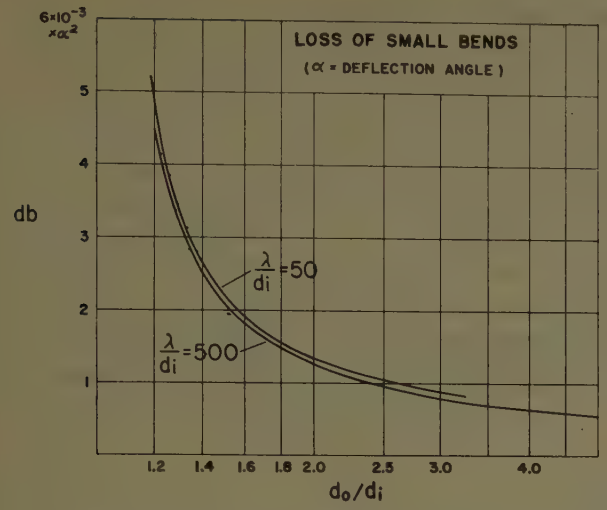

Fig. 3— Radiation loss of bends with small deflection angles (α=in degrees) for $\lambda/d_i=50$ and $\lambda/d_i=500$ as a function of d_0/d_i.

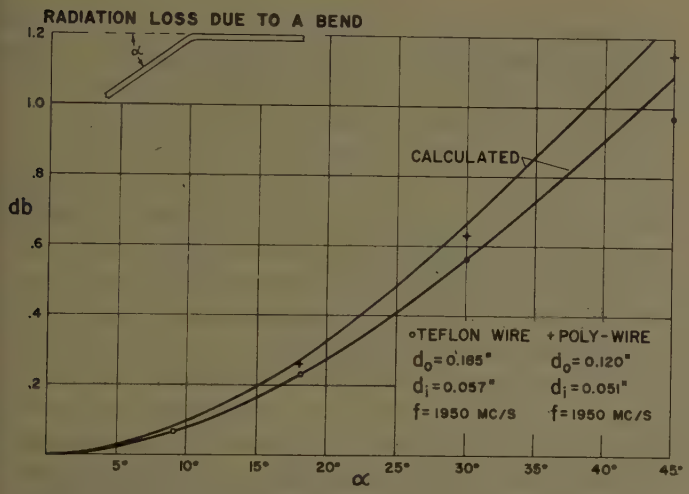

Fig. 4—Measured loss of bends with various deflection angles compared with calculated curves.

half the loss of the single bend. In general, replacing a single bend by n smaller bends each having $1/n$th of the deflection angle of the original single bend should reduce the loss to $1/n$th. This reasoning, however, is not conclusive because it implies the assumption that the "sub-bends" into which the large bend is divided are radiating independently. Actually their radiation fields form a resulting radiation field and the corresponding loss may differ considerably from that of independently radiating bends. It is obvious that as the distance between the sub-bends is continuously decreased, the radiation approaches that of a single bend having a deflection angle equal to the sum of the deflection angles of the sub-bends.

The experimental study of bends has demonstrated that if a single bend is split into two sub-bends, there is an optimum spacing between the sub-bends such that the loss is a minimum. Fig. 5 is an example of the variation in loss when three 30° bends in the line at three consecutive suspension points are divided into pairs of

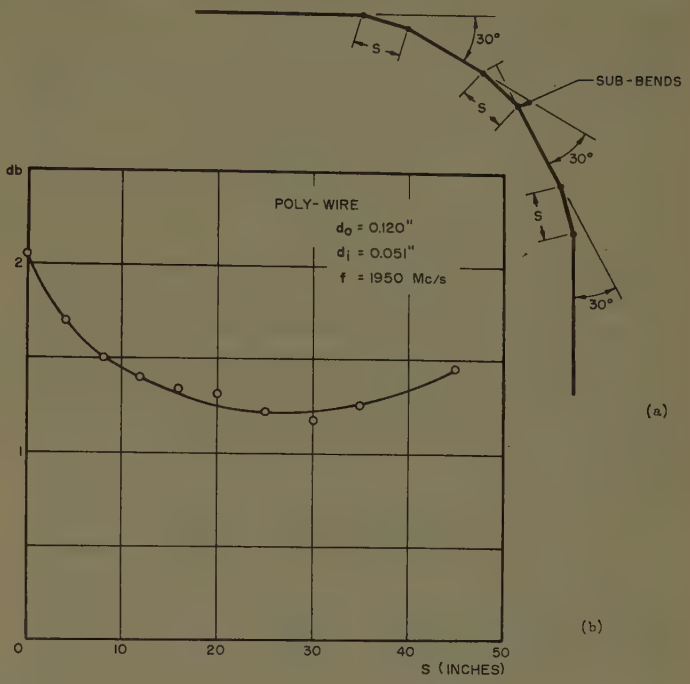

Fig. 5—(a) A 90° turn consisting of three 30° bends each of which is split in two sub-bends. The spacing between the 30° bends is approximately 24 wavelengths. (b) Loss measured for the 90° turn shown in (a) as a function in spacing of the sub-bends.

equal sub-bends and the spacing between the sub-bends is varied. The optimum spacing equals a few wavelengths. The minimum loss is somewhat higher than predicted for independently radiating sub-bends. It is noted that the optimum spacing is not critical. Spacing the sub-bends by two wavelengths is sufficient to obtain a considerable improvement. A further small improvement is obtained by introducing an additional small bend between each pair of sub-bends. The loss of the 90° turn is then reduced to about 1 db. This loss is actually somewhat smaller than the loss which occurs when all the sub-bends are equally distributed around the 90° turn.

Effect of Sags

The sags between supports in a swt line also produce some radiation loss, mainly due to the bends which are introduced at each point of support. Theoretical considerations show that the loss increases with the square of the sag. Assuming that the radiation is due only to the bends, the loss can be calculated with (3). But since the bends in the line at the supports are not sharp, and the line on either side of the bend is curved in the opposite direction, some compensating effect takes place. The measured loss therefore is less than that calculated for the bends. Fig. 6 shows an example of the measured loss per span as a function of the relative sag (sag s divided by the length l of the span). The dimensions of the line are given in the figure. The scale on the abscissa is proportional to $(s/l)^2$, thus permitting a linear representation of the loss. The dotted curve is calculated for

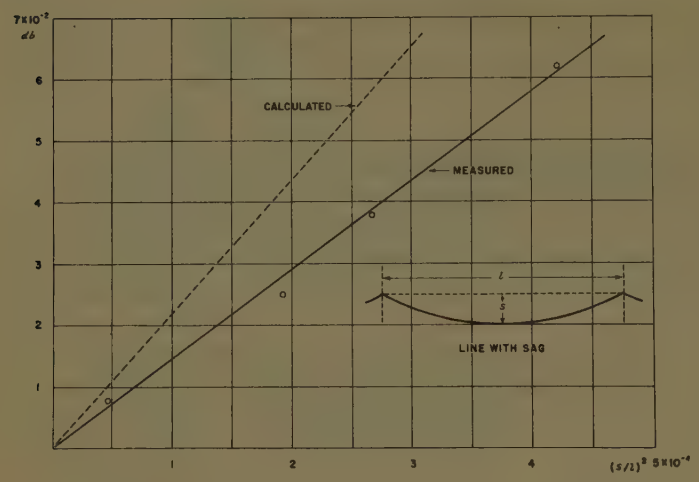

Fig. 6—Loss due to sag as a function of the square of the ratios between sag and span. $d_0/d_i=2.35$; $\lambda/d_i=120$.

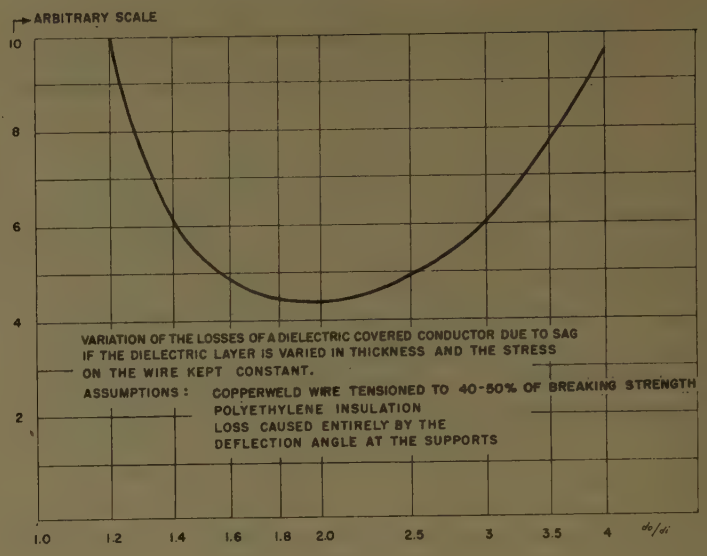

Fig. 7.

the bends at the points of support. The measured loss is only about 65 to 70 per cent of the calculated loss.

The measured curve in Fig. 6 can be used for determining approximately the loss due to sag of any line. If, for instance, the sag of a full-size line is 1 foot at the center of a 120-foot span, then $(s/l)^2=0.7\times10^{-4}$. Assume d_0/d_i and λ/d_i are the same as in Fig. 6; the loss due to sag per span is then 1.0×10^{-2} db. If d_0/d_i is different, say 1.5, then Fig. 3 may be used to correct for the different ratio d_0/d_i. According to Fig. 3, the loss in a bend is about twice as large for $d_0/d_i=1.5$ as it is for $d_0/d_i=2.35$. The loss per span will thus be about 2.0×10^{-2} db. The loss due to sag for 44 spans per mile will be about 0.9 db. Since this loss is rather high; the ratio d_0/d_i should be increased to at least 2.0.

There is an optimum thickness of the dielectric layer with respect to the sag. Increased dielectric thickness causes increased sag due to increased weight, assuming the tension on the line is kept constant. Although the thicker dielectric layer tends to reduce the line loss, this reduction can be overcompensated by the effect of the increased sag. This is illustrated in Fig. 7. In this figure a copperweld wire of fixed diameter is considered; the dielectric layer is varied while the tension on the line is kept constant (40 to 50 per cent of the breaking strength). The loss due to the sag is plotted in an arbitrary scale vs the ratio d_0/d_i. The loss is shown to have a broad minimum at $d_0/d_i=2$.

Coupling Between Two SWT Lines

The coupling effects between two swt lines have been investigated theoretically by Meyerhoff.[3] Since this theory contains certain simplifying assumptions, it was desirable to verify experimentally some of the predictions of this theory.

The coupling phenomenon between two swt lines may be explained as follows: A system of two parallel lines, when considered as a unit, is a system which propagates two wave modes. If the propagation constants of the lines differ and the lines are not very close together the two modes are almost identical with the surface waves on the individual lines. However, each wave induces a small current in the adjacent line, and the reaction causes a slight modification of the phase velocity. In the case where the propagation constants of the two lines are identical, the two modes differ considerably from the individual surface wave, independent of the spacing of the lines. Each mode has equal currents in both lines. The currents are in phase for one mode, and 180° out of phase for the other mode. The phase velocities of the two modes are different. The difference increases with decreasing spacing. If energy is fed to one line only, then both modes are excited simultaneously in such a phase relation that at the excitation point, the currents add in the first line, and cancel in the second line. As the two waves propagate along the lines, the phase relation varies in accordance with the difference in phase velocities. When the mutual phase difference has changed by π, the currents cancel in the first line and add in the second line. The total energy is then concentrated around the other line. After a further change of the mutual phase difference by π, the energy has returned to the first line, and so on.

In order to obtain complete power transfer the lines must have a minimum length which is dependent on the spacing of the lines. Assume one line is very long and the other is short; either one, say the long line, is excited at A (see right-hand side of Fig. 8). If the lines are very far apart, the current in the short line is zero. Now, when the lines are brought together, a current is induced in the second line. For a certain spacing this current has a maximum at the termination C. At the same time the current at the termination B of the long line is zero. If the spacing is further decreased, the current in the short line decreases and reaches zero when the coupling is such that the energy is transferred twice, first from the long

[3] A. A. Meyerhoff, "Interaction between surface wave transmission lines," Proc. IRE, vol. 40, pp. 1061–1065; September, 1952.

line to the short line, and then back to the long line. Further decrease of the spacing brings the energy back to the short line, and so on.

Fig. 8 also demonstrates the energy transfer. The curve shows the measured attenuation between the lines as a function of their spacing. Zero attenuation means the entire energy is transmitted to the short line. The measured attenuation between A and C is actually somewhat below zero. There is somewhat more energy received at the short line than there was received at the end of the long line, before the short line was coupled. The explanation is that the system of two parallel lines has somewhat lower loss than one line alone.

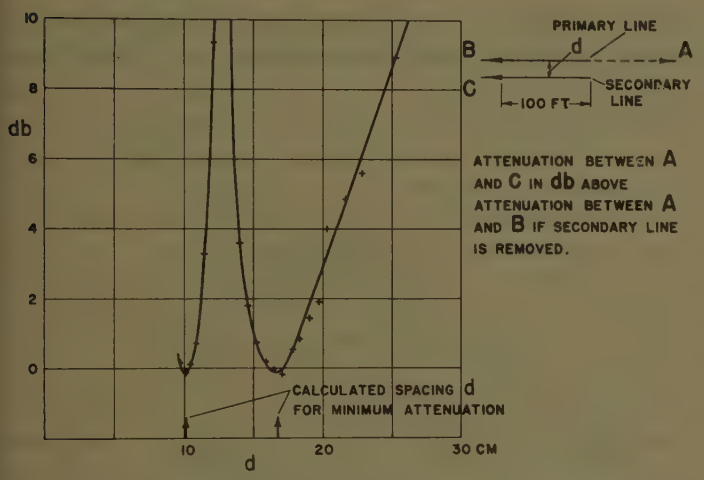

Fig. 8—Coupling between two surface wave transmission lines with identical wires.

The calculated spacings for complete power transfer are in perfect agreement with the measurements. The line sections used in above measurements were carefully selected because variations of the dielectric layer of the wire by a few per cent will upset the conditions for complete energy transfer.

From the foregoing it is obvious that two identical long-distance swt lines intended to operate independently, should not be strung parallel. However, if the dielectric coats differ by a few per cent the energy exchange becomes very small. The crosstalk between such lines still may be considerable if they are only a wavelength apart. This crosstalk will be large, however, only if the lines transmit signals in the same direction, because the coupling is directional.

Conclusion

SWT lines for long-distance transmission can be supported in such a manner that the increase in transmission loss effected by poles, crossarms, supporting nylon ropes, and the sags between spans is less than a db per mile. In order to secure this small loss, the ratio d_0/d_i between outer (conductor plus dielectric) and inner diameter (conductor alone) of the line should be at least 2. Since the loss of a swt line increases little with increasing thickness of the dielectric layer, such a ratio is permissible for a low-loss line. If a line for long-distance transmission contains curves, the transmission loss is further increased by the bends necessary in the curves. The amount of additional loss will depend on the layout of the line. If d_0/d_i is greater than 2 and radiation reducing support methods previously described are used, the loss in curves can be kept within reasonable limits, say about 1 db for a 90° turn.

As the result of the information obtained from the scale model tests and theoretical studies, it appears entirely practical to construct a swt line for low-loss long-distance transmission with 100 mc or more bandwidth. For example, if the conductor diameter is 0.4 inch and the outer diameter of the line is 1 inch, and if the dielectric layer consists of brown polyethylene, the calculated loss is 2.5 db/mile at 100 mc and 4.7 db/mile at 200 mc. The actual loss will be about 10 per cent higher due to imperfections of the conductor surface which, are always present. If the loss due to supports is 0.5 db/mile, then the loss of a straight line section will be about 3.3 db/mile at 100 mc and 5.7 db/mile at 200 mc. At these frequencies the efficiency of the line is not affected by rain. Also dry snow and thin layers of ice have little effect on the transmission loss.

Antenna-to-Medium Coupling Loss*

HAROLD STARAS†

Summary—**This paper presents an improved estimate of one of the more important systems parameters on a scatter circuit, namely, the antenna-to-medium coupling loss. The work presented in this paper differs from the earlier work of Booker and de Bettencourt[1] in that it permits evaluating the coupling loss even when nonconical, nonidentical antennas are used at either end of the scatter circuit, and it also permits taking the anisotropy of atmospheric turbulence into account. An important conclusion is reached that the coupling loss is not shared equally by the two antennas (*i.e.*, transmitting and receiving) even if they are identical. This is a phenomenon which should be fully appreciated by engineers designing a scatter circuit or when measuring the coupling loss experimentally.**

Introduction

In an earlier paper, Booker and de Bettencourt[1] presented an excellent discussion of the effect of very narrow beams on the systems parameters on a scatter circuit. In particular, they discussed the phenomenon of antenna-to-medium coupling loss and presented estimates of the loss. However, they restricted their consideration to identical conical antenna beams, a restriction which is removed in this paper. Furthermore, in the important region where the antenna beamwidths are approximately equal to the medium beamwidths, their estimate is obtained by interpolation from the case of very broad antenna beams and very narrow antenna beams while the estimates presented in this paper are evaluated quantitatively in this region. In addition, these estimates permit taking into account the statistical anisotropy of atmospheric turbulence which recent measurements by RCA and other laboratories indicates does exist. Finally, the analysis developed in this paper points out clearly that the coupling loss on a scatter circuit is *not* shared equally between the transmitting and receiving antennas. An understanding of this fact is essential for properly designing a scatter circuit and even more so, when conducting experimental tests to measure the coupling loss.

Basic Formulation

We begin by referring to the development presented by the author[2] in an earlier paper. This starting point can be written for our purposes as follows.

$$\langle P\rangle \sim \int_{H_0}^{\infty}\int_{-\infty}^{\infty} \frac{(h-H_0)(f_0\cdot f)^2}{(x^2+r^2h^2)^2(h-H_0/2)^2}\,dxdh \quad (1)$$

where $\sim$ means "proportional to," $\langle P\rangle$ is the average received scattered power measured relative to free space, $(f_0\cdot f)^2$ represents the antenna power patterns of the transmitting and receiving antennas normalized to unity along the beam axes, and r is the anistropy parameter defined as follows:

$$r = \frac{\text{scale of turbulence in vertical dimension}}{\text{scale of turbulence in horizontal dimension}}.$$

The other variables x, h, and H_0 refer to the coordinate system being used and are shown in Fig. 1, which by

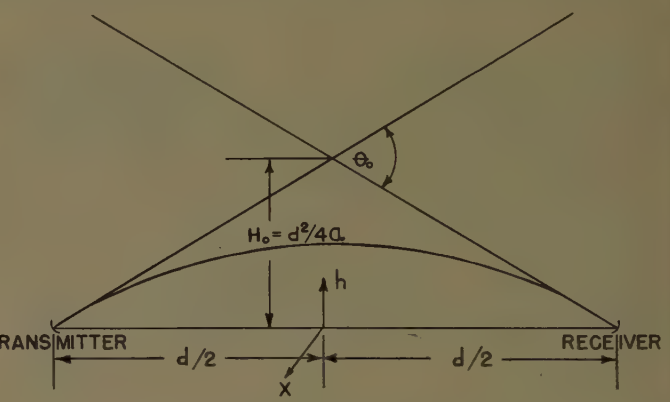

Fig. 1—Geometry for scatter propagation.

now has become the symbol of the scatter propagationist. "a" is the radius of a 4/3 earth.

Before proceeding to evaluate (1), it may be of interest to point out that the factor $(h-H_0/2)^{-2}$ in (1) represents the assumption that the intensity of turbulence varies inversely as the square of the height above the earth. This particular assumption leads to a distance dependence of d^{-5} for $\langle P\rangle$. Some investigators believe that the distance dependence is more closely approximated by d^{-6}. This would imply that the negative exponent in the term $(h-H_0/2)$ lies between 2 and 3. A more detailed discussion of this point is presented by Gordon.[3] On the other hand, the frequency dependence of the average scatter loss, $\langle P\rangle$, is not affected by the term just discussed. A change in the frequency dependence would imply a change of the scattering cross section. The only factor of the scattering cross section which appears in (1) is $(x^2+r^2h^2)^{-2}$. In order to accommodate a $1/f$ frequency dependence, for example, this factor would be changed to $(x^2+r^2h^2)^{-5/2}$. This change would also increase the distance dependence even without changing the exponential in the term $(h-H_0/2)$. Thus, very minor modifications of the integrand in (1)

* Manuscript received by the PGAP, May 31, 1956; revised manuscript received, January 12, 1957. This work was supported by the Signal Corp. under Contract DA-36-039-sc-64555 on a Study and Investigation of Tropospheric Scattering.

† RCA Labs., Princeton, N. J.

[1] H. G. Booker and J. T. de Bettencourt, "Theory of radio transmission by tropospheric scattering using very narrow beams," Proc. IRE, vol. 43, pp. 281–290; March, 1955.

[2] H. Staras, "Forward scattering of radio waves by anistropic turbulence," Proc. IRE, vol. 43, pp. 1364–1380; October, 1955. See, in particular, eqs. (8) and (9) of Sec. V, and the accompanying discussion.

[3] W. E. Gordon, "Radio scattering in the troposphere," Proc. IRE, vol. 43, pp. 23–28; January, 1955.

are necessary in order to accommodate different estimates of the frequency and distance dependence of the scatter loss. We will, therefore, attempt to evaluate (1) as it stands because the minor modifications necessary to explain the distance or frequency dependence will hardly change the coupling loss estimate.

To make progress in evaluating (1), an explicit analytical approximation must be made for the antenna beam pattern functions. Making a usual assumption that the beam shape is approximately Gaussian, then each antenna pattern may be considered to have the following form in each dimension:

$$\exp\left\{-0.7(\tan\beta/\tan\beta_0)^2\right\}$$

where β is the angle measured from the antenna beam axis and β_0 is the semi-beamwidth, *i.e.*, the angle between the antenna axis and the 3-db down point in the particular direction in question. Each antenna may have two different β_0, one for each dimension. It was not possible to evaluate (1) as it stands even with the Gaussian assumption for the antenna patterns; however, to a good approximation we can evaluate it as follows: First consider antennas which have broad beams in the vertical dimension but which may have narrow beams in the horizontal dimension and thus suffer a coupling loss due to their horizontal beamwidth. Then reverse the situation and consider antennas which have broad beams in the horizontal dimension but which may have narrow beams in the vertical dimension and thus suffer a coupling loss due to their vertical beamwidth. Finally, for antennas with narrow beams in both dimensions, the total coupling loss would be approximately the db sum of the coupling losses in each dimension.

Evaluating the Coupling Loss

With the above approximation, the first integral we evaluate (for measuring coupling loss in the horizontal dimension) becomes

$$\langle P\rangle \sim \int_{-\infty}^{\infty} \frac{\exp\left\{-(x/b_1)^2-(x/b_2)^2\right\}}{(x^2+H^2)^2}\,dx \qquad (2)$$

where H is the parameter rh evaluated approximately in the center of the scatter volume. From Fig. 3 and the accompanying discussion there, we can estimate that $H\cong 1.2\,rH_0$. In (2) b_1 and b_2 are related to the antenna beamwidths by $b_1=(d/2\sqrt{0.7})\tan\beta_1$, and $b_2=(d/2\sqrt{0.7})\tan\beta_2$. In the present context β_1 is the semi-beamwidth in the horizontal dimension for one antenna while β_2 would be the semibeamwidth in the horizontal dimension for the second antenna. If we define $b^{-2}=b_1^{-2}+b_2^{-2}$, (2) becomes

$$\langle P\rangle \sim \int_{-\infty}^{\infty} \frac{e^{-(x/b)^2}}{(x^2+H^2)^2}\,dx. \qquad (3)$$

It is to be noted that in (3), it was explicitly assumed that the antenna axes lie in the great circle plane between transmitter and receiver. The integral is evaluated in the Appendix, yielding

$$\langle P\rangle = e^{(H/b)^2}[1-2(H/b)^2][1-\Phi(\sqrt{2}H/b)] + \frac{2}{\sqrt{2\pi}}(H/b) \qquad (4)$$

where $\Phi(x)$ is the probability integral defined by

$$\Phi(x)=\frac{1}{\sqrt{\pi}}\int_{-x}^{x} e^{-t^2/2}dt.$$

Eq. (4) has been normalized so that $\langle P\rangle=1$ at $b=\infty$, *i.e.*, for broad-beam antennas. A graphical presentation of (4) is shown on Fig. 2 where the coupling loss is

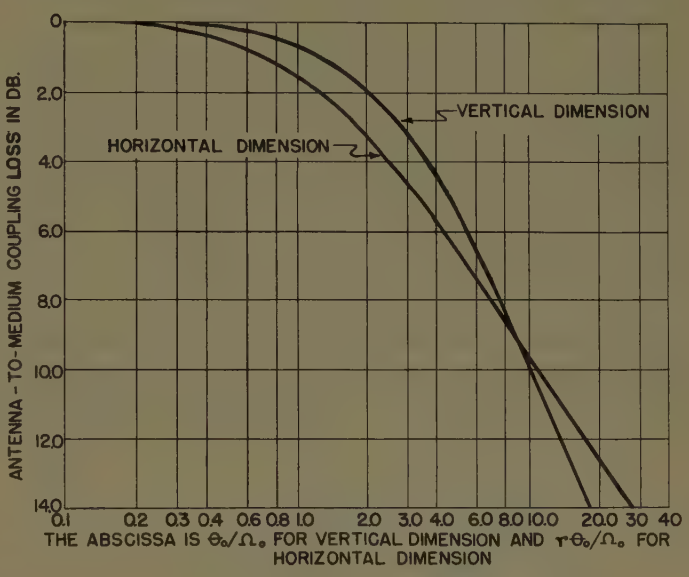

Fig. 2—Estimate of antenna-to-medium coupling loss.

plotted as a function of $r\theta_0/\Omega_0$, r being the anistropy parameter, θ_0 being the angular distance between transmitter and receiver and Ω_0 being the effective beamwidth in the horizontal dimension of the transmitting and receiving antennas. The effective beamwidth Ω_0 is defined in terms of the individual beamwidths by

$$\Omega_0^{-2}=\Omega_1^{-2}+\Omega_2^{-2}$$

where Ω_1 and Ω_2 are the beamwidths between 3-db points of antennas 1 and 2. If one antenna is broad and the other narrow in the horizontal dimension, then the effective beamwidth is that of the narrow one. If both antennas have identical beamwidths, then the effective beamwidths is 0.707 that of either antenna. We next evaluate the coupling loss due to mismatching antenna beamwidths with medium beamwidth in the vertical dimension. In this case, we assume that the antennas have broadbeams in the horizontal dimension. Integrating over x in (1) and introducing the Gaussian beamwidth assumption with the antenna axes along the horizon planes, we obtain

$$\langle P\rangle \sim \int_{H_0}^{\infty} \frac{(h-H_0)\exp\left\{-\left(\frac{h-H_0}{b_1}\right)^2-\left(\frac{h-H_0}{b_2}\right)^2\right\}}{h^3(h-H_0/2)^2}\,dh. \tag{5a}$$

Introducing

$$b^{-2}=b_1^{-2}+b_2^{-2} \text{ and } z=\frac{h-H_0}{H_0/2},$$

(5a) can be rewritten as

$$\langle P\rangle \sim \int_0^{\infty} \frac{z\exp\left\{-\left(\frac{H_0 z}{2b}\right)^2\right\}}{(z+2)^3(z+1)^2}\,dz. \tag{5b}$$

It is to be noted that since these integrals are all normalized to unity at $b=\infty$, multiplicative factors are always neglected. Returning to (5b), it was not possible to evaluate it in terms of tabulated functions. However, since we are dealing with real positive definite quantities, a satisfactory approximation to the denominator of the integrand is obtained by the following reasoning. A function of the form $(z+\text{const})^{-n}\cong c_0e^{-az}$ for n large. This suggests that the denominator of the integrand in (5b) can be approximated by an exponential. To fit the first two terms of a McLaurin series, the approximation is $1/8e^{-3.5z}$. This approximation was improved by a correction factor of the form $(1+1.33z^2)$. A comparison of the given integrand (without the antenna pattern factor) and the approximate integrand used is shown in Fig. 3.[4] It would seem that a quite satisfactory approximation has been made. The integral we then evaluate becomes

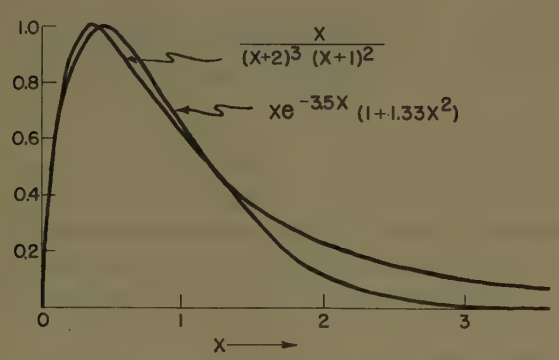

Fig. 3—A comparison of an approximate integrand with the true integrand.

$$\langle P\rangle \sim \int_0^{\infty} ze^{-(H_0zb/2b)^2}(1+1.33z^2)e^{-3.5z}dz. \tag{5c}$$

This integral can be evaluated by standard techniques yielding

$$\frac{p^2}{1.816}\left\{(1+0.272p^2+0.136p^4)-\sqrt{\pi/2}\,p(1+0.408p^2+0.136p^4)e^{p^2/2}[1-\Phi(p)]\right\} \tag{6}$$

where $p\cong 6\Omega_0/\theta_0$.

This function is also plotted in Fig. 2. As a check, (5b) was evaluated for several values of $H_0/2b$ by numerical integration using Simpson's rule with 18 points. The results were within 1 db of those shown in Fig. 2, thus confirming the validity of our approximation.

An important conclusion to be reached from this analysis is that the coupling loss is not shared equally by the antennas at either end of the scatter circuit. For example, utilizing the curves presented in Fig. 2, it can be seen that introducing a second narrow-beam antenna into a system that has already suffered a coupling loss of 6 db, say, in each dimension will not double the coupling loss (in db) but will increase it only by about 1.5 db to 2.0 db in each dimension. It might be of some interest to note that when using very high gain paraboloid antennas, the introduction of a second very high gain dish will introduce a coupling loss of about 4.0 db. It is to be noted that Booker and de Bettencourt guessed that their coupling loss estimate would be too large because of their assumptions of isotropic turbulence, a scattering parameter constant with height and very simplified approximations to the antenna beam shapes. A comparison of the Booker-de Bettencourt estimate with ours (see Fig. 4) indicates that theirs *is* too large. For our estimate, it was assumed that the anistropy parameter, r, was $\frac{1}{4}$ and that identical parabolic antennas were being used at each end of the scatter circuit, Ω being the beamwidth of each antenna.

To utilize Fig. 2 most effectively, a satisfactory estimate for the anisotropy parameter, r, should be used. In an earlier paper already referred to,[2] it was found that $r\cong\frac{3}{5}$ fitted NBS data quite satisfactorily. Using the same graphical procedure, a comparison was made between Kurihara's data[5] with theory. It was found that $r\cong\frac{2}{5}$ for the Buffalo-Ithaca path and $r\cong\frac{1}{3}$ for the Wethersfield-Ithaca path. RCA's own measurements on a 153-mile path indicated that an average value for r is $\frac{1}{5}$. All these estimates are in the same direction, namely, $r<1$ ($r=1$ would represent isotropic turbulence) even though the quantitative estimates are fairly variable. At the present state of our knowledge, it would seem that an estimate of $r=\frac{1}{4}$ should be quite satisfactory.

It is of interest to compare our theory with some data

[4] Both integrands are normalized to have a maximum value of unity.

[5] Y. Kurihara, "Trans-horizon microwave propagation over hilly terrain," PROC. IRE, vol. 43, pp. 1362–1368; October, 1955.

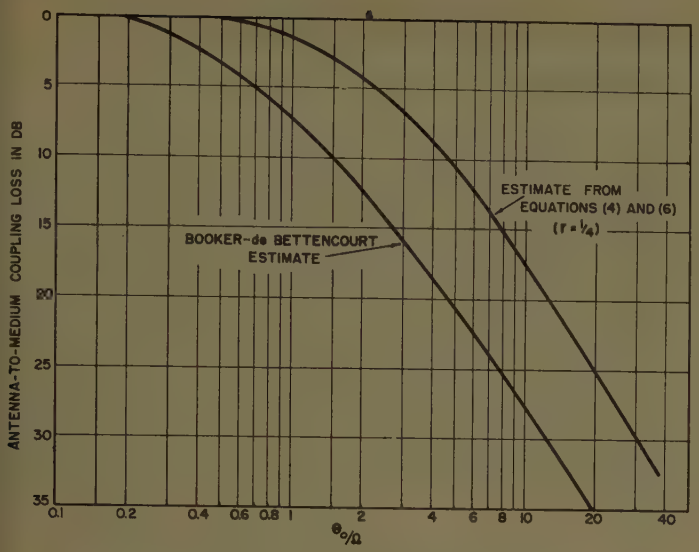

Fig. 4—A comparison of two estimates for coupling loss assuming identical parabolic antennas at each end.

that has come to our attention. Recent Lincoln Laboratory data (unpublished) have indicated that on the average, no noticeable coupling loss has been observed on a 618-mile path utilizing a 60-feet dish (freq. = 400 mc) at the transmitting end while comparing a 60-feet dish with a 28-feet dish on the receiving end. For this particular situation, our estimates (Fig. 2) would suggest that a 2.5-db coupling loss would occur. It is not possible to utilize the Booker-de Bettencourt[1] estimates properly for this situation since their estimates are for identical antennas at each end of the scatter circuit. However, their estimate for the coupling loss between two 60-feet antennas on this path is about 13 db. It would appear that our estimates are more consistent with Lincoln Laboratory data and it would furthermore appear that it is quite essential to be able to estimate coupling loss for dissimilar antennas at either end of the scatter circuit.

Another source of data of interest in this connection is the Bell Laboratory data[6] obtained on a Labrador path. In this experiment, a coupling loss of 2.5 db was measured (650 hours of data) at 4000 mc when a 28-feet transmitting antenna was used and a comparison between the received signal on a 5 feet and 28 feet antenna was made at the receiving end. For this particular situation our estimate as obtained from Fig. 2 is 2 db. Again it appears that our theory is in substantial agreement with experiment.

[6] K. Bullington, W. J. Inkster, and A. L. Durkee, "Results of propagation test at 505 mc and 4,090 mc on beyond-horizon paths," Proc. IRE, vol. 43, pp. 1306–1316; October, 1955.

Appendix

In evaluating an integral of the form

$$F(q) = \int_{-\infty}^{\infty} \frac{e^{-q^2x^2}}{(x^2 + H^2)^2}\, dx \tag{7}$$

the following technique was used. It is to be noted that

$$F(q) = -\frac{d}{d(H^2)} \int_{-\infty}^{\infty} \frac{e^{-q^2x^2}}{x^2 + H^2}\, dx \tag{8}$$

and that

$$\frac{1}{x^2 + H^2} = \frac{1}{2H} \int_{-\infty}^{\infty} e^{-|k|H - jkx} dk. \tag{9}$$

Substituting (8) and (9) into (7) yields

$$F(q) = -\frac{d}{d(H)^2} \left\{ \frac{1}{2\pi} \int\int_{-\infty}^{\infty} e^{-|k|H - q^2x^2 - jkx} dx\, dk \right\}.$$

Integrating over x by completing the square in the exponent of the integrand leaves

$$F(q) = -\frac{d}{d(H^2)} \frac{\sqrt{\pi}}{2Hq} \int_{-\infty}^{\infty} e^{-k^2/4q^2 - |k|H} dk$$

$$= -\sqrt{\pi}\, \frac{d}{d(H^2)} \frac{1}{qH} \int_{0}^{\infty} e^{-k^2/4q^2 - kH} dk. \tag{10}$$

Eq. (10) is easily evaluated by completing the square, evaluating the integral and then performing the indicated differentiation recognizing that

$$\frac{d}{d(H^2)} = \frac{1}{2H} \frac{d}{dH}.$$

The result for $F(q)/F(0)$ is that given in (10).

Precipitation Particle Impact Noise in Aircraft Antennas*

ROBERT L. TANNER†

Summary—**It has been found that precipitation static noise is produced in antennas under plastic surfaces, even though these surfaces are covered by conductive films. In this paper, the noise is shown to be due to a noise-producing mechanism associated with the acquisition of charge by individual precipitation particles upon impact in the antenna field region. The existence of such a mechanism is demonstrated theoretically and substantiated by experiment. Production of such noise in antennas is analogous to production of shot noise in vacuum tubes. Calculated results indicate that in practical antennas this process is capable of generating noise voltages sufficient to disable lf and mf equipment such as the adf radio compass.**

Introduction

THE TYPE of radio interference known as precipitation static has long been familiar to aircraft radio engineers. Precipitation static is peculiar to aircraft in flight, and derives its name from the fact that it was first associated with flight through snow storms.

It is now known that several distinct basic mechanisms contribute to precipitation static interference. The best known of these is associated with what has been called "autogenous charging." Particles of snow, or the ice crystals found in high clouds, strike the aircraft, charging it to a high voltage. The charging continues until corona discharges occur at the wing tips and other extremities, producing noise which couples into the radio receivers. The production of noise by corona discharges and the mechanism by which the noise couples into the receivers have received considerable attention, and are quite well understood.[1,2] Progress has been made in alleviating noise from this source, although no completely satisfactory method is yet available. The familiar wick discharger, incidentally, is directed at overcoming this type of noise.

Another type of precipitation static noise is produced in antennas mounted under plastic surfaces such as canopies and radomes. The plastic surface is an insulator and ice particles striking it charge it to a high voltage relative to the surrounding metal portions of the aircraft. The charge rapidly builds up until a sparking or "streamering" discharge occurs between the plastic surface and the surrounding metallic structure, with consequent coupling of noise into the antenna. The solution to this type of interference seemed obvious: to coat the dielectric surfaces with a film having a conductivity sufficiently high to prevent the accumulation of static charge, but not so high as to act as an rf shield. Conductive coating materials have been developed, and this solution has been tested. Although the application of conductive material eliminated the discharges, it failed to eliminate the noise. This result made it evident that some mechanism besides sparking—one capable of producing noise in spite of the conductive coating—was contributing significantly to the observed noise. An explanation for the residual noise is proposed in the present paper.

* Manuscript received by the PGAP, April 23, 1956; revised manuscript received, January 15, 1957. The work was supported by the U. S. Air Force under Contracts AF 33(616)-2761 and AF19(604)-1296.

† Stanford Res. Inst., Menlo Park, Calif.

[1] R. Gunn, W. C. Hall, and G. D. Kinzer, "Army-Navy precipitation static project, part I," PROC. IRE, vol. 34, pp. 156P–161P; April, 1946.
G. D. Kinzer and J. W. McGee, "Army-Navy precipitation static project, part IV," PROC. IRE, vol. 34, pp. 234–240; May, 1946.

[2] R. L. Tanner, "Radio Interference from Corona Discharges," Stanford Res. Inst., Menlo Park, Calif., Tech. Rep. No. 37, Contract No. AF 19(604)-266; April, 1953.

A Coupling Theorem

In discussing the phenomena of precipitation static and the manner in which electrical disturbances couple into nearby antennas it is convenient to employ a coupling theorem developed in the investigation of interference from corona discharges.[2] The theorem is a reciprocity relationship, and can be derived in a manner similar to that in which the familiar Lorentz reciprocity theorem is derived. The derivation will not be given in the present paper. To state the theorem it is necessary first to define the two situations illustrated in Fig. 1.

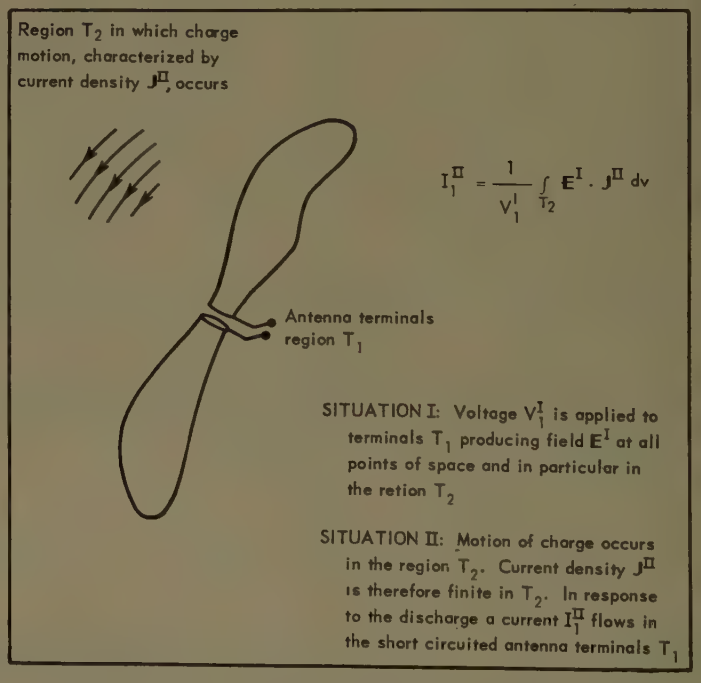

Fig. 1—Coupling of electrical effects due to charge motion in antenna field.

For the conditions outlined in these situations the coupling theorem states that

$$I_1^I(\omega) = \frac{1}{V_1^I(\omega)} \int_{T_2} \vec{E}^I \cdot \vec{J}^{II} dv. \qquad (1)$$

Eq. (1) is derived using the Fourier-transformed form of Maxwell's equations, so that, in general, all quantities are functions of frequency. The field quantities $\vec{E}^I$ and $\vec{J}^{II}$ are also, as indicated, functions of the spatial coordinates. To obtain the response as a function of time it is necessary to perform the inverse Fourier transform. A special condition exists, however, when the electrodynamic situation can be adequately described by the quasistatic approximation. Such a condition exists when the dimensions of the region in which it is necessary to define the field $\vec{E}^I$ are small compared to the wavelength of the highest frequencies of interest.

If the quasistatic approximation is valid, the ratio of field to applied voltage is a function of spatial coordinates only and not of frequency. For such a situation (1) can be shown to reduce to

$$I_t^{II}(t) = \int_{T_2} \frac{E^I}{V_1^I}(x) \cdot J^{II}(x, t)dv \qquad (2)$$

which expresses the terminal current as a function of time directly in terms of the current describing the motion of charge, also given as a function of time. The presence of conducting material in the field, such as conducting films surrounding the antenna, tends to render the quasistatic assumption invalid. It can be shown in the case of such coatings, however, that if the conductivity is not so high as to reduce the sensitivity of the antenna no appreciable error results.

Processes Capable of Producing Noise in the Antenna

It is evident from (1) and (2) that any process involving the motion of charge in the field of the antenna will produce a short-circuit current at the antenna terminals. Whether such currents have significant components at frequencies sufficiently high to cause radio interference depends upon the time-space distribution of the charges and their motions. In the case of discharge phenomena such as corona and over-surface streamering the motion of the charge is extremely rapid, resulting in short duration pulses of terminal current having high frequency spectral components. Discharge phenomena are excluded from consideration in the present investigation, however, and we are obliged to search for other mechanisms.

Although previous investigations had established quite conclusively that impinging precipitation in general carries negligible charge at the time of impingement, the possibility that the motion of charged precipitation particles is responsible again suggests itself. Perhaps particles charged by impact on the forward portions of the aircraft could cause noise upon passing through the fields of antennas located further to the rear. An additional objection to this possibility, however, is the relatively low velocity of such particles, which raises some doubt as to whether the moving precipitation particles could cause output current pulses sufficiently short to contain appreciable spectral components at radio frequencies. This question can be investigated with the aid of (2) which for a single moving point charge can be shown to simplify still further to

$$I_t(t) = qv \frac{E^I}{V_1^I}(x') \qquad (3)$$

where x' represents the coordinates of the particle, and q is the particle charge.

Eq. (3) states that the instantaneous terminal current induced by the motion of the particle is proportional to the magnitude of the reciprocal field at the point occupied by the particle. It is evident, therefore, that if the field is highly concentrated or has sufficiently rapid variation in space, sharp current pulses might be produced even without high particle velocities. To obtain a quantitative estimate indicating whether conditions exist in actual aircraft capable of producing rf noise by this mechanism, an investigation was carried out using the idealized model illustrated in Fig. 2. The field situation illustrated corresponds approximately to that which would exist at the metal border surrounding a canopy in which an antenna is installed, and has the advantage that it can be treated analytically with relative ease.

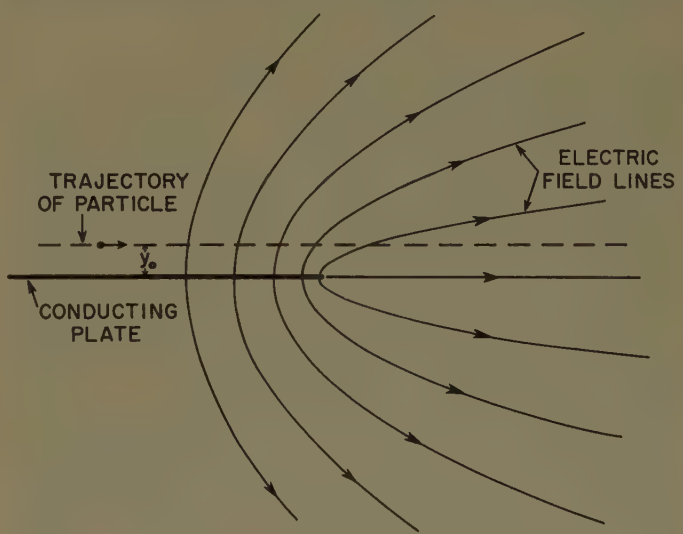

Fig. 2—Field model used in computing terminal current pulses due to induction.

For the model shown the output current pulse as a function of time is given by

$$I(t) = k_1 \left[\frac{t + \sqrt{t^2 + \left(\frac{y_0}{v}\right)^2}}{t^2 + \frac{y_0^2}{v}} \right]^{1/2}, \qquad (4)$$

where k_1 is a constant which depends upon the velocity and charge magnitude of the particle and upon the absolute magnitude of the fields at the edge of the plate.

The spectrum function of the pulse thus produced can also be obtained analytically. It is

$$g(\omega) = \frac{1}{\sqrt{j\omega}} e^{-(y_0/v)|\omega|}. \qquad (5)$$

Fig. 3 shows the output current pulses produced by

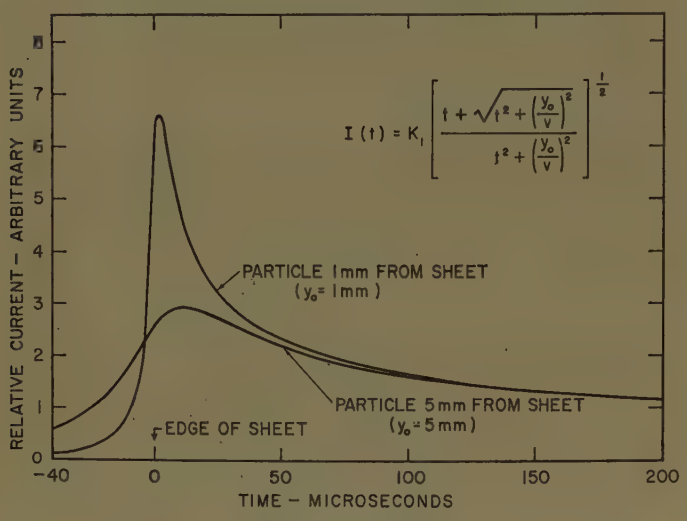

Fig. 3—Terminal current pulses produced by induction.

particles having similar charges but moving in trajectories spaced different distances from the conducting plate. The more peaked pulse corresponds to a spacing, y_0, equal to 1 millimeter, while the other corresponds to a spacing of 5 millimeters. In both cases a particle velocity of 250 meters per second, approximately 500 miles per hour, is assumed. The corresponding spectral functions are shown in Fig. 4. Consideration of the spectra of the induction pulses shown, taken in conjunction with the fact that in an actual aircraft the field areas capable of producing pulses as sharp as those illustrated are extremely small, if any at all exist, indicates that this mechanism can probably be neglected as a source of noise. It is necessary, therefore, to search further for an explanation.

The situation illustrated by the diagram of Fig. 5, together with the result stated in (3), provides the key to the production of noise. Eq. (3) states that the instantaneous value of the terminal current is proportional to the product of the charge and velocity of the particle and of the reciprocal field at the position of the particle. In the induction process considered previously the field varies with position and the position varies with time. The terminal current therefore varies with time and thus contains ac components. It is evident that the terminal current will also vary with time if the charge varies with time, even though the field is constant. This is the situation illustrated in Fig. 5. Until the time of impact the particle carries no charge and therefore produces no reaction in the external circuit. At the time of impact, t_0, the particle acquires charge instantaneously and rebounds with the magnitude of its velocity essen-

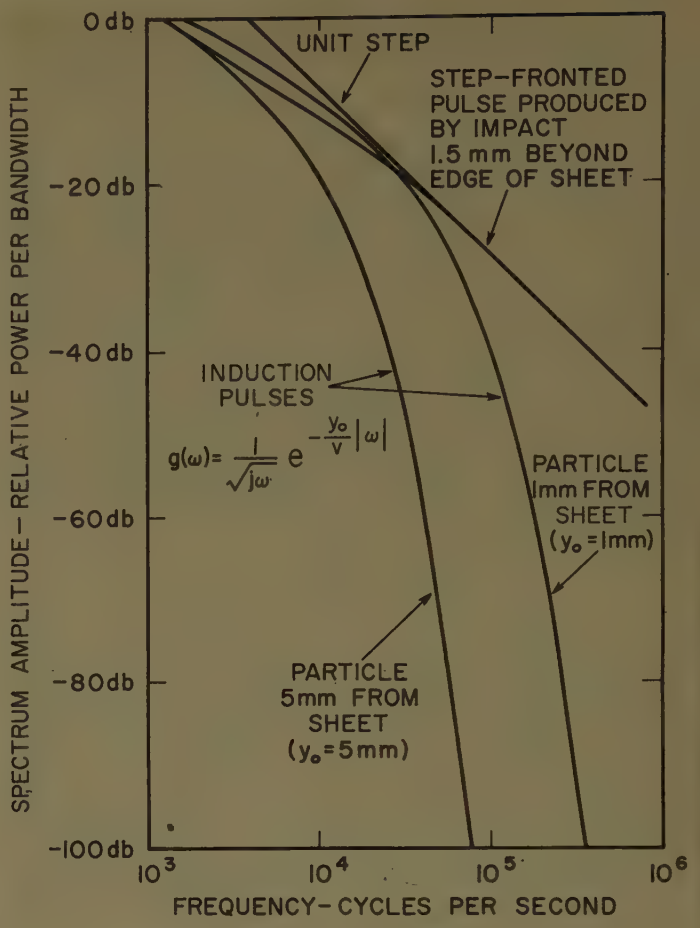

Fig. 4—Pulse spectra.

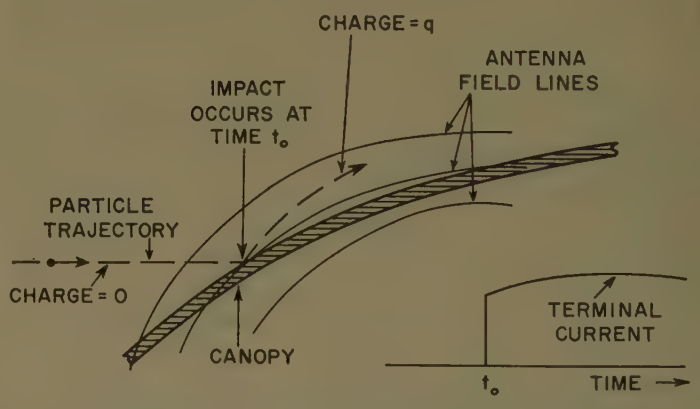

Fig. 5—Production of terminal current pulses by particle impact in antenna field region.

tially unchanged. This produces a discontinuous or step-fronted pulse similar to the one shown in the figure.

The mechanism of instantaneous charge acquisition in the field region appears able to account for the observed noise. The step-fronted pulses thus produced have noise current spectra which at high frequencies drop off only inversely with increasing frequency rather than exponentially as did the induction pulses. Furthermore, since the high-frequency components are introduced by the stepped leading edge, it is obviously not necessary to postulate concentrated fields in order to

explain the production of high levels of interference at relatively high frequencies.

Experimental Confirmation

That the step-fronted pulses which have been postulated do indeed occur and are responsible for the noise experienced has been confirmed in an interesting series of laboratory experiments. A small draw-down wind tunnel, consisting of a 150-gallon vacuum tank fitted with an inlet orifice and valve, was placed in a large refrigerated chamber in which ice fogs could be produced by introduction of steam followed by seeding with dry ice. After air was pumped from the tank, ice fogs were seeded in the chamber and the inlet valve opened. A stream of ice fog was drawn into the tank at speeds approaching Mach 1 and allowed to impinge upon an instrumented surface, permitting observation of the effects by oscillographic and other electronic techniques.

The crystals occurring in ice fogs are very much smaller and more numerous than those found in clouds, and consequently have much smaller individual charging effects. This fact in addition to the great numerical density of the particles—the stream of air flowing into the tank is only $\frac{3}{4}$ inches in diameter but carries approximately 15 million particles per second—creates considerable difficulty in distinguishing the effects of individual particles. By designing an electrode arrangement in which the reciprocal fields are large and highly concentrated in an area of approximately 0.5 square millimeter, but negligibly small over the remainder of the surface upon which the airstream impinges, it was possible to obtain oscillograms of pulses due to individual particles corresponding exactly to those predicted. One of these is shown in Fig. 6. The pulse as recorded has a finite rate of rise rather than the instantaneous step pictured in Fig. 5. The discrepancy was shown, however, to correspond exactly to that which would be introduced by unavoidable time constants associated with the measuring equipment. The short duration of the pulses is due to the particles passing out of the region of high coupling fields. As explained, the region of high fields was made very small in order to isolate the effects of single particles.

The data obtained in the ice-fog tests indicate that the charge deposited by the individual particles averages approximately 10^{-13} coulombs. It is believed that the charging effect per particle of cirrus particles or snow will average at least 100 times greater than that observed for ice-fog crystals.

In addition to the oscillographic investigation of individual particle effects, measurements were made with apparatus devised to permit spectral analysis of the noise generated when the stream of ice fog was allowed to impinge upon a simulated antenna. The rms noise voltage per unit bandwidth was observed to have a distribution which fell close to a curve representing a distribution proportional to the inverse of the frequency.

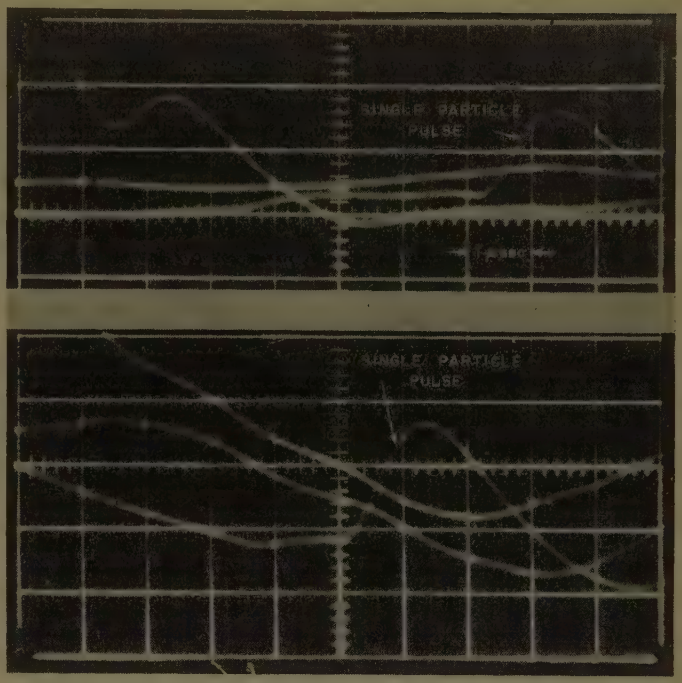

Fig. 6—Oscillograms of pulses produced by ice-fog particle impact.

It can be shown that such a spectral distribution would be expected if the basic noise-generating mechanism were a step-fronted pulse of the type postulated.

Flight Test Program[3]

To confirm that the mechanism involving instantaneous acquisition of charge in the field region is responsible for the noise observed in flight, a series of flight tests was carried out at Wright Air Development Center using a specially instrumented B-47. The results of the flight tests substantiate very satisfactorily the theoretical predictions and, in addition, provide much additional information on particle numerical densities and particle charge distributions in typical precipitation conditions.

The flight test data show that in both cirrus clouds and in upper levels of cumulo-nimbus clouds particle densities ranged between 10^4 and 10^5 particles per cubic meter. Individual particle charges ranged between 1 and 40-$\mu\mu$ coulomb, the highest values being encountered in thunderheads. Maximum particle charging encountered in cirrus clouds were under 20-$\mu\mu$ coulombs. Average charge values were usually between 5 and 10-$\mu\mu$ coulombs although for one cirrus flight the average particle charge was only 3.1-$\mu\mu$ coulombs. Distribution of particle charges was such that the rms charge values exceeded the average values by 15–20 per cent.

Oscillographic records of the electrical effects produced by individual particle impacts reveal information concerning the actual course of events during impact. In most cases the impulse produced by the particle has a leading edge which is not a single large step, as shown

[3] A more detailed account of the results of the flight tests and of other aspects of the program is given in the report of Tanner and Nanevicz, footnote 5.

in Fig. 5, but consists instead of a sequence of small steps. This is interpreted as being caused by particle shattering. As the particle collides with the surface it grinds itself to pieces, and each fragment, as it flies off, carries a part of the total charge, thereby producing an incremental step.

Flight test data also revealed some interesting effects regarding the dependence of aircraft charging upon speed. Earlier investigators found charging rate to be approximately proportional to the third power of aircraft speed,[1] while more recent unpublished results obtained by Wright Air Development Center personnel indicate that at higher speeds charging rate increased approximately as the sixth power of the speed. It has been assumed previously that the particles impinging on the aircraft are those in the volume swept by out it, so that the number increased in proportion to the speed. From this it was inferred that the charge per particle must increase as the second to fifth power of the speed. The results of the flight tests, while not entirely conclusive, indicate that if particle charge is dependent on speed the dependence is certainly much weaker than the fifth power, and probably much weaker than the second power. Other data were obtained, however, which indicate that the particle trajectories are strongly dependent upon aerodynamic factors which vary rapidly with speed, so that the number of particles impinging can vary as a rather high power of speed. This result is corroborated by theoretical work performed at the Lewis Laboratory of the NACA by R. J. Brun, R. G. Dorsch and their co-workers.[4] In connection with the problem of aircraft icing, the NACA investigators have calculated the trajectories of spherical particles impinging upon various aerodynamic shapes. While the aerodynamics of ice crystals producing precipitation static are much more complicated than the aerodynamics of the spherical droplets assumed in the NACA investigations, the NACA results apply qualitatively to the problem at hand and indicate that the number of particles impinging can quite probably increase as rapidly as the sixth power of the speed.

Computation of Noise in Idealized Antenna

The production of noise in an antenna by the mechanism just described is similar to the production of shot noise in a vacuum tube but considerably more complicated in detail. Whereas in shot effect the contribution of each electron is exactly the same as every other one, the contribution to the total "particle impact noise" of each precipitation particle depends on its size, its point of impact in the antenna field, and its trajectory subsequent to impact. To accurately include all of these factors for any practical antenna configuration is beyond the capability of available analytical techniques. Valuable insight and good approximations can be achieved, however, by calculations using simplified analytical models of the antenna together with particle statistics determined in the flight tests. Such calculations have been made[5] and give surprisingly good quantitative agreement with measured noise values. For a typical canopy-mounted adf sense antenna flight test data and calculations indicate that particle impact effects produce equivalent noise fields in excess of 100 $\mu v/m$ in a 2-kc bandwidth at a frequency of 300 kc.

Conclusion

From the foregoing it is clear that the particle impact effect is capable of accounting well for the magnitude and spectral characteristics of the noise observed in antennas under dielectric surfaces coated with conductive films, leaving little doubt this is the responsible mechanism. It is important, therefore, to consider the implications of this fact for the design of aircraft lf and mf antennas. One of the more significant conclusions is that there is no simple remedy which will eliminate noise in existing antenna designs. So long as appreciable antenna fields exist in areas exposed to particle impingement, noise will be produced. Furthermore, the fact that particle impact noise is closely analogous to shot noise—of a nonimpulsive nature—precludes the use of special tricks of circuitry such as interference blankers which have been under development as an antiprecipitation static measure. The only measure which appears to hold reasonable hope of overcoming particle impact noise is to develop antenna designs which do not expose the antenna field regions to particle impact.

Another very significant result of the present investigation is assessment of the relative effectiveness of conductive coatings in reducing noise. While noise produced by particle impact is generated whether a conductive film is present or not, and while this type of noise may be high enough to disable radio equipment in conditions of heavy precipitation, flight test data as well as subsequent theoretical investigations indicate that impact noise is less by about 40 db than noise produced by surface discharge. Thus, with a properly applied conductive coating there should be many circumstances—light precipitation or high signal—where equipment should remain operable. Without a conductive coating, the same precipitation conditions would almost certainly result in complete disablement of the equipment regardless of signal level. This suggests that a renewed effort to develop satisfactory conductive coatings is warranted.

Acknowledgment

The author wishes to acknowledge the assistance of J. E. Nanevicz, G. R. Hilbers, and A. Vassiliadis, all members of the Stanford Research Institute staff, who participated in the investigations reported here.

[4] NACA, Washington, D. C., Tech. Notes, TN 2476, TN 3147, TN 3153, TN 3099, TN 3410, TN 3587.

[5] R. L. Tanner and J. E. Nanevicz, "Radio Noise Generated on Aircraft Surfaces," Stanford Res. Inst., Menlo Park, Calif., Final Rep., Contract No. AF 33(616)-2761; September, 1956.

communications

The Exact Solution of the Field Intensities from a Linear Radiating Source*

RABINDRA N. GHOSE†

THE EVALUATION of field intensities in the immediate vicinity of a linear antenna of any arbitrary length is often of some interest. In this region the electric and magnetic field intensities consist of contributions from the radiation, induction, and electrostatic fields. An exact solution of these field intensities which will be particularly suitable for the immediate neighborhood of the antenna can be obtained both for the electric and the magnetic type of linear radiating sources with sinusoidal current or voltage distribution along the axis of the source.

The generalized solution[1] of the field intensities for any source can be expressed as

$$E = -\text{grad } V - \mu\dot{A} - \text{Curl } F$$
$$H = -\text{grad } \Phi - \epsilon\dot{F} + \text{Curl } A \qquad (1)$$

where A, F, and Φ are the magnetic vector potential, the electric vector potential, and the magnetic scalar potential, respectively.

For a thin filamentary line source[2] with sinusoidal current distribution along the s or z direction (Fig. 1),

$$E_z = \frac{1}{j\omega\epsilon}\left(\frac{\partial^2}{\partial z^2} + \beta^2\right)A_z \qquad (2)$$

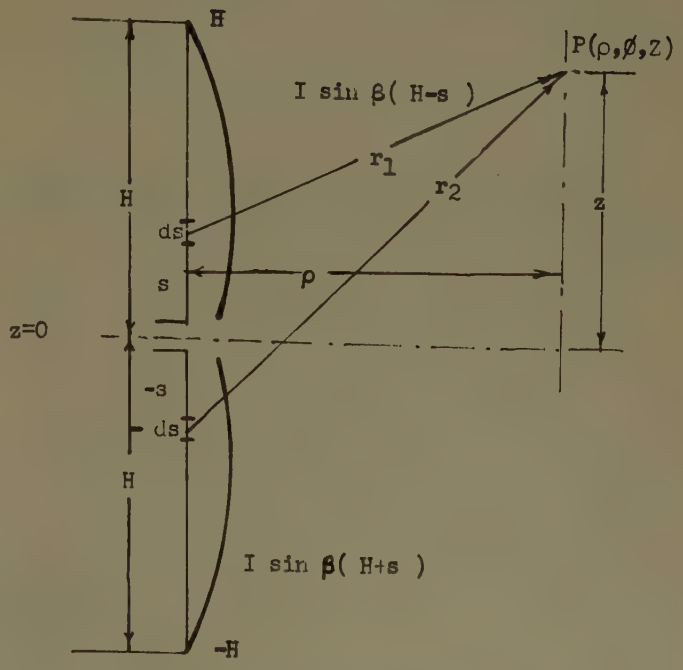

Fig. 1—Radiation from a linear electric dipole with sinusoidal current distribution.

and

$$A_z = \frac{1}{4\pi}\left[\int_0^H \frac{I\sin\beta(H-s)e^{-i\beta\sqrt{\rho^2+(z-s)^2}}}{\sqrt{\rho^2+(z-s)^2}}\,ds + \int_{-H}^0 \frac{I\sin\beta(H+s)}{\sqrt{\rho^2+(z-s)^2}}\,e^{-i\beta\sqrt{\rho^2+(z-s)^2}}ds\right]. \qquad (3)$$

* Received by the PGAP, November 29, 1956.
† Ramo-Wooldridge Corp., Los Angeles, Calif.
[1] E. C. Jordan, "Electromagnetic Waves and Radiating Systems," Prentice-Hall, Inc., New York, N. Y.; 1950.
[2] S. A. Schelkunoff, "Advanced Antenna Theory," John Wiley and Sons, Inc., New York, N. Y.; 1952.

Upon expanding $\sin\beta(H-s)$ and $\sin\beta(H+s)$, one obtains

$$A_z = \frac{I}{8\pi i}\left[e^{i\beta H}\int_0^H \frac{e^{-i\beta s}e^{-i\beta\sqrt{\rho^2+(z-s)^2}}}{\sqrt{\rho^2+(z-s)^2}}\,ds - e^{-i\beta H}\int_0^H e^{i\beta s}\frac{e^{-i\beta\sqrt{\rho^2+(z-s)^2}}}{\sqrt{\rho^2+(z-s)^2}}\,ds + e^{i\beta H}\int_{-H}^0 \frac{e^{i\beta s}e^{-i\beta\sqrt{\rho^2+(z-s)^2}}}{\sqrt{\rho^2+(z-s)^2}}\,ds - e^{-i\beta H}\int_{-H}^0 \frac{e^{-i\beta s}e^{-i\beta\sqrt{\rho^2+(z-s)^2}}}{\sqrt{\rho^2+(z-s)^2}}\,ds\right]. \quad (4)$$

Making use of the following transformation:

$$z - s = \rho\sinh\alpha, \quad (5)$$

the magnetic potential A, can be expressed as

$$A_z = \frac{I}{8\pi i}\left[-e^{i\beta(H-z)}\int_b^a e^{-i\beta\rho e^{-\alpha}}d\alpha + e^{-i\beta(H-z)}\int_b^a e^{-i\beta\rho e^{\alpha}}d\alpha - e^{i\beta(H+z)}\int_a^b e^{-i\beta\rho e^{+1}}d\alpha + e^{-i\beta(H+z)}\int_a^b e^{-i\beta\rho e^{-1}}d\alpha\right] \quad (6)$$

where

$$a = \sinh^{-1}\frac{z-H}{\rho}, \qquad b = \sinh^{-1}\frac{z}{\rho},$$

and

$$\bar{a} = \sinh^{-1}\frac{z+H}{\rho}.$$

Expanding the integrand into binomial series and interchanging the order of integration and summation, one finds

$$A_z = \frac{I}{4\pi i}\sum_{k=0}^{\infty}\frac{(-i\beta\rho)^k}{k\cdot k!}\left[\cosh\left(i\beta H - i\beta z - k\sinh^{-1}\frac{z-H}{\rho}\right) - 2\cos\beta H\cosh\left(i\beta z + k\sinh^{-1}\frac{z}{\rho}\right) + \cosh\left(i\beta H + i\beta z + k\sinh^{-1}\frac{z+H}{\rho}\right)\right]. \quad (7)$$

Once the magnetic potential is determined, the electric and magnetic field components can be determined uniquely by the following relations:

$$H_\phi = -\frac{\partial A_z}{\partial\rho} \qquad E_\rho = \frac{1}{j\omega\epsilon}\frac{\partial^2 A_z}{\partial z\partial\rho}$$
$$H_\rho = 0 \qquad E_z = \frac{1}{j\omega\epsilon}\left(\frac{\partial^2}{\partial z^2}+\beta^2\right)A_z.$$
$$H_z = 0 \qquad E_\phi = 0. \quad (8)$$

It may be remarked that as no approximation is involved in determining A_z, the field evaluated by (8) will be exact. In particular, the numerical computation of the field will be much simpler for very small $(\beta\rho)$; that is, for a region very close to the antenna, as only a few terms of the infinite series need be considered.

A direct application of this analysis may be helpful to determine the region, about a very high power broadcast or television antenna, which may not be safe for maintenance personnel because of the harmful effect of radiation on human bodies. Another application of the analysis will be the determination of self-impedance of an antenna or the mutual impedances of parallel antennas of unequal heights which are often encountered in broadcast-antenna phasing problems.

The problem of determining the field from a slot antenna with sinusoidal distribution of E along the axis of the slot can be solved as a dual problem. If I is replaced by E, the electric field at the center of the slot, in the expression of A_z, one may obtain the electric vector potential F_z for the slot antenna. The remaining field components can be determined by usual vector operations on F_z.

Experimental Measurement of the Absorption of Millimeter Radio Waves Over Extended Ranges*

C. W. TOLBERT† AND A. W. STRAITON†

A SERIES of measurements of the attenuation of radio waves has been made using path lengths up to 61 miles for a wavelength of 8.6 millimeters and up to 7.2 miles for a wavelength of 4.3 mm.

Although some uncertainty exists as to mean meteorological conditions over the paths, it is possible to draw some general conclusions as to the water vapor and oxygen absorption of the atmosphere.

The approximate values obtained from these measurements are listed in Table I.

TABLE I

Wavelength in MM	Average Elevation in Feet	Oxygen		Water Vapor	
		Loss in db/km	Line-Breadth Const. Cm^{-1}	Loss in (db/km) (g/m^3)	Line-Breadth Const. Cm^{-1}
4.3	850	0.5	0.09	0.024	0.3
8.6	850	—	—	0.010	0.28
8.6	6,500	—	—	0.011	0.32
8.6	14,000	—	—	0.0020 to 0.0027	0.045 to 0.06

Introduction

As part of the millimeter propagation research sponsored at The University of Texas jointly by The Office of Naval Research and the Signal Corps, measurements of the loss of 4.3 and 8.6-mm radio waves have been made over a number of paths. These included 3.5, 7.2, and 12.1-mile paths in the vicinity of Austin, Texas, a 50-mile path from Cheyenne Mountain in Colorado to the plains east of the mountains, and a 61-mile path between Pikes Peak and Mount Evans in Colorado.

The measurement technique and the details of each set of measurements are described in a series of technical reports[1] prepared for the sponsoring agencies. This paper is for the purpose of summarizing the results of these measurements as they relate to the energy absorption of the radio waves by oxygen and water vapor in the atmosphere.

4.3-Millimeter Measurements

Paths in the vicinity of Austin, Texas, with lengths of 3.5 and 7.2 miles were used at two slightly different wavelengths of approximately 4.3 mm. The frequencies were 69.45 and 70.10 kilomegacycles. Calibration was made by reference to a 1000-foot path and the median signal level was determined for a number of 5-minute sampling periods.

Sling psychometer readings were made at each end of the path and the moisture content of the air as determined from these soundings was found to be in good agreement with that obtained from the local Weather Bureau. All of these measurements were made in the absence of precipitation.

The attenuation of these signals below the free space values was determined in decibels per mile for each sample and the results plotted as a function of the water vapor content of the air in Fig. 1. The line shown in this figure was plotted to minimize the square of deviation of the points from the line.

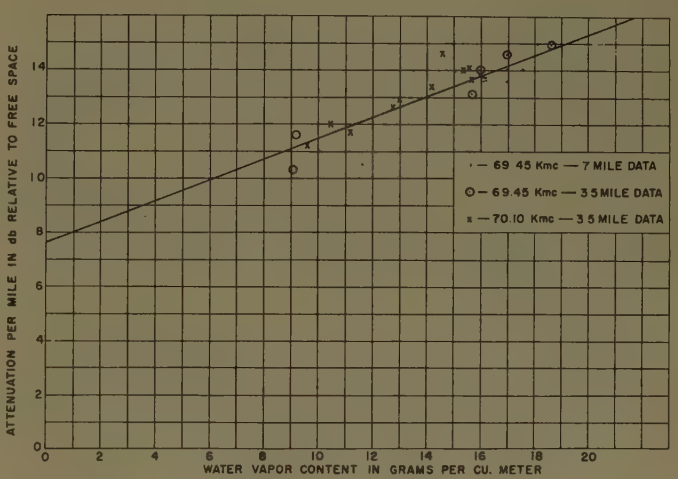

Fig. 1—Loss of radio signal per mile vs water-vapor content.

The accuracy of the data did not justify attempting to separate the effects of the two frequencies and all of the data were given equal weight.

The oxygen loss is determined from the y intercept to be 0.8 db/mile or 0.5 db/km. This value agrees within the limit of accuracy with that predicted by Van Vleck[2] based on laboratory measurements and corresponds to the loss that would be predicted for a line-breadth constant of 0.09 cm^{-1}.

The water-vapor absorption in grams per cubic meter is determined from the slope of the line in Fig. 1 and found to be 0.038 db/mile/g/m^3 or 0.024 db/km/g/m^3. This value is approximately three times that predicted by Van Vleck and corresponds to a line-breadth constant of 0.3 cm^{-1}.

* Manuscript received by the PGAP, February 23, 1956; revised manuscript received, May 14, 1956.

† Elec. Eng. Res. Labs., Univ. of Texas, Austin, Texas.

[1] Elec. Eng. Res. Lab., Univ. of Texas, Tech. Reps. Nos. 63, 69, 70, 73, and 77.

[2] D. E. Kerr, ed., "Propagation of Short Radio Waves," M.I.T. Radiation Lab. Series, No. 13, sec. 8; 1951.

8.6-MM Measurements on 3.5, 7.2, and 12.1-Mile Paths

Loss measurements were made at 8.6 mm on paths in the vicinity of Austin, Texas, with lengths of 3.5, 7.2, and 12.1 miles. The attenuation below the free space values are plotted in Fig. 2 on a per mile basis as a function of the water-vapor content of the atmosphere. The losses at 8.6 mm are distinctly reduced over those at 4.3 mm and the total magnitude of the absorption over these paths is small. For this reason, there is a very large scatter of the points plotted in Fig. 2. These data are inadequate in themselves to separate the oxygen and water-vapor effects. The oxygen loss is, however, small at 8.6 mm and is known with sufficient accuracy to assume a zero water-vapor loss value in Fig. 2 of 0.03 db as predicted from a line-breadth constant of 0.02 cm^{-1}. With this value as the y intercept, a line was so drawn that half of the points fell on either side of it. It is felt that the accuracy of the data does not justify more elaborate methods of drawing this line.

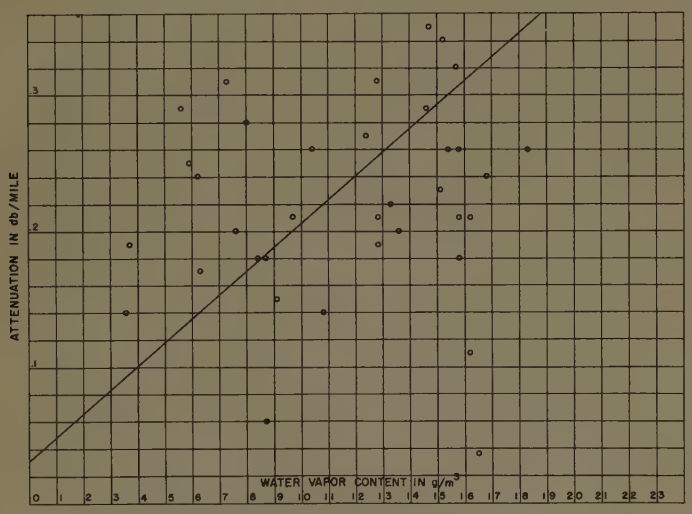

Fig. 2—Water-vapor absorption over 3.5, 7.2, and 12.1-mile path at Austin, Texas.

Using the slope of the line in Fig. 2, a water-vapor absorption of 0.17 db/mi/g/m^3 or 0.10 db/km/g/m is found. This value is that which would be predicted from line breadth constant of 0.28 cm^{-1}.

8.6-MM Measurements Over a 50-Mile Path

The data obtained at 8.6 mm over a path from Cheyenne Mountain to the plains east of Colorado Springs, Colo., were treated in the same manner as that discussed in the previous section. In this case, however, the 8.6-mm signals were compared to a 3.2-cm level with a small height-gain correction to this reference level.

The data for this test are shown in Fig. 3 and the line is drawn on the same basis as used in the previous section except that a small correction in the oxygen absorption for its change in the density-temperature ratio is made in accordance with the approximation proposed by Van Vleck.[2]

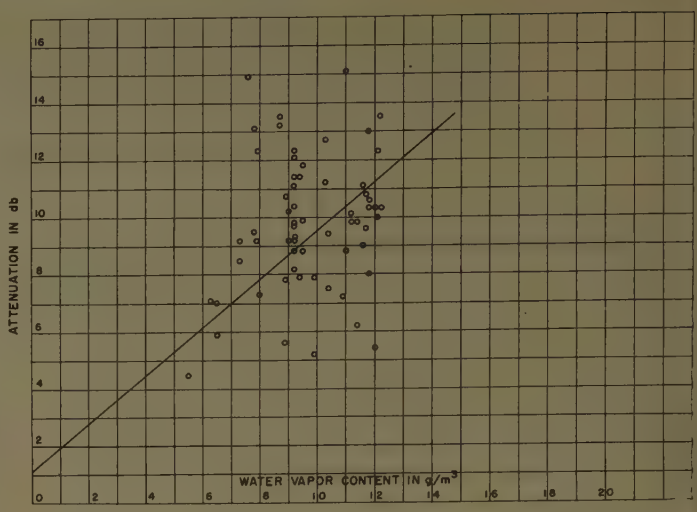

Fig. 3—Water-vapor absorption over 50-mile path in Colorado.

The slope of this line is found to be 0.18 db/m/g/m^3 or 0.11 db/km/g/m^3. This value is that which would be predicted from a line-breadth constant of 0.3 cm^{-1} for water-vapor absorption.

8.6-MM Measurements Over A 61-Mile Peak-to-Peak Path

Measurements were made on a path 60.9 miles in length between Pikes Peak and Mount Evans at a mean elevation of approximately 14,000 feet. Frequent precipitation was encountered on this path, whereas the previous measurements were made at time free of rain, snow or sleet. The results of the measurements are shown in Fig. 4 as a function of the average of the water-vapor content measured at the two ends. The loss of 8.6-mm radio waves is again compared to a 3.2-cm signal recorded simultaneously. In Fig. 4, there are seven samples of millimeter data with losses of less than 3 db and the remaining samples had losses greater than 5 db. The lower-loss group contains all of the cases when it was reasonably certain that no precipitation was occurring on the path and the samples with the higher losses contain all of the cases where there was evidence of precipitation. For this reason, the lower-loss points were assumed to be those associated with no precipitation.

The oxygen loss was again calculated, using the approximate correction for altitude, and a line drawn dividing the lower loss points equally. From the slope of this line it is found that water-vapor absorption is 0.032 db/mi/g/m^3 or 0.002 db/km/g/m^3, corresponding to a line-breadth constant of 0.045 cm^{-1}.

There is some question as to whether the water-vapor content as measured on the peaks is representative of the whole path. Radiosonde data taken by the Air Force at Lowry Field near Denver were analyzed to obtain the water-vapor content at 14,000 feet. The data taken at 0800 were compared to data taken on the peak at 0930 and they were found to be approximately 25 per cent less than humidity measurements taken on the peaks on four days when comparison was possible. The mete-

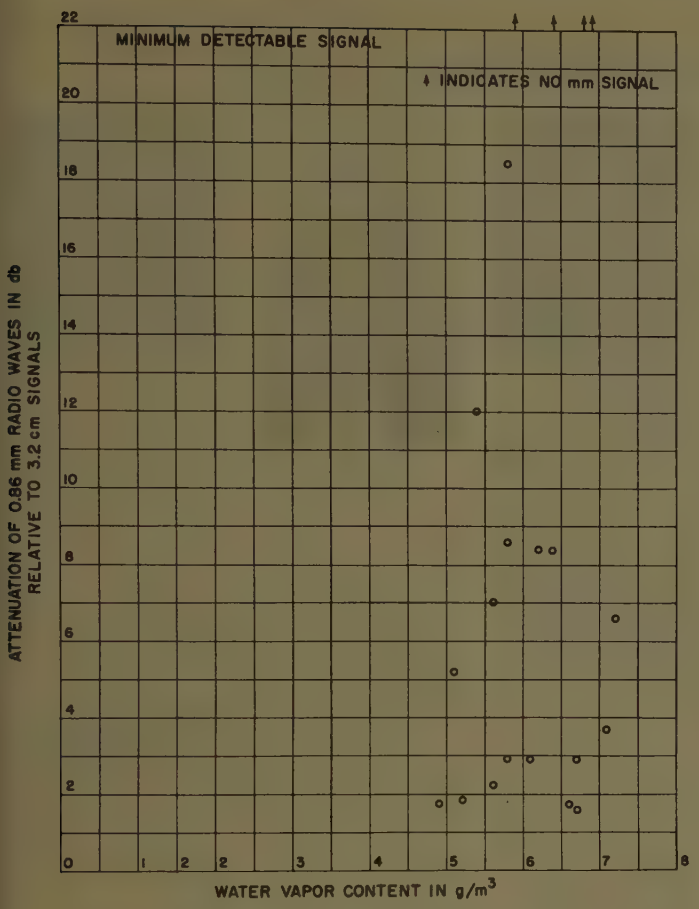

Fig. 4—8.6-mm attenuation as a function of water-vapor content of the atmosphere.

orological situation was such that lower water-vapor content would be expected over Lowry Field at the earlier hour, but it is doubtful whether the difference would be as great as noted. If the water-vapor contents are all decreased by 25 per cent of those used in Fig. 4, the slope of the water-vapor line would be increased by $\frac{1}{3}$. The resulting absorption by water-vapor would then be 0.0043 db/mi/g/m^3 or 0.0027 db/km/g/m^3. The associated line breadth constant is 0.06 cm^{-1}. It is felt that absorption calculated with and without taking into account the radiosonde data provides approximate limits to the loss values and the average of the extremes is taken as the best estimate of the loss values.

There is considerable uncertainty in the results due to lack of complete moisture content data along the paths and to the interference from other propagation factors such as refraction or reflection. Some general conclusions can, however, be drawn from the measurements concerning the absorption of millimeter radio waves by oxygen and water-vapor in the atmosphere.

Only the 4.3-mm measurements provided data on oxygen absorption. These measurements agreed within the limits of accuracy with the losses predicted from laboratory measurements.[2]

The water-vapor losses for the measurements at 850-foot and 6500-foot elevations for both 4.3 and 8.6 mm gave approximately the same line-breadth constant. This value was, however, many times larger than recent predictions[3] based on laboratory measurements.

On the other hand, the measurements made between two 14,000-foot peaks gave losses distinctly less than those predicted. Becker and Autler[3] indicated a dependence on the line-breadth constant on the water-vapor content, but of a much smaller value than predicted by these measurements.

It is hoped that additional measurements will resolve the discrepancy between the measured and theoretical results.

[3] G. E. Becker and S. H. Autler, "Water vapor absorption of electromagnetic radiation in the centimeter wave length range," *Phys. Rev.*, vol. 70, September, 1946.

Contributors

Charles I. Beard (SM'56) was born in Ambridge, Pa., on November 30, 1916. He received the B. S. degree in E.E. from Carnegie Institute of Technology in 1938. One and one-half years at Westinghouse Research Laboratories on dielectrics were followed by two years at M.I.T. as a teaching fellow in physics. In the U. S. Army Signal Corps he served during 1942 and 1943 as an instructor in the Harvard radio and the M.I.T. radar schools. During 1944 and 1945 he was at the Fort Monmouth Signal Corps Publication Agency preparing technical manuals for microwave radar sets. Returning to M.I.T. in 1946, he became a research associate in physics and obtained the Ph.D. degree in physics in February, 1948 performing his research in microwave spectroscopy. In January, 1948 he joined the Magnolia Petroleum Co. Field Research Laboratories and conducted experiments in electromagnetic wave propagation in conducting media. In August, 1950 he joined the Applied Physics Laboratory of Johns Hopkins University and engaged in microwave spectroscopy and in the propagation of microwaves over the ocean.

C. I. Beard

Since August, 1956 Dr. Beard has been at Sylvania Electronics Defense Laboratory, Mountain View, Calif., doing research in microwave scattering.

He is a member of the American Physical Society, Tau Beta Pi, and Sigma Xi.

❖

Jesse G. Chaney (SM'46) was born in Moody, Texas, on August 9, 1906. He received the B.A. degree from Southwestern University in 1924 and the M.A. degree from the University of Texas in 1930.

J. G. Chaney

In addition, he took graduate courses in communication engineering and mathematics at the University of Texas and the Agricultural and Mechanical College of Texas. He was an instructor in mathematics in Southwestern University during 1924–1925, taught in high schools of Texas, 1925–1928, and in the Agricultural and Mechanical College of Texas from 1928 until April, 1942. He was on duty as a Naval Reserve Officer during World War II and is a Commander, U.S.N.R. (Ret.).

Since October, 1944, he has been professor of electronics at U. S. Naval Postgraduate School, Monterey, Calif., first as an officer, and later as a civilian.

Professor Chaney is a member of the American Physical Society, Pi Mu Epsilon, Pi Kappa Delta, and Pi Gamma Mu.

❖

William S. Cook was born in Moncton, New Brunswick, Canada, on March 16, 1932. He attended Mount Allison University in Sackville, New Brunswick, for four years in fulfillment of the requirements for the B.Sc. degree.

W. S. Cook

From 1954 until the fall of 1956, he was affiliated with the Defence Research's Radio Physics Laboratory in Ottawa, Canada. At the present time, Mr. Cook is affiliated with the Federal Electric Corporation, located in Streator, Ill.

❖

John H. Crysdale was born on April 12, 1925, in Toronto, Ontario, Canada. He received the B.A. degree in physics and chemistry from the University of Toronto in 1948 and the M.Sc. degree in physics from McGill University in 1953.

J. H. Crysdale

With the exception of a year spent at McGill University, he has been associated with the Defence Research Board's Radio Physics Laboratory in Ottawa, Canada, since graduation from the University of Toronto. At the present time he is a member of the Laboratory's Upper Atmospheric Physics Section.

Mr. Crysdale is a member of the Canadian Association of Physicists.

❖

John W. B. Day (M'56) was born on December 14, 1931, in Vancouver, British Columbia. He received the B.A.Sc. degree in engineering physics from the University of British Columbia in 1954.

J. W. B. Day

Since his graduation, he has been associated with the Radio Physics Laboratory of the Defence Research Board in Ottawa, Canada. At the present time, he is with the Lower Atmosphere Research Group at the Laboratory.

Georg Goubau (A'49–SM'56–F'57) was born in Munich, Germany, on November 29, 1906. He received the Dipl. Phys. degree in 1930, and the Dr. Ing. degree in 1931, both from the Munich Technical University. From 1931 to 1939, he was employed in research and teaching in the physics department of the same university. During this time he was principally concerned with ionospheric research. He established the first German Ionospheric Research Station (Herzogstand/Kochel) and was in charge of research work there.

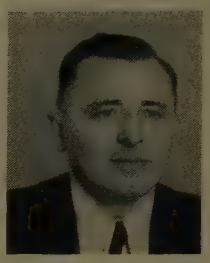

G. Goubau

In 1930, Dr. Goubau became professor and director of the department of applied physics at the Friedrich-Schiller University in Jena, Germany. Since 1948, he has been a consultant at the Signal Corps Engineering Laboratories, Fort Monmouth, N. J.

Dr. Goubau is senior author of the volumes on electronics of the "FIAT Review of German Science," organized by the Military Government of Germany. He also is the senior author of a book on microwave circuits published in 1955 in Germany. In 1957, Dr. Goubau received the "Harry Diamond Award" of the IRE.

❖

Isadore Katz (SM'56) was born in Philadelphia, Pa., on October 21, 1916. He received the B.S. degree with majors in physics and mathematics from Temple University in 1937. From 1938 until 1941 he worked for the U.S. Weather Bureau. In 1942 he joined the staff of M.I.T. Radiation Laboratory where he was engaged in research in radiometeorological problems. In 1946 he joined the Naval Research Laboratory staff in Washington, D.C., where he carried out research on microwave propagation and atmospheric physics. Since 1952 he has been with the Applied Physics Laboratory of the Johns Hopkins University where he continues the study of various phases of radar propagation and atmospheric turbulence.

I. Katz

He is a member of the American Physical Society and a professional member of the American Meteorological Society.

❖

Robin I. Primich (S'48–A'50–M'55) was born in Johannesburg, South Africa, on June 17, 1927. He received the B.S. degree in elec-

trical engineering from the University of the Witwatersrand in 1949.

From 1950 to 1954 he studied at Imperial College, London, Eng., on a scholarship from the Witwatersrand University and with financial assistance from the Department of Scientific and Industrial Research, England.

R. I. PRIMICH

In 1954 he was awarded the diploma of Imperial College and the Ph.D. degree from the University of London. Since the beginning of 1955, he has been with the Radio Physics Laboratory, Defence Research Board, Ottawa, Can., engaged in microwave work.

❖

Michael E. Psutka was born on October 23, 1920, in Kitchener, Ontario, Canada.

In 1939, he was graduated from Kitchener-Waterloo Collegiate, Kitchener, Ont. He then spent four years in the Canadian Army, where he specialized in radar direction finding.

M. E. PSUTKA

Resuming his education, he attended the Radio College of Canada in Toronto, graduating in 1947.

Since that time, Mr. Psutka has been a member of the Radio Physics Laboratory of the Defence Research Board in Ottawa, Canada.

❖

Paul E. Robillard was born on September 26, 1932 in Belle River, Ontario, Canada.

He was graduated from the Ryerson Institute of Technology in Toronto, Canada, in 1954.

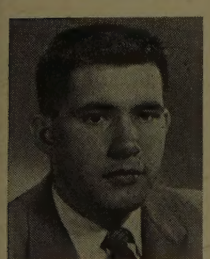

P. E. ROBILLARD

Upon his graduation from the Institute of Technology, he joined the Radio Physics Laboratory of the Defence Research Board in Ottawa, Canada.

At the present time, Mr. Robillard is associated with the Microwave Measurements Group at the Radio Physics Laboratory.

❖

Chester E. Sharp (A'51) was born on June 2, 1906, in Long Branch, N.J. In 1940, he joined the Field Radio Section of the Squier Signal Laboratory at Fort Monmouth, N. J., where he was responsible for the design and development of portable frequency-modulated field radio equipment. In 1943, Mr. Sharp was assigned to the Radio Communication Research Branch, Coles Signal Laboratory, for investigation work on microwave receivers and components. Later, as a project engineer with the Radio Relay and Microwave Section he was responsible for the development of man-pack portable and SHF radio relay equipments. He received War Department commendation from the Office of the Chief Signal Officer in 1946.

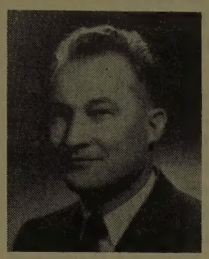

C. E. SHARP

From 1950 to 1955, while with the Radio Communication Research Section, he investigated improved designs of microwave filters and transmission lines.

Since 1955, Mr. Sharp has been assigned to radio wave propagation research and consultation with the Communication Division Research Staff, Signal Corps Engineering Laboratories, Fort Monmouth, N. J.

❖

Harold Staras (M'50–SM'53) was born in New York, N. Y., on December 24, 1922. Upon receiving the B.S. degree from City College, New York, in January, 1944, he joined the Langley Field Laboratories of the National Advisory Committee for Aeronautics as a junior physicist where he did development work on electronic instruments for use in aeronautical research.

H. STARAS

In 1945, he entered the U. S. Army and served as a Counter-Intelligence Corp officer. After leaving military service in 1947, Mr. Staras returned to full time graduate study, receiving the M.S. degree in physics in 1948 from New York University. He then joined the Central Radio Propagation Laboratory of the National Bureau of Standards where he was engaged in the study and analysis of tropospheric propagation phenomena. During this time, Mr. Staras continued this graduate studies in physics at the University of Maryland, obtaining the Ph.D. degree in 1955.

In March, 1954, he joined the Advanced Development section of RCA, Camden, N. J., where he was engaged in the analysis of radar performance in presence of target scintillation and ground clutter, as well as in the performance of communication systems on a scatter circuit.

In 1956, Dr. Staras transferred to the Research Laboratories of RCA where, in addition to continuing to work on scatter systems, he has become involved in bandwidth compression studies of television signals.

Dr. Staras is a member of the American Physical Society, Sigma Xi, and of Commission II, URSI.

❖

Louis Stark (M'54) was born on April 5, 1926 in Detroit, Mich. He enrolled at Massachusetts Institute of Technology, Cambridge, Mass., in 1944 and after completing one semester there, he served with the U. S. Navy for two years. He then resumed his studies at M.I.T. and received the B.S. degree in 1950 and the M.S. degree in 1952, both in electrical engineering. From 1950 to 1952, he was a research assistant in the M.I.T. Research Laboratory of Electronics.

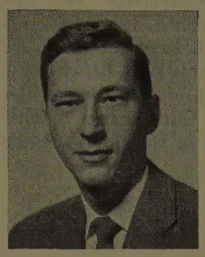

L. STARK

In 1953, he joined the staff of M.I.T.'s Lincoln Laboratory and worked on antennas and microwave components for radar systems. In June, 1954, he joined the Hughes Aircraft Co., Culver City, Calif., where he has been doing antenna work.

Mr. Stark is a member of Sigma Xi and Eta Kappa Nu.

❖

Robert L. Tanner was born in Idaho Falls, Idaho, on December 4, 1921. He attended Stanford University where he received the B.S. degree in 1944, the M.S. degree in 1947, and the Ph.D. degree in 1953.

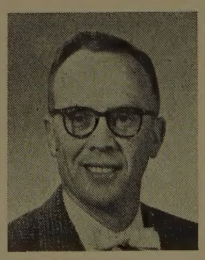

R. L. TANNER

From 1944 to 1946, he served in the Signal Corps, working with pulse modulated communication equipment and with voice coding equipment. In 1947, Dr. Tanner joined the electrical engineering faculty of the University of Washington and remained there until 1950.

During 1950, he was employed by the Boeing Airplane Company where he was engaged in Antenna research.

Since January, 1951, Dr. Tanner has been with Stanford Research Institute where his interests have been largely in the field of aircraft antennas and related systems problems.

He presently holds the position of Group Head in the Antenna Research Group of the Antenna Systems Laboratory.

Dr. Tanner is a member of Phi Beta Kappa, Tau Beta Pi, Sigma Xi, and the Scientific Research Society of America.

J. R. WAIT

J. R. Wait (SM'56) was born in Ottawa, Canada, in January, 1924. He attended McGill University for a brief period before enlisting in the Canadian Army in 1942. By the end of the war he was a foreman in a radar workshop at Kingston, Ontario.

He received the B.A.Sc. and M.A.Sc. degrees in engineering physics from the University of Toronto in 1948 and 1949 respectively. At this time he was employed as a junior research engineer at the Hydro Electric Power Commission of Ontario where he assisted in the development of an infra-red bolometer. Returning for further graduate work to the University of Toronto, he obtained the Ph.D. degree in electromagnetic theory in 1951.

From 1949 to 1952, Dr. Wait was associated with Newmont Exploration Ltd. of Jerome, Ariz. where he conducted theoretical and experimental research in electrical prospecting. From 1952 to 1955 he was a section leader in the Defence Research Telecommunications Establishment in Ottawa where he was mainly concerned with theoretical problems in radiation. He is now a consultant with the Central Radio Propagation Laboratory of the National Bureau of Standards in Boulder, Colo.

He is a member of the Research Society of America, the Society of Exploration Physicists, Commissions III and VI of URSI, and the Canadian Association of Physicists.

W. E. WILLIAMS

William Elwyn Williams was born in Llangefni, Anglesey, Wales, in July 1931. He received B.Sc. degree in mathematics from Manchester University in 1951, the M.Sc. degree in 1952 and Ph.D. degree in 1954. From 1954–1955 he was visiting research associate with the Institute of Mathematical Science, N. Y. Recently he has been concerned with acoustic and electromagnetic scattering problems and radio propagation. Since 1955, he has been employed by the English Electric Company at Luton, Eng.

INSTITUTIONAL LISTINGS

The IRE Professional Group on Antennas and Propagation is grateful for the assistance given by the firms listed below, and invites application for Institutional Listing from other firms interested in the field of Antennas and Propagation.

ANDREW CORPORATION, 363 E. 75th St., Chicago 19, Illinois
Antennas, Antenna Systems, Coaxial Transmission Lines, Design, Development, Production

ANTLAB, 4950 North High St., Columbus 14, Ohio
Antenna Pattern Range Measuring Systems

COLLINS RADIO COMPANY, Cedar Rapids, Iowa
Antenna Design and Propagation Research Related for Airborne and Ground Communication Systems.

DEVELOPMENTAL ENGINEERING CORP., 1001 Conn. Ave, N.W., Washington, D. C. and Leesburg, Va.
Research, Development, Installation of Antennas and Antenna Equipment for Super Power Stations

DORNE AND MARGOLIN, INC., 30 Sylvester Street, Westbury, L. I., New York
Antenna Research and Development—Radiation Pattern Measuring Services.

THE GABRIEL LABORATORIES, Div. of the Gabriel Co., 135 Crescent Road, Needham Heights 94, Mass.
Research and Development of Antenna Equipment for Government and Industry.

HUGHES AIRCRAFT COMPANY, Culver City, California
Research, Development, Mfr.: Radar, Missiles, Antennas, Radomes, Tubes, Solid State Physics, Computers.

JANSKY & BAILEY, INC., 1339 Wisconsin Ave. N.W., Washington 7, D.C.
Radio & Electronic Engineering; Antenna Research & Propagation Measurements; Systems Design & Evaluation

MARYLAND ELECTRONIC MANUFACTURING CORPORATION, College Park, Md.
Antenna and System Development and Production for Civil and Military Requirements.

THE RAMO-WOOLDRIDGE CORPORATION, Los Angeles 45, California

TRANSCO PRODUCTS, INC., 12210 Nebraska Ave., Los Angeles 25, Calif.
Antenna Design and Production—Radiation Pattern Measuring Services

WHEELER LABORATORIES, INC., 122 Cutter Mill Road, Great Neck, New York
Consulting Services, Research and Development, Microwave Antennas and Waveguide Components.

The charge for an Institutional Listing is $25.00 per issue or $75.00 for four consecutive issues. Application may be made to the Technical Secretary, The Institute of Radio Engineers, 1 East 79th Street, New York 21, N.Y.